







EX LIBRIS  
UNIVERSITATIS  
ALBERTENSIS


---

The Bruce Peel  
Special Collections  
Library









Digitized by the Internet Archive  
in 2025 with funding from  
University of Alberta Library

<https://archive.org/details/0162014920480>







**University of Alberta**

**Library Release Form**

**Name of Author:** Barbara Marie Djurfors

**Title of Thesis:** Pulsed Electrodeposition of Au/Sn Eutectic Solder

**Degree:** Master of Science

**Year this Degree Granted:** 2001

Permission is hereby granted to the University of Alberta Library to reproduce single copies of this thesis and to lend or sell such copies for private, scholarly or scientific research purposes only.

The author reserves all other publication and other rights in association with the copyright in the thesis, and except as herein before provided, neither the thesis nor any substantial portion thereof may be printed or otherwise reproduced in any material form whatever without the author's prior written permission.







University of Alberta

**Pulsed Electrodeposition of Au/Sn Eutectic Solder**

By

**Barbara Marie Djurfors**



A thesis submitted to the Faculty of Graduate Studies and Research in partial fulfillment of the requirements for the degree of Master of Science

in

Materials Engineering

Department of Chemical and Materials Engineering

Edmonton, Alberta

Fall, 2001





University of Alberta

Faculty of Graduate Studies and Research

The undersigned certify that they have read, and recommend to the Faculty of Graduate Studies and Research for acceptance, a thesis entitled **Pulse Electrodeposition of Au/Sn Eutectic Solder** in partial fulfillment of the requirements for the degree of **Master of Science in Materials Engineering**.





# Acknowledgments

I would like to acknowledge the contributions of my supervisor Dr. Ivey for his superior supervision and guidance during the past two years of my degree.

In addition, I acknowledge Dr. Anquiang He for allowing me to use one of his images in my thesis (Figure 29c).

I would also like to acknowledge funding from Nortel Networks and the Natural Science and Engineering Research Council of Canada.





# Table of Contents

1	INTRODUCTION.....	1
2	LITERATURE SURVEY .....	3
2.1	AU/SN ALLOY SYSTEM .....	3
2.1.1	<i>Phase Diagram</i> .....	3
2.1.1.1	$\xi$ and $\xi'$ Phases .....	4
2.1.1.2	$\delta$ Phase.....	5
2.1.2	<i>Diffusion</i> .....	5
2.1.2.1	Bulk Diffusion.....	6
2.1.2.2	Grain Boundary Diffusion.....	7
2.2	SINGLE METAL PLATING.....	8
2.2.1	<i>Cell Components and Reactions</i> .....	8
2.2.2	<i>Electrode Potentials</i> .....	9
2.2.3	<i>Electrical Double Layer</i> .....	11
2.2.4	<i>Overpotential</i> .....	12
2.2.4.1	Concentration Overpotential .....	12
2.2.4.2	Activation Overpotential .....	13
2.2.4.3	Resistance Overpotential.....	14
2.2.5	<i>Electrodeposition</i> .....	14
2.3	ALLOY PLATING.....	15
2.3.1	<i>Sequential Layer Plating and Diffusion</i> .....	15
2.3.2	<i>Co-deposition Theory</i> .....	17
2.3.2.1	Types of Alloy Plating .....	18
2.3.2.1.1	Normal.....	18
2.3.2.1.1.1	Regular .....	19
2.3.2.1.1.2	Irregular.....	19
2.3.2.1.1.3	Equilibrium.....	20
2.3.2.1.2	Abnormal.....	20





2.3.2.1.2.1	Anomalous .....	20
2.3.2.1.2.2	Induced .....	22
2.3.2.1.3	Non-Interactive.....	22
2.3.2.1.4	Charge Transfer Coupled .....	22
2.3.2.1.5	Mass Transport Coupled .....	23
2.3.2.2	Electrode Potentials.....	23
2.3.2.2.1	Predicting Co-deposition From Static Potentials .....	24
2.3.2.2.2	Altering Static Potentials.....	24
2.3.2.2.2.1	Concentration .....	25
2.3.2.2.2.2	Complex Ion Addition.....	25
2.3.2.2.3	Dynamic Potentials .....	26
2.3.2.2.3.1	Effect of Current Density .....	26
2.3.2.2.3.2	Effect of Complexing Ions .....	27
2.3.2.2.3.3	Effect of Addition Agents .....	27
2.3.2.3	Factors Influencing Alloy Composition.....	28
2.3.2.3.1	Bath Composition.....	28
2.3.2.3.1.1	Ratio of Metal Ions.....	28
2.3.2.3.1.1.1	Normal Deposition .....	29
2.3.2.3.1.1.2	Abnormal Co-deposition.....	30
2.3.2.3.1.2	Total Metal Concentration .....	33
2.3.2.3.2	Complexing Agents.....	34
2.3.2.3.2.1	Regular Co-deposition.....	34
2.3.2.3.2.2	Irregular Co-deposition .....	35
2.3.2.3.2.3	Induced, Equilibrium, and Anomalous Co-deposition.....	36
2.3.2.3.3	Effect of pH.....	36
2.3.2.3.4	Effect of Addition Agents .....	37
2.3.2.3.5	Effect of Plating Variables on Alloy Composition .....	38
2.3.2.3.5.1	Current Density .....	38
2.3.2.3.5.2	Current Efficiency .....	39
2.3.2.3.5.3	Temperature .....	40
2.3.2.3.5.4	Agitation.....	41





2.3.2.4	Structure of Alloy Electrodeposits .....	42
2.4	PULSE PLATING .....	43
2.4.1	<i>Components</i> .....	44
2.4.1.1	Waveform.....	44
2.4.1.2	Current Density .....	46
2.4.1.3	Duty Cycle.....	47
2.4.2	<i>Electrical Double Layer-Capacitance Effects</i> .....	47
2.4.3	<i>Cathode Diffusion Layer-Mass Transport Effects</i> .....	49
2.4.3.1	Pulsating Diffusion Layer .....	50
2.4.3.2	Stationary Diffusion Layer.....	51
2.4.3.3	Limiting Currents .....	51
2.4.4	<i>Kinetics Effects</i> .....	52
2.4.4.1	Electrical Double Layer Effect.....	52
2.4.4.2	Surface Concentration Effect .....	53
2.4.5	<i>Alloy Pulse Plating</i> .....	53
2.4.5.1	Prediction of Pulsed Alloy Composition.....	53
2.4.5.2	Gold Alloy Pulse Plating.....	55
2.5	ELECTROCRYSTALLIZATION.....	55
2.5.1	<i>Effects of Pulse Deposition on Crystal Growth</i> .....	59
2.6	GOLD-TIN SOLDER DEPOSITION.....	60
2.6.1	<i>Sequential Deposition</i> .....	60
2.6.2	<i>Co-deposition</i> .....	61
2.6.2.1	Co-electrodeposition .....	61
2.6.2.2	Cyanide System.....	62
2.6.2.3	Chloride System .....	64
3	EXPERIMENTAL METHODS.....	69
3.1	SOLUTION PREPARATION .....	69
3.2	PLATING EXPERIMENTS.....	70
3.2.1	<i>Wafer Preparation</i> .....	70
3.2.2	<i>Plating Power Supply</i> .....	71





3.2.3	<i>Multi-Layer Plating</i> .....	72
3.2.4	<i>Solution Stability</i> .....	72
3.3	SCANNING ELECTRON MICROSCOPY (SEM) .....	72
3.4	TRANSMISSION ELECTRON MICROSCOPY (TEM) .....	73
3.5	X-RAY DIFFRACTION ANALYSIS .....	74
4	RESULTS AND DISCUSSION .....	75
4.1	BATH STABILITY .....	75
4.2	CURRENT DENSITY/COMPOSITION RELATIONSHIP .....	78
4.3	X-RAY DIFFRACTION ANALYSIS .....	81
4.4	EUTECTIC ALLOY DEPOSITION .....	85
4.4.1	<i>Deposition Rate</i> .....	85
4.4.2	<i>Multi-Layer Deposition</i> .....	89
4.5	PHASE MORPHOLOGY AND FILM GROWTH MECHANISM.....	95
4.5.1	<i>AuSn</i> .....	95
4.5.1.1	Film Growth Mechanism-Imaging.....	95
4.5.1.2	Film Growth Mechanism-Compositional Analysis.....	104
4.5.2	<i>Au<sub>5</sub>Sn</i> .....	110
4.5.2.1	Film Growth Mechanism-Imaging.....	110
4.5.2.2	Film Growth Mechanism-Compositional Analysis.....	119
5	CONCLUSIONS.....	121
5.1	SOLUTION STABILITY .....	121
5.2	CURRENT DENSITY/COMPOSITION RELATIONSHIP .....	121
5.3	PHASE MORPHOLOGY .....	121
5.3.1	<i>AuSn</i> .....	121
5.3.2	<i>Au<sub>5</sub>Sn</i> .....	122
6	FURTHER RECOMMENDATIONS.....	123
7	REFERENCES.....	125



# List of Tables

Table 1. Lattice Spacings at 30°C for $\zeta$ Phase in Au/Sn Alloy System [Massalski and King, 1960].....	4
Table 2. Extrapolated Room Temperature Diffusivity for Au and Sn in Au/Sn Alloys [Nakahara et al, 1981]. ....	7
Table 3. Table of Standard Electrode Potentials [Bradford, 1993].....	10
Table 4. Electrolyte composition for gold-tin deposition [Holmbrom et al, 1998]. ....	62
Table 5. Operating conditions for Au-Sn alloy plating chemistry [Holmbrom et al, 1998]. .....	62
Table 6. Chemical composition of chloride based plating bath [Sun and Ivey, 1999]. ...	64
Table 7 Composition of plating solution for Au/Sn Alloy plating.....	69
Table 8. Intensity calculations from EDX spectrum of solder layer.....	105
Table 9. Intensity calculations from EDX spectrum of gold seed layer. ....	107





# List of Figures

Figure 1. Au/Sn equilibrium phase diagram [Mastijasevic et al].....	3
Figure 2. Activation and concentration polarization for the cathode. $\eta_A$ and $\eta_C$ refer to the activation and concentration polarizations while $i_o$ and $i_l$ refer to the exchange and limiting current densities respectively [Bradford, 1993].....	13
Figure 3. Activation overpotential for the anode and cathode. $i_o$ refers to the exchange current density and $b_c$ and $b_a$ are the tafel slopes for the cathode and anode respectively [Bradford, 1993]. ....	14
Figure 4. Schematic for the electrodeposition of metals. $i_d$ is the limiting current [Lyons, 1967].....	15
Figure 5. Graph showing the effect of current density on electrode potential. Curve 1 is a copper solution, curve 2 is a copper solution with gelatin, curve 3 is a mixed copper and lead solution with gelatin, and curve 4 is a lead solution with gelatin [Brenner, 1963]. ....	27
Figure 6. Graph showing the effects of bath composition on alloy composition for normal deposition. Curve 1 represents the Bi-Cu alloys, curve 2 represents the Cu-Zn alloys, curve 3 represents the Pb-Sn alloys, curve 4 represents the Bi-Cu curve plotted against percentage of Bi, and curve 5 represents a hypothetical curve. Line AB is the compositional reference line [Brenner, 1963]. In all cases, the copper and lead are the more noble metals.....	30
Figure 7. Graph showing the effects of bath composition on alloy composition for anomalous deposition. Curve 1a represents the Fe-Zn alloys deposited from a bath with 1M total metal content. Curve 1b represents Fe-Sn alloys deposited from a bath with 0.5 M total metal content. Curve 2 represents the Ni-Co alloys deposited from a bath with 0.5M total metal content. Curve 3 represents Ni-Zn alloys deposited from a bath with a variable total metal content. Line AB is the compositional reference line [Brenner, 1963]. ....	32
Figure 8. Graph showing the effects of bath composition on alloy composition for induced deposition. Curve 1 represents W-Fe alloys where W is the reluctant metal. Curve 2 represents P-Ni deposits where P is the reluctant species. Curve 3 represents Mo-Ni alloys where Mo is the reluctant metal. Line AB is the composition reference line [Brenner, 1963].....	33
Figure 9. Graph showing the effect of a complexing agent on alloy composition for In-Ag alloys [Brenner, 1963].....	35
Figure 10. Graph showing the effects of complexing agents on alloy composition for Cu-Sn alloys. Curve 1 represents the effects of cyanide on the deposit composition. Curve 2 represents the effects of NaOH on the deposit composition[Brenner, 1963]. ....	36
Figure 11. Schematics of various pulsed deposition waveforms [Duva, 1984(1)]. ....	45
Figure 12. Schematic representation of modified square waveforms [Puipe, 1986]. ....	46
Figure 13. Schematic illustrating pulse plating parameters [Tannenberger, 1985].....	47
Figure 14. Schematics showing the influence of the capacitance of the electrical double layer on the pulsed current [Ibl, 1980]. ....	49





Figure 15. Schematic showing the concentration profile for the two diffusion layers in pulsed deposition [Puipe, 1986].	50
Figure 16. Schematic diagram of different types of polycrystalline deposits as a function of current density and inhibition intensity [Winand, 1994].	58
Figure 17. Effect of current density on the alloy composition [Sun and Ivey, 1999].	66
Figure 18. Micrographs showing the effects of current density on the grain size of the deposits. a), b) and c) are pulsed current deposits; d), e), and f) are direct current deposits [Sun and Ivey, 1999].	66
Figure 19. Deposit composition for solutions containing 5g/L $\text{KAuCl}_4$ and 5g/L $\text{SnCl}_2 \cdot 2\text{H}_2\text{O}$ with various ethylenediamine concentrations [Doesburg and Ivey, 2000].	68
Figure 20. Schematic of plating wafer preparation.	70
Figure 21. Schematic diagram of experimental plating set-up.	71
Figure 22. Graph of film composition vs. time for deposition at $3 \text{ mA/cm}^2$ for 90 minutes.	76
Figure 23. SEM secondary electron plan view images of solder layer at a) 0 hours;	77
Figure 24. Graph of current density vs. film composition.	79
Figure 25. Plot of current density vs. film composition showing phase analysis.	82
Figure 26. XRD pattern from (a) $\text{Au}_5\text{Sn}$ ordered phase in bold and $\text{Au}_5\text{Sn}$ disordered in italics, (b) $\text{AuSn}$ phase, and (c) mixed phase ( $\text{AuSn}/\text{Au}_5\text{Sn}$ ) sample.	83
Figure 27. Deposition rate data for a) $0.8 \text{ mA/cm}^2$ and b) $2.4 \text{ mA/cm}^2$ .	86
Figure 28. SEM backscattered electron (BSE) image of a two-layer cross-section.	90
Figure 29. a) and b) SEM BSE cross-section images of a multi-layer deposit: a) $2.4 \text{ mA/cm}^2$ for 5 minutes; $0.8 \text{ mA/cm}^2$ for 20 minutes and b) $2.4 \text{ mA/cm}^2$ for 2.5 minutes; $0.8 \text{ mA/cm}^2$ for 10 minutes. c) FE-SE SEM image showing multi-layers deposited at $2.4 \text{ mA/cm}^2$ for 5 minutes; $0.8 \text{ mA/cm}^2$ for 21 minutes.	93
Figure 30. SEM BSE plan view image of composite multi-layer post melting.	94
Figure 31. Film growth progression of $\text{AuSn}$ phase. Depositions were done at $2.4 \text{ mA/cm}^2$ using a pulsed current with an on-time of 2ms and an off-time of 8ms.	97
Figure 32. SEM SE images of $\text{AuSn}$ deposit a) plan view and b) cross-sectional view.	99
Figure 33. TEM cross-section bright field images of $\text{AuSn}$ deposit at a) 18s and b) 120s.	101
Figure 34. a) Plan view TEM bright field image of $\text{AuSn}$ , b) diffraction pattern showing the $\delta$ phase, and c) EDX spectrum confirming the composition of $\text{AuSn}$ .	103
Figure 35. a) Diffraction pattern from a solder layer grain which was indexed as gold (b). The zone axis was indexed as [01-1]. The extra spots (denoted by x's) are due to twinning of the Au grain. The twin plane is (111).	104
Figure 36. EDX spectrum from the grain in Figure 35.	105
Figure 37. EDS spectrum from gold seed layer directly beneath the solder layer.	107
Figure 38. XRD spectra from deposits done for 18, 60, 180, and 300 seconds.	109
Figure 39. SE SEM images showing film growth progression of $\text{Au}_5\text{Sn}$ phase. Depositions were done at $0.8 \text{ mA/cm}^2$ using a pulsed current with an on-time of 2ms and an off-time of 8ms.	112
Figure 40. SEM SE images of $\text{Au}_5\text{Sn}$ deposit a) plan view b) cross-sectional view	115
Figure 41. TEM cross-section images of solder layer at a) 66s and b) 1200s.	116



Figure 42. a) Plan view TEM brightfield image of $\text{Au}_5\text{Sn}$ , b) diffraction pattern showing the $\zeta$ phase, and c) EDS spectra confirming the composition of $\text{Au}_5\text{Sn}$ . .....	118
Figure 43. XRD spectra from deposits done for 66, 180, 400, and 600 seconds. ....	119





# 1 Introduction

One of the lead-free solders currently being used in optoelectronic packaging applications is the eutectic Au/Sn alloy (30 at%Sn). Like the other hard solders, Au/Ge and Au/Si, it also has excellent thermal and mechanical properties making it well suited for packaging applications in which long-term device reliability is important [Plumbridge, 1996]. In addition, its comparatively low melting temperature of 280°C makes it ideally suited for applications in which the structures, often GaAs and InP based devices, are temperature sensitive [Matijasevic, 1993].

Presently, most eutectic Au/Sn alloys are prepared as solder preforms. The major drawback of this technique is that it requires expensive robots to place the preforms or it must be done manually, which is very labor and time intensive. Thin film deposition by evaporation or sputtering of the solder is an attractive alternative, since the oxide content is reduced relative to preforms and process control is better in terms of thickness uniformity and solder alignment [Ivey, 1998]. However, standard thin-film equipment is costly from a production viewpoint.

An alternate thin film deposition technique is electrodeposition. The benefits include reduced oxide formation, thickness uniformity, improved solder alignment (relative to preforms) and significantly reduced capital costs, suggesting a strong commercial viability for this technique. Electrodeposition of an alloy solder can be either done sequentially or simultaneously. With sequential deposition, a pure Sn layer is deposited on top of a pure Au layer. The disadvantage of this technique is that a post-deposition anneal is required to homogenize the composition through interdiffusion [Matijasevic, 1993]. In addition to being a time consuming, multi-step process, such treatments often lead to segregation of the tin to the surface of the alloy layer resulting in the formation of an oxide layer or brittle intermetallics that interfere with bonding [Matijasevic, 1993].

Unfortunately, direct alloy co-electroplating can be a difficult process to control, but the application of pulse plating can vastly improve the properties of the deposit [Avila,



1989]. Most importantly, it is a one-step deposition procedure that requires no further heat treatment or diffusion during bonding.

This thesis is a continuation of the work done by Sun and Doesburg. Using the solution originally developed by Sun, this work focuses on developing a reproducible, simple method for depositing the eutectic Au/Sn alloy directly onto the chip carrier without the need for further processing. The second half of the work is concerned with the film formation of the individual eutectic phases:  $\text{Au}_5\text{Sn}$  and  $\text{AuSn}$ . This portion of the thesis focuses on the nucleation and growth characteristics of the films along with an analysis of their final morphology.

The thesis is organized into six chapters. Chapter two is an extensive literature survey covering the Au/Sn alloy system, fundamentals of electrodeposition, alloy deposition, pulsed deposition, electrocrystallization, and finally a survey of the prior work on the Au/Sn co-deposition system. Chapter 3 outlines the experimental methods, and chapter 4 contains the results and discussion of the thesis work. Chapter 4 has essentially two parts. The first part of the chapter deals with the deposition of the eutectic composition, while the second half of the chapter is devoted to the film formation studies. Chapter 5 is a summary of the appropriate conclusions followed by Chapter 6 which gives some recommendations for further study.





## 2 Literature Survey

### 2.1 Au/Sn Alloy System

Before considering alternate methods for depositing the gold/tin eutectic alloy, it is important to understand the chemistry of the gold/tin alloy system. This particular alloy system has many unique properties that make it extremely well suited for applications as a hard solder.

#### 2.1.1 Phase Diagram

Figure 1 is a representation of the Au/Sn phase diagram between 0%Sn and 50at%Sn.

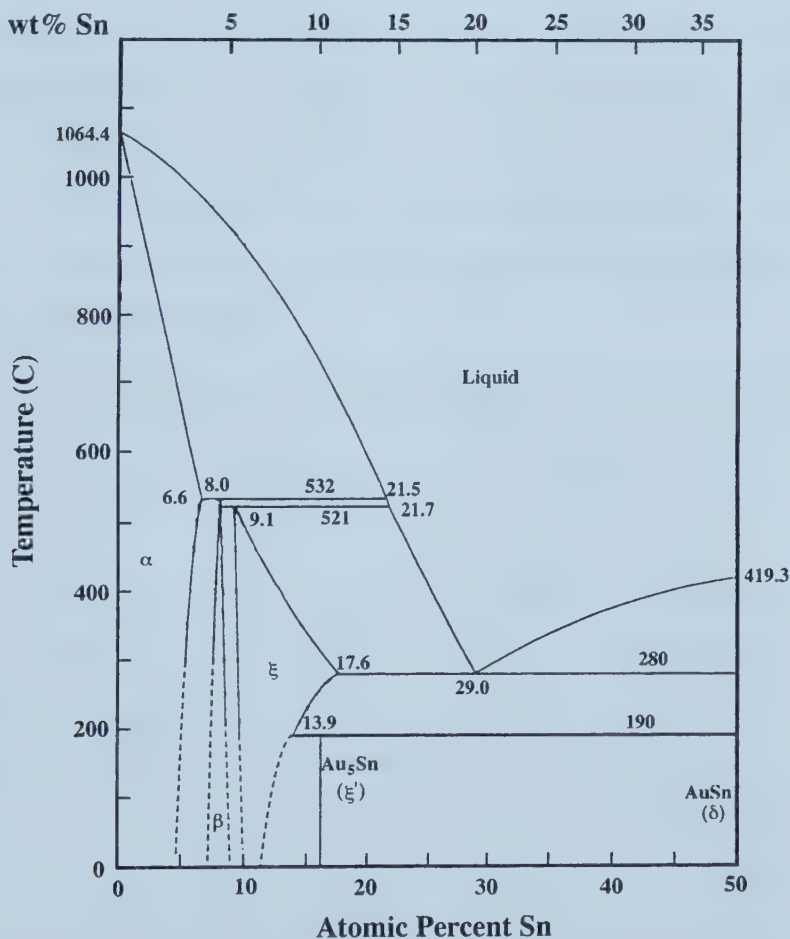
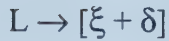


Figure 1. Au/Sn equilibrium phase diagram [Mastijasevic et al].



In the Au/Sn binary system, there are four stable intermetallic compounds,  $\xi'$  (16.7at%Sn),  $\delta$  (50at%Sn),  $\varepsilon$  (66.7at%Sn), and  $\eta$  (80at%Sn), in addition to the two eutectic and three confirmed peritectic points. The eutectic point that is used in the solder applications is at 29.5 at%Sn and 280°C and is described by the following equation.



#### 2.1.1.1 $\xi$ and $\xi'$ Phases

One of the phases making up the eutectic is the  $\xi$ , or  $\text{Au}_5\text{Sn}$ , phase. The  $\xi$  phase is the disordered  $\text{Au}_5\text{Sn}$  phase that is thought to exist at the stoichiometric composition only at higher temperatures. As indicated by the phase diagram, it has quite a large homogeneity range. It extends from 9.1at%Sn at 521°C to 17.6at%Sn at 280°C [Matijasevic et al, 1993]. It has a magnesium type close-packed-hexagonal structure with lattice constants varying with the tin content. Table 1 lists the lattice parameters for this phase as a function of composition.

**Table 1. Lattice spacings at 30°C for  $\xi$  phase in Au/Sn alloy system [Massalski and King, 1960].**

Composition (at%)		Structure	$a$ (nm)	$c$ (nm)	$c/a$
Au	Sn				
88.93	11.07	$\xi$	0.29084	0.47864	1.6457
88.00	12.00	$\xi$	0.29117	0.47874	1.6442
87.00	13.00	$\xi$	0.29170	0.47856	1.6406
86.00	14.00	$\xi$	0.29228	0.47823	1.6362
84.74	15.26	$\xi$	0.29305	0.47761	1.6298
84.00	16.00	$\xi$	0.29350	0.47717	1.6258
83.83	16.17	$\xi$	0.29362	0.47707	1.6248
83.69	16.31	$\xi$	0.29368	0.47694	1.6240



As the tin content of the alloy increases, the lattice parameter  $a$  increases consistently, while the lattice parameter  $c$  first increases and then decreases.

Below 190°C, the  $\xi$  phase is no longer stable, and the  $\xi'$  phase, the ordered intermetallic  $\text{Au}_5\text{Sn}$ , will form. It has a composition of 16.7at%Sn with a homogeneity range of less than 1at%Sn [Matijasevic et al, 1993]. It is known to be a close-packed-hexagonal structure with the unit cell of the superstructure containing 15 Au atoms and 3 Sn atoms. The unit cell has an  $a$  parameter of 0.5092 (nm) and a  $c$  parameter of 1.4333 (nm).

#### 2.1.1.2 $\delta$ Phase

The second constituent phase of the eutectic is the  $\delta$ , or  $\text{AuSn}$ , phase. Like the  $\xi'$  phase,  $\text{AuSn}$  is an intermetallic compound, with a composition of 50at%Sn. However, unlike most intermetallic compounds,  $\text{AuSn}$  has a homogeneity range between 50.0 and 50.5at%Sn.  $\text{AuSn}$  has a NiAs-type hexagonal close-packed structure with two molecules of  $\text{AuSn}$  associated with the unit cell [Matijasevic et al, 1993]. The NiAs hexagonal structure has the unique feature that it can easily incorporate or lose atoms from its lattice. In the case of  $\text{AuSn}$ , gold atoms can be easily gained or lost allowing  $\text{AuSn}$  to transform easily into a gold-rich or tin-rich phase [Nakahara et al, 1981].

#### 2.1.2 Diffusion

It is very important to understand the diffusion characteristics of the gold/tin solder system since many device failures occur along the solder interface. The most significant problem with the gold/tin solder is the reactivity of the system. A typical solder base will consist usually of Ti/Pt/Au layers. However, due to the reactivity and high diffusivity of both the gold and tin, there are often complications with the existing Ti/Pt/Au metallization [Lee et al, 1992; Katz et al, 1994]. Significant interaction can take place between the Pt and Sn resulting in the formation of the  $\text{PtSn}$  and  $\text{PtSn}_4$  intermetallics. This in turn results in a non-eutectic solder layer that forms a non-uniform solder joint, which deteriorates quickly and is a major cause of device failure [Lee et al, 1992; Katz et al, 1994]. More successful solder metallization systems have been designed to prevent





this type of interaction. Au-Sn/W, Au-Sn/Cr, and Au-Sn/Ni have all been shown to reduce the formation of tin intermetallics and tin diffusion out of the solder layer giving a more homogeneous solder joint [Lee et al, 1992; Katz et al, 1994].

#### **2.1.2.1 Bulk Diffusion**

The Au/Sn alloy system enjoys extremely fast interdiffusion, which accounts for the difficulty in obtaining an appropriate solder metallization system. Generally in group Ib/IVb alloy systems, the group Ib elements will be the most rapidly diffusing species [Nakahara et al, 1981]. This is the case with the Au/Sn system, where the Au moves through the Sn lattice via an interstitial diffusion mechanism. However, bulk diffusion in the Au/Sn system is strongly concentration dependent, with relatively small diffusivities for both species in gold-rich regions, and high diffusivities for gold in the Sn-rich regions [Nakahara et al, 1981]. This difference is attributed to a different diffusion mechanism in each region. As mentioned earlier, the Au will diffuse quickly through the tin-rich regions using an interstitial mechanism, while a vacancy diffusion mechanism is employed in the Au-rich regions. In addition, the structural differences between the two metals also accounts for the concentration dependence of the diffusivity. Gold tends to exhibit more metallic bonding, while tin is predominantly covalently bonded. As a result, their alloys will exhibit properties of both types of bonding and the variation in the diffusivity is an example of this combined property [Nakahara et al, 1980].

Because of the relatively high diffusivity of both species outside of the pure phases, room temperature diffusion can occur readily causing Au/Sn intermetallics to form [Gregersen et al, 1981]. Table 2 lists extrapolated room-temperature diffusivities for each species in the different alloy compositions.



**Table 2. Extrapolated room temperature diffusivity for Au and Sn in Au/Sn alloys [Nakahara et al, 1981].**

Phase	$D_{\text{Sn}} \text{ (cm}^2\text{/s)}$	$D_{\text{Au}} \text{ (cm}^2\text{/s)}$
<i>Au</i>	$10^{-26}$	$10^{-30}$
<i>AuSn</i>	$10^{-14}$	$10^{-14}$
<i>AuSn<sub>2</sub></i>	$10^{-16}$	$10^{-16}$
<i>AuSn<sub>4</sub></i>	$10^{-15}$	$10^{-15}$
<i>Sn</i>	$10^{-27}$	$10^{-10}$

In addition, studies by Gregersen et al in 1981 indicated that the diffusion of gold through the AuSn phase is three times as fast as the diffusion of Sn through the AuSn.

Studies done by Nakahara et al in 1981 discovered that the formation of gold/tin intermetallics occurred within a few hours of deposition. Immediately upon deposition, there is an initial rapid diffusion of Au interstitially into the Sn to form the AuSn<sub>4</sub> phase. The reason that the AuSn<sub>4</sub> phase forms first is that it can nucleate easily within the existing tin structure without significantly changing it. At the Au-rich interface, AuSn will also begin to nucleate and grow, although not at the speed of AuSn<sub>4</sub>. Other phases in the Au/Sn alloy system will subsequently form, but at the expense of the two initial phases AuSn<sub>4</sub> and AuSn. This type of interdiffusion, however, can lead to induced stresses that are a few orders of magnitude higher than the yield stresses of many strong materials. As a result, plastic deformation will occur and the interfacial bonding will be compromised [Nakahara and McCoy, 1981(1)].

#### **2.1.2.2 Grain Boundary Diffusion**

In numerous instances, it appears that Au is not the most rapidly diffusing species as predicted by the bulk diffusion data. Sn diffusion can, in many cases, exceed gold diffusion using a grain boundary diffusion mechanism. In these instances, the Sn will diffuse rapidly through the gold grain boundaries [Nakahara et al, 1981; Nakahara and McCoy, 1980(1); Nakahara and McCoy, 1980(2)]. An estimated diffusivity for Sn diffusing along the grain boundaries of the gold is listed at  $10^{-14} \text{ cm}^2\text{/s}$  [Nakahara and McCoy, 1980(1)]. Comparing this value to the values given for the diffusivities of gold





and tin in Table 2, it becomes clear that Sn grain boundary diffusion is only a real concern in gold rich alloys where typical diffusivities for gold and tin are  $10^{-30}$  and  $10^{-26}$   $\text{cm}^2/\text{s}$  respectively. In these situations, the diffusivity for grain boundary Sn is ten orders of magnitude larger than the values for bulk diffusion. This type of diffusion carries with it similar problems to bulk diffusion. As the tin rapidly disappears into the gold layer, Kirkendall voids quickly form along the interface ultimately compromising the solder bond. Indeed for most typical metallization systems, the thickness ratio for the gold and tin deposits tends to be on the gold-rich side, suggesting that grain-boundary diffusion of Sn through the gold lattice is the predominant diffusion mechanism. There has been great success in reducing this phenomenon by using single crystal gold although this is not always practical [Nakahara and McCoy, 1980(1)].

## 2.2 Single Metal Plating

Before the specifics of alloy plating can be dealt with, it is important to have basic background knowledge of the plating process, which requires a brief treatment on single metal plating and the associated phenomena.

### 2.2.1 Cell Components and Reactions

An electrochemical cell consists of four major components; the anode, the cathode, the electrolyte, and an electronic conduction path between the anode and cathode. The anode is where oxidation, or loss of electrons, occurs. A typical oxidation reaction for an electrochemical cell is as follows.

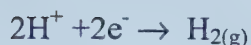


The cathode is where reduction, or a gain of electrons, occurs. Typically, the cathode reaction will look as follows for metal plating.





However, for many electrochemical cells, the actual cathodic reaction involves the evolution of gas, usually hydrogen, instead of the production of a metal product according to the following equation.



The electrolyte acts as the charge-carrying medium, maintaining charge equilibrium in the solution while the electrical conduction path between the anode and cathode is required to allow the electrons to flow.

### 2.2.2 Electrode Potentials

Within the electrolytic solution, as the reactions at the electrodes are occurring, electrons are interchanged between the electrode and the chemical species within the electrolyte that are close to the electrode. The potential of the electrode is therefore defined as the potential of these electrons and is used to determine which reaction will occur. In a sense the electrode potential reflects the relative ability of a substance to enter into a chemical reaction either by gaining or losing electrons. Table 3 is the standard reduction table and lists various chemical reactions and their corresponding potentials at 25°C and 1M solution of ions. Those reactions with the most positive potential are most likely to undergo reduction, while those reactions with the most negative potentials are most likely to undergo oxidation.



**Table 3. Table of standard electrode potentials [Bradford, 1993].**

<i>Reaction</i>	<i>E<sup>0</sup> (V)</i>
$\text{Au}^{3+} + 3\text{e}^- \rightarrow \text{Au}$	1.498
$\text{Cl}_2 + 2\text{e}^- \rightarrow 2\text{Cl}^-$	1.358
$\text{O}_2 + 4\text{H}^+ + 4\text{e}^- \rightarrow 2\text{H}_2\text{O}$	1.229
$\text{Pt}^{2+} + 2\text{e}^- \rightarrow \text{Pt}$	1.118
$\text{Pd}^{2+} + 2\text{e}^- \rightarrow \text{Pd}$	0.951
$\text{Ag}^+ + \text{e}^- \rightarrow \text{Ag}$	0.800
$\text{Fe}^{3+} + \text{e}^- \rightarrow \text{Fe}^{2+}$	0.771
$\text{O}_2 + 2\text{H}_2\text{O} + 4\text{e}^- \rightarrow 4\text{OH}^-$	0.401
$\text{Cu}^{2+} + 2\text{e}^- \rightarrow \text{Cu}$	0.342
$2\text{H}^+ + 2\text{e}^- \rightarrow \text{H}_2$	0.000
$\text{Pb}^{2+} + 2\text{e}^- \rightarrow \text{Pb}$	-0.126
$\text{Sn}^{2+} + 2\text{e}^- \rightarrow \text{Sn}$	-0.138
$\text{Mo}^{3+} + 3\text{e}^- \rightarrow \text{Mo}$	-0.200
$\text{Ni}^{2+} + 2\text{e}^- \rightarrow \text{Ni}$	-0.257
$\text{Co}^{2+} + 2\text{e}^- \rightarrow \text{Co}$	-0.277
$\text{Cd}^{2+} + 2\text{e}^- \rightarrow \text{Cd}$	-0.403
$\text{Fe}^{2+} + 2\text{e}^- \rightarrow \text{Fe}$	-0.447
$\text{Cr}^{3+} + 3\text{e}^- \rightarrow \text{Cr}$	-0.744
$\text{Zn}^{2+} + 2\text{e}^- \rightarrow \text{Zn}$	-0.762
$\text{Ti}^{2+} + 2\text{e}^- \rightarrow \text{Ti}$	-1.630
$\text{Al}^{3+} + 3\text{e}^- \rightarrow \text{Al}$	-1.662
$\text{Na}^+ + \text{e}^- \rightarrow \text{Na}$	-2.771
$\text{Li}^+ + \text{e}^- \rightarrow \text{Li}$	-3.040

These standard potentials, however, apply only under the conditions mentioned. If the temperature or ion concentration change, then the reaction potential will also change.





The Nernst equation is used to describe the effects of temperature and ion concentration on the potential of the reaction.

$$E = E^{\circ} - \frac{RT}{zF} \ln (\text{red})/(\text{ox})$$

$E^{\circ}$  is the standard reduction potential given in Table 3;  $R$  is the gas constant;  $T$  is the temperature;  $z$  is the amount of charge transferred;  $F$  is Faraday's constant;  $(\text{red})$  indicates the activities of all species on the reduction side of the equation multiplied together; and  $(\text{ox})$  refers to the activities of all the species on the oxidation side of the equation multiplied together. Using this equation, the electrode potential of reactions can be determined.

### 2.2.3 Electrical Double Layer

If two phases of differing chemical composition are in intimate contact, an electric potential difference will develop between them. Consider the example with metal in solution assuming a negative charge on the metal. Cations will therefore be attracted to the region of the metal surface in order to provide electro-neutrality. The electrical double layer refers to the two regions of opposite charge across the metal/solution interface. There are several possibilities for the distribution of the cations within the double layer, including the Helmholtz, Gouy and Stern double layer. The Helmholtz double layer has a matching positive charge at a certain fixed distance away from the surface of the metal. This distance is dependant on the how far the ions' inner solvation shells will allow them to approach. The Gouy double layer assumes that the positive charge is distributed in a diffuse manner throughout the solution. The Stern double layer is a combination of the Helmholtz and Gouy double layer [Castellan, 1983]. This electrical double layer is very important since it, in a sense, controls the reactions that occur at the electrode surface. The diffusion of cations to the cathode surface is controlled by the structure of the two charge layers.



## **2.2.4 Overpotential**

Once current begins to flow in the electrochemical cell, the potential of the system shifts. This potential shift is referred to as polarization. The anode will experience a more positive potential as current flows from the anode into the electrolyte, and the cathode will experience a more negative potential. In electroplating, polarization is often referred to as overpotential since extra voltage must be applied to the system to overcome the effects of polarization and allow for the deposition of metal. There are three main types of overpotential: concentration, activation, and resistance. All three are present when an electrochemical cell is working, and therefore their effects must be summed in order to gain a complete understanding of overpotentials.

### **2.2.4.1 Concentration Overpotential**

Concentration overpotential arises as a result of concentration changes at the surface of the working electrode. This in turn causes a concentration gradient between the solution at the electrode surface and in the bulk of the electrolyte. This gradient will cause ions to diffuse from regions of high concentration to regions of low concentration. Thus concentration overpotential is a diffusion controlled process and will therefore be limited by the maximum diffusion rate of ions. This gives rise to the concept of the limiting or diffusion current.

The cathode, not the anode, is usually diffusion controlled since the reactants in the electrolyte must diffuse to the surface of the cathode in order to gain an electron. During normal cell activity, the reactant often becomes depleted in the immediate vicinity of the cathode, forcing the cathode to become increasingly negatively charged in order to attract more reactant. However, at some point, the diffusion distances will become so large that the increasing negative charge of the cathode cannot attract any more reactant electrostatically, and a maximum, or limiting, current density is reached. This is illustrated schematically in Figure 2 [Bradford, 1993]. Notice that concentration polarization is most pronounced at the higher current densities.





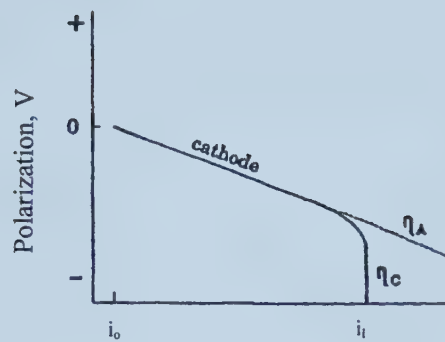


**Figure 2. Activation and concentration polarization for the cathode.  $\eta_A$  and  $\eta_C$  refer to the activation and concentration polarizations while  $i_0$  and  $i_l$  refer to the exchange and limiting current densities respectively [Bradford, 1993].**

#### 2.2.4.2 Activation Overpotential

Unlike concentration overpotential, activation overpotential has significant effects for both the cathode and the anode. Activation polarization is a reaction-controlled phenomenon instead of a diffusion-controlled phenomenon. Every reaction has a certain energy barrier that must be overcome in order for the reaction to take place. In an electrochemical cell, the activation energy is overcome not only by thermal agitation, but also by the electrode potential. Thus, the electrode must polarize in order to provide sufficient energy for the reaction to take place. The anode tends to become more positive and drives the metal ions off faster, and the cathode becomes more negative allowing the reacting species in the electrolyte to receive the electrons more rapidly as illustrated in Figure 3 [Bradford, 1993].



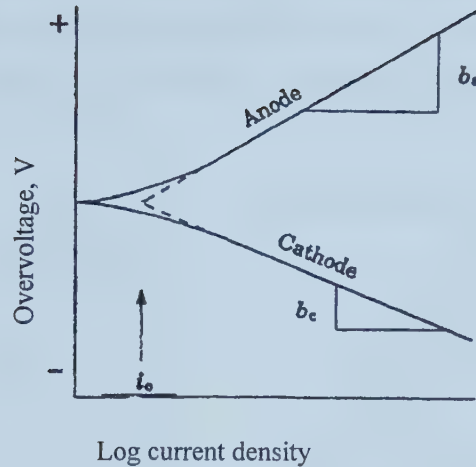


**Figure 3. Activation overpotential for the anode and cathode.  $i_0$  refers to the exchange current density and  $b_c$  and  $b_a$  are the tafel slopes for the cathode and anode respectively [Bradford, 1993].**

#### 2.2.4.3 Resistance Overpotential

The final type of overpotential is the resistance overpotential. This is due entirely to the intrinsic resistance of the electrolyte. When current flows, a portion of it must be used to overcome the solution resistance. The overpotential is defined by Ohm's law where

$$\eta_r = IR$$

$\eta_r$  is the overpotential and  $R$  is the resistance of the solution.

#### 2.2.5 Electrodeposition

The typical current-potential behavior for electrodeposition of a metal is illustrated schematically in Figure 4 [Lyons, 1967]. From the graph it can be seen that at potentials positive to the rest or equilibrium potential, anodic dissolution will occur. However, as the potential becomes more negative, the current reverses, and metal deposition occurs. As the potential continues to become more negative, eventually the limiting current density for the deposition process is reached. If the potential is made even more



negative, then hydrogen evolution and metal deposition will take place simultaneously. Thus, in order for an efficient deposition process, it is often best to operate near the limiting current density to prevent the evolution of hydrogen.

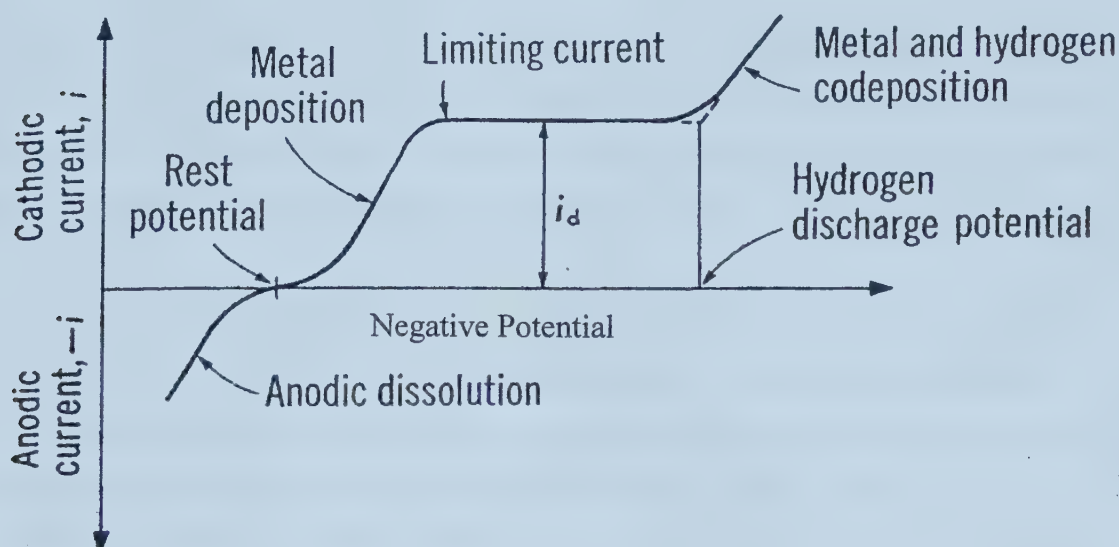


**Figure 4.** Schematic for the electrodeposition of metals.  $i_d$  is the limiting current [Lyons, 1967].

## 2.3 Alloy Plating

Plating alloys is obviously more difficult than single metal deposition since the composition of the bath must be more complex and therefore the process will be much more difficult to control. There are two standard ways of plating an alloyed metal. The first method, sequential layer plating followed by a diffusion process, is by far the easiest to control. The second method, co-deposition, has far more stringent requirements for successful plating, but results in superior control over the plated alloy, and in many instances where precision is required, it is the desired technique.

### 2.3.1 Sequential Layer Plating and Diffusion

Sequential layer plating and subsequent heating is an easy method of forming a plated alloy. The sequential plating method requires separate plating baths to plate several





alternating layers of each individual metal. The layers are then heated to form a diffused alloy. Thus, the technology is only as advanced as single metal plating since the same solutions used to plate the single metal are used in forming the layered alloy.

The only restriction on sequential layer plating is that the metals involved must form a solid solution or compound to allow the diffusion of the different species to take place. The phases that will form for each of the cases can be predicted from the low-temperature region of the pertinent phase diagram [Mohler, 1969].

There are two possible scenarios for solid solution formation. In the case of continuous solid solubility, an alloy zone will be formed that ranges in composition from 0% to 100% of the metal species. If the diffusion process is allowed to continue until one of the pure metals is completely consumed, then the alloy zone will homogenize. Thus, an alloy will form with composition depending on the amount of the pure metals originally plated onto the substrate. For a situation of limited solid-solubility, the same mechanism will occur, except that the homogenization process will result in the presence of two distinct phases [Mohler, 1969]. If the phase diagram indicates that compounds or intermediate phases will form, then they can be expected to form during the diffusion process. The phases will appear in the order indicated on the diagram, but the quantity of each phase must be determined experimentally or through a first hand knowledge of the diffusion rates of the individual species. Again, once one of the pure metals has been completely consumed, then homogenization will tend to occur with the final amount of each compound depending upon the original amount of metal present in the system [Mohler, 1969].

There is an important advantage to this particular method of alloy plating that is not readily achievable with a co-deposition method. It is possible, using the appropriate metal layer sequence and the appropriate diffusion cycles, to achieve alloy deposits in layers, or as a homogenous structure. Thus, a range of alloy properties that extend from the surface of the substrate to the free surface of the plated layers may be produced, or one layer with relatively uniform properties may be produced. Depending on the desired



application of the plated layer, this option can be very advantageous. For instance, in corrosion, it is desirable to have a range of metal layers instead of a homogeneous structure. For steel, an undercoat of nickel is first plated followed by a zinc or tin overcoat. The substrate is then heated to 370°C and a protective coating for the steel is produced. There is approximately 80 wt% zinc at the free surface to provide sufficient corrosion protection against the atmosphere, while the layer is virtually 100% nickel next to the steel to provide superior wear properties [Mohler, 1969]. This method is also used in composition-modulated alloys which are multilayered structures consisting of layers of pure and alloyed materials [Leisner et al, 1996]. Again, the advantages are unique magnetic, mechanical, wear, elasticity, ductility, electrical, optical, and chemical properties.

### **2.3.2 Co-deposition Theory**

An alternate method to sequential plating is to directly deposit the alloy from a single plating bath. This method is termed co-deposition since both metal species deposit at the same time from the same plating bath. Obviously, the requirements for co-deposition are more stringent than for sequential plating as the metals must be compatible both metallurgically and electrochemically.

Metallurgically, the two species must form a solid solution or an intermetallic compound. As with sequential plating, the phases can be roughly predicted by looking at the low-temperature region of the phase diagram. However, deviations from the phase diagram will occur because the electrodeposit will be more finely crystalline which will promote greater solubility than that estimated by the phase diagram. Thus, the phase diagram can only be used as a guide to determine which phases are expected to be present, but not the quantity or composition of any particular phase.

Electrochemically, it is necessary that the two metals deposit at or near the same voltage and have a general affinity for each other [Mohler, 1969]. If the deposition potentials of the two species are far apart, then one species will deposit preferentially effectively preventing the other species from depositing. If the metals are able to co-deposit, but



have no affinity for each other, then the deposited layer will be mechanically weak, and therefore limited in application.

### **2.3.2.1 Types of Alloy Plating**

There are two major schools of thought governing alloy deposition. The pioneering work by Brenner in 1969 is concerned with primarily the thermodynamic criteria of alloy deposition, and does not consider mass transport effects. Later theories, however, tend to focus more on the charge transport and mass transport mechanisms. However, both treatments of alloy plating contain valuable information, and therefore both will be presented in the following discussion.

According to Brenner, there are two major types of alloy co-plating, normal and abnormal, which can be further subdivided to encompass all types of alloy co-deposition. However, the mixed potential theory, where the total current in a system is the sum of the partial currents of that system, tends to categorize the plating types as non-interactive systems, charge transfer coupled systems, and mass transport coupled systems [Landolt, 1994]. The latter treatment of alloy plating categorizes the types based on the mechanism of deposition while Brenner's is based more on experimental observation and is therefore limited in its predictive ability. The following sections will briefly describe the various types of alloy deposition systems as defined by both Brenner and the mixed potential theory.

#### **2.3.2.1.1 Normal**

Normal co-deposition, according to Brenner, is so termed because the more noble metal of the alloy system deposits preferentially as expected by standard electrochemical theory. In any alloy system, there will always be one metal that is more noble, or has the more positive potential. The plating of the noble metal is dependent only on the concentration of the noble metal species within the bath, and independent of the ratio of the two metal species [Mohler, 1969]. Within the normal alloy plating system, there are three different types of plating possible [Brenner, 1963].





#### **2.3.2.1.1.1 Regular**

The regular plating process is a normal plating system that is controlled by diffusion phenomena [Brenner, 1963]. The effects of the plating variables (current density, agitation, and temperature) on the composition of the deposit are determined solely by any changes in the concentrations of metal ions in the cathode diffusion layer. Thus, the composition of the deposit can be predicted from basic diffusion theory. The percentage of the more noble metal in the deposit will be increased by any variable that increases the concentration of the metal ion in the cathode diffusion layer. For instance, an increase in the total metal content of the bath, a decrease in current density, an increase in bath temperature, and increased agitation of the bath system will all increase the metal ion concentration in the diffusion layer, and thereby increase the percentage of the noble metal in the deposit.

Experimentally, regular co-deposition is most likely to occur in baths containing simple metal ions, but may occur in the more complex baths. It is also most likely to occur in a bath where the static potentials of the metals are quite far apart, and when the metals do not tend to form solid solutions [Brenner, 1963].

#### **2.3.2.1.1.2 Irregular**

Irregular co-plating is a form of normal plating that is controlled by the cathode potentials. It is the least understood of all the plating systems, and serves to encompass those alloy plating systems that do not readily fit into the other types of plating systems. It is also a much more complex plating system than the regular system. In this system, the plating is controlled more by the potentials of the various metals against the solution than by diffusion phenomena. Thus, the effects of the plating variables on the composition of the deposit are, at times, in accordance with diffusion theory, and at other times, contrary to diffusion theory. As well, when compared to the regular plating system, the effects of the plating variables on the composition of the deposits are much smaller.



It has been found that irregular co-deposition is most likely to occur with complex ion solutions, particularly when the static potentials of the metals are significantly affected by the complex ion concentration. It is also more likely to occur in systems where the static potentials of the parent metals are relatively close together, and solid solutions are readily formed [Brenner, 1963].

#### **2.3.2.1.1.3 Equilibrium**

This particular type of co-deposition is characterized by deposition from a solution that is in equilibrium with both of the parent metals. This system is unique in that the ratio of the metals in the deposit is the same as the ratio of the metals in the bath. Unfortunately, only a few alloy systems of this type are known. For instance, Cu-Bi, Pb-Sn alloys deposited from an acid bath, and Cu-Ni alloys deposited from a thiosulfate bath are some common examples of equilibrium co-deposition [Brenner, 1963].

#### **2.3.2.1.2 Abnormal**

Abnormal plating, unlike normal plating systems, does not necessarily require that the more noble metal of the system deposit preferentially. There are two plating systems that fall under the abnormal category: anomalous and induced.

##### **2.3.2.1.2.1 Anomalous**

Anomalous plating systems are quite simply those plating systems in which the less noble metal deposits preferentially. Within a certain plating system, anomalous co-deposition will occur only if certain conditions are met regarding the bath concentration and the operating conditions. Therefore, most baths have the potential to be anomalous plating systems if the right conditions are met. If they are not, then the plating system will fall under the category of one of the other three types: regular, irregular, and equilibrium.

Unlike many of the other plating systems, anomalous co-deposition can occur in solutions of either complex or simple ions. It is, however, quite rare, and most prevalent in the electrodeposition of alloys containing iron, cobalt, or nickel [Brenner, 1963].

However, the iron family of alloys has many commercial applications, and recently work has been undertaken in an effort to better understand anomalous co-deposition. The new



model is developed based on the effects of hydrogen evolution in the process of plating [Li et al, 1999].

The model covers seven "rules" that are used to describe all anomalous behaviors. First, it must be recognized that hydrogen evolution will always accompany an alloy deposition, and that the less noble metal ion will have relatively faster intrinsic kinetics [Li et al, 1999]. However, it is important to remember that the deposition rate will be higher only if a sufficient overpotential is applied (increased current density) because the deposition potential of the less noble metal ion is relatively more negative. Secondly, the effect of the hydrogen evolution during plating is mainly to enhance mass transfer by convection. The third rule states that the convection induced by hydrogen evolution will slow the processes with the slower kinetics (charge transfer controlled processes) and enhance processes with intrinsically faster kinetics (diffusion controlled processes) [Li et al, 1999]. Fourthly, the amount of convective flow depends only on the absolute quantity of hydrogen bubbles, which generally increases as current is increased. Fifthly, an increase in overpotential will increase charge transfer controlled processes, but will not affect diffusion controlled processes. Sixthly, a process can change from charge transfer control to diffusion control by increasing the overpotential (current density). This is easily accomplished at lower ion concentrations, high temperatures, larger exchange current densities, and a relatively weaker convection [Li et al, 1999]. The final part of the model deals with the parallel reactions that occur during co-deposition. If both are diffusion limited, then they will not interfere with each other's deposition processes. If one is charge transfer controlled, then the diffusion limited deposition reaction may affect the rate of the other reaction. Similarly, if both are charge transfer controlled, then it is likely that they will interact with each other during co-deposition [Li et al, 1999].

Since this type of model was developed to explain the seemingly inconsistent behaviour of anomalous co-deposition, it is likely that a similar type of model could be developed to describe the other co-deposition processes although this has not been done.





### 2.3.2.1.2.2 Induced

Induced alloy plating systems are those systems where metals that cannot be plated individually can be co-deposited in the presence of another metal. Such metals include molybdenum, tungsten, and germanium. The metals that will not deposit by themselves are termed *reluctant* metals, while those metals that stimulate the deposition process are termed *inducing* metals. This type of co-deposition has an extremely complicated mechanism, and therefore, the effect of the plating variables on this particular deposition system is difficult to predict [Brenner, 1963].

### 2.3.2.1.3 Non-Interactive

In this type of plating system, the partial currents of the two metal components are independent of each other meaning that the kinetics of the individual metals can be used to predict the alloy composition [Landolt, 1994]. The partial current of any given alloy component during co-deposition is the same as if it was being deposited singly. This suggests that the presence of one metal ion in the solution does not affect the deposition behavior of the other metal ion. It has been found that Ni-Cu alloys and tin-lead alloys exhibit this type of behavior. However, this type of alloy deposition is not very common.

### 2.3.2.1.4 Charge Transfer Coupled

The charge transfer coupled co-deposition plating system is far more common. In this type of plating, the partial currents of deposition are dependent on one another. As opposed to the non-interactive system, the partial current of an alloy component during co-deposition is not the same as if it was being deposited alone. The reason that the partial polarization curves are different is a result of the change in activity or nature of the ions when compounds of the two metals are together in the same solution [Gorbunova and Polukarov, 1969]. There are two major types of charge transfer coupled co-deposition: inhibited and catalyzed. In the former type, the partial current density of one of the parent metals is much lower than it would be in pure metal deposition while the other metal usually remains unaffected by the presence of the other metal [Landolt, 1994]. This is the case for the zinc-nickel plating system, where the zinc remains unaffected by the nickel, but the partial current density for the nickel is greatly reduced



by the presence of the zinc. It is suggested that this type of behavior is a result of competitive adsorption of reaction intermediates influencing the surface coverage of nickel [Landolt, 1994]. Catalyzed co-deposition is characterized by one of the parent metals having a catalytic effect on one of the co-deposited alloy components. For instance, in the nickel-molybdenum system, although molybdenum cannot be deposited from an aqueous solution alone, the presence of the nickel makes the deposition possible. It is suggested that this is a result of the formation of a nickel-molybdenum reaction intermediate that allows for the deposition of the molybdenum [Landolt, 1994]. This type of catalyzed system seems analogous to the induced plating system described by Brenner.

#### **2.3.2.1.5 Mass Transport Coupled**

This type of alloy plating refers to the situation wherein the rate of alloy deposition of a given component is controlled by the mass transport of the species being consumed or produced at the cathode as a result of the codeposition of another alloy component [Landolt, 1994]. For instance, simultaneous hydrogen evolution will increase the pH of the plating bath, and therefore change the metal deposition kinetics, and alter the deposition rate. Charge transfer kinetics may or may not be coupled with mass transport co-deposition making the mechanism, at times, quite difficult to determine.

#### **2.3.2.2 Electrode Potentials**

As with single metal plating, the electrode potentials are what control the deposition of the metals in alloy plating. The major requirement for alloy plating is that the deposition potentials of the two metals be relatively close together in the electrochemical series. As discussed earlier, the major reason for this is that the more noble metal will most often deposit preferentially to the complete exclusion of the other metal. Thus, in order to obtain co-deposition, the potentials of the two metals must be close enough that the less noble of the two metals can also be deposited without using an extremely high current density. A large current density not only wastes energy, but also results in a poorly deposited layer.



#### **2.3.2.2.1 Predicting Co-deposition From Static Potentials**

As mentioned previously, co-deposition requires that the electrode potentials of the two metals be relatively close together. As a preliminary estimate, the standard electrode potentials can be used to predict co-deposition from a simple salt or acid solution [Brenner, 1963]. Thus, any two metals with standard potentials relatively close together, and with metallurgical compatibility, should be able to be co-deposited. Unfortunately, there is no standard value by which the standard potentials may be separated for co-deposition to still occur, since the tendency for co-deposition depends so greatly on the individual conditions of the plating bath. It has been found through experience that a separation less than 0.2V usually results in satisfactory co-deposition [Brenner, 1963].

The value of the standard, or static, potentials as a predictor is actually quite limited. The static potential is the most positive potential at which a metal can be deposited. Due to polarization effects, the actual deposition potential will be more negative than the standard value. As well, the tables of standard potentials apply to specific conditions, often 25°C and 1M concentration of ions, and can therefore not be universally applied to all situations.

Beyond these limitations, there is the further difficulty that the electrode potential takes into consideration only the thermodynamic effects. In fact, the potential only refers to the total energy involved in the reaction, but does not give any consideration to kinetic effects.

#### **2.3.2.2.2 Altering Static Potentials**

Looking at the table of standard electrode potentials, it becomes obvious that there are very few metals that have static potentials less than 0.2 V apart at the given conditions. Even with polarization effects, this greatly restricts the alloys that are able to be co-deposited. However, if the static potentials of the individual metals can be moved closer together, then the number of alloys that can be successfully electrodeposited can be increased. The two easiest ways of altering the static potential are to change the concentration of the metal ions, and the addition of complexing agents.





#### **2.3.2.2.2.1 Concentration**

The effect of changing the concentration on the value of the standard electrode potential can be readily predicted from the Nernst equation. Lowering the concentration of the more noble metal in the solution will, in fact, bring the static potentials of the two metals closer together since it will cause the static potential of the more noble metal to become more negative. However, since the standard potential of the metal is a logarithmic function of the metal ion concentration, a large change in ion concentration results in only a very small change in the actual potential of the metal. A further complication is that alloy deposition is not readily possible from a very dilute solution. If the concentration of the noble metal is less than 1% of the less noble metal concentration, then concentration changes in the bath during the plating process are so severe that it is impossible to obtain an alloy with a reproducible composition [Brenner, 1963]. Thus, altering the concentration of the metal ions in the plating bath, although it changes the electrode potentials, is not very effective in practice.

#### **2.3.2.2.2.2 Complex Ion Addition**

As a result of the impracticality of changing the metal ion concentration to bring the static electrode potentials closer together an alternate method had to be developed: complex ion addition. This method is so effective that virtually all of the electrodeposited alloys are obtained from solutions of complex ions. There are two main types of complex ion solutions, single baths and mixed baths. Single complex baths are those baths in which the complex ions of both parent metals can be formed by a single complexing agent. A mixed complex bath, on the other hand, is a bath in which one of the parent metals is in a complex form and the other is not, or when both parent metals are in a complex form as a result of two different complexing agents.

According to Brenner, the use of complex ions is the most important method of altering the electrode potentials of the parent metals. In a solution of complex ions, the electrode potentials all become more negative regardless of their position in the electrochemical series. The potential shift is often larger for the more noble metal, and smaller for the



less noble metal. This results in a crowding together of the electrode potentials in the negative region. In fact, if the appropriate complexing agent is used, then the potentials of the two metals can be made almost equal [Gorbunova and Polukarov, 1969].

Unfortunately, the simple addition of a complexing agent is often not sufficient by itself to bring the potentials of two metals close enough to allow for co-deposition. In addition to complexing, the concentration of the more noble metal may also be reduced, the concentration of the complexing agent may be varied, or the metal ions may be introduced into the bath in the form of different complexes [Brenner, 1963]. The specifics of complex ion addition must therefore depend on experimental observation and will differ depending on the parent metals in the system.

#### **2.3.2.2.3 Dynamic Potentials**

As mentioned earlier, the static electrode potential listed for a metal, is never the actual deposition potential due to polarization effects. The dynamic potential, then, is the actual deposition potential and therefore far more important in determining the ability of two metals to co-deposit. The dynamic potential of a metal is always more negative than the static potential. Therefore, if the polarization of the more noble metal is larger than the polarization of the less noble metal, then the dynamics of potential may, in fact, bring the potentials of the two metals closer together. Thus, understanding the dynamic potentials of the alloy plating system is important since it may allow for co-deposition of a system that was otherwise deemed impossible to co-deposit based solely on static potentials.

##### **2.3.2.2.3.1 Effect of Current Density**

Current density can have a large effect on the dynamic potentials of the metals involved. Unfortunately, the effect of current density is individual for each alloy plating system. Figure 5 shows some examples of the effect of current density on the dynamic potentials. It can be seen that increasing the current density will make the electrode potential increasingly negative thereby helping to bring the deposition potentials of the metals closer together.



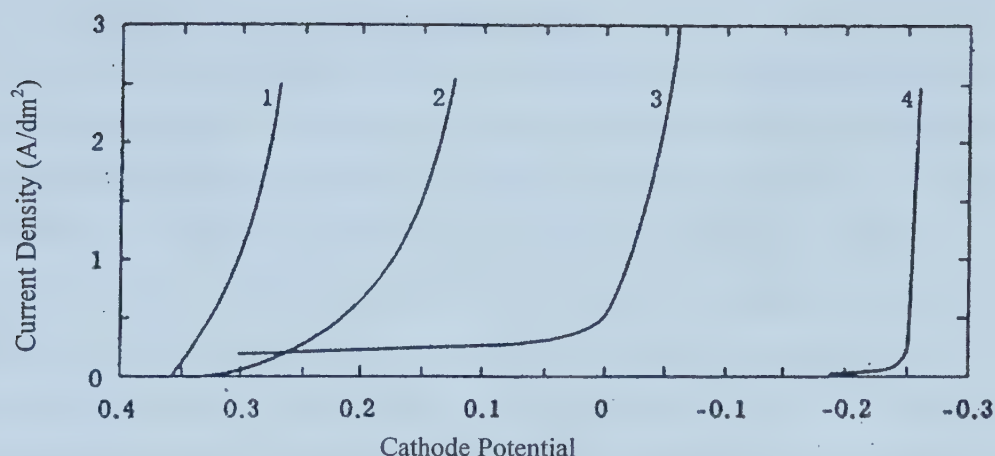


**Figure 5.** Graph showing the effect of current density on electrode potential. Curve 1 is a copper solution, curve 2 is a copper solution with gelatin, curve 3 is a mixed copper and lead solution with gelatin, and curve 4 is a lead solution with gelatin [Brenner, 1963].

#### 2.3.2.2.3.2 Effect of Complexing Ions

As with the static potentials, the addition of complexing ions also brings together the dynamic potentials of the two parent metals. In many cases, the effect of the complexing agent is more pronounced on the dynamic potential, thereby increasing the possibility of co-deposition.

#### 2.3.2.2.3.3 Effect of Addition Agents

Addition agents are another means by which alloy deposition can be brought about. Like complexing agents, the addition agents are used to bring the dynamic deposition potentials of the parent metals closer together. However, unlike complexing agents, addition agents do not need to complex with the metal ion. The effect of the addition agent is unique to the plating system within which it acts, and therefore it is difficult to make generalizations. In many instances, it is possible to find an addition agent that will more greatly affect the polarization of the more noble metal. The result is that the deposition potentials are brought closer together, and co-deposition becomes possible.





### **2.3.2.3 Factors Influencing Alloy Composition**

As with any industrial process, it is of utmost importance to understand the effect of the variables involved on the final product. Electrodeposition of alloys is no exception. The final composition of the alloy will be determined both by the composition of the bath, the use of additional chemicals, and by the operating parameters of the plating bath.

However, in order to make precise predictions, information regarding the specific individual kinetic behavior of the components in the alloy is necessary, and is unfortunately often unavailable [Landolt, 1994; Sanchez et al, 1997]. Thus the following discussion concerning the effects of bath and plating parameters on the alloy composition will be presented as a qualitative review.

#### **2.3.2.3.1 Bath Composition**

One of the most important relationships in alloy plating is the relationship between the composition of the plating bath and the final composition of the electroplated alloy. The composition of the plating bath can be altered by changing the ratio of the parent metal ions within the bath, and also by changing the total metal concentration within the bath. The effects of both are discussed below. However, the mixed potential theory does not discuss in any detail the effects of the bath composition on the resulting alloy composition. Therefore, this topic will be treated with respect to the theory developed by Brenner.

##### **2.3.2.3.1.1 Ratio of Metal Ions**

The ratio of the parent metal ions within the plating bath greatly affects the composition of the deposited alloy. The effect of changing the ratio, however, is distinctive for some of the plating systems that were discussed earlier. In fact, the effects are so distinctive that it is often possible to characterize the type of alloy plating system simply by constructing the graph of alloy composition vs. bath composition [Brenner, 1963]. As a general trend, an increase in the concentration of the more noble metal with respect to the



concentration of the less noble metal, results in an increase in the concentration of the more noble metal in the alloy deposit.

#### **2.3.2.3.1.1.1 Normal Deposition**

Generally, for all normal deposition plating systems, the curves look similar to those illustrated in Figure 6 [Brenner, 1963]. Note that the composition-reference line indicates a situation wherein the composition of the alloy is equal to the composition of the plating bath. In curves 1-3, there is an initially steep rise from the origin where a small change in the concentration of an ion in the plating bath results in a significant increase in that metal in the alloy. Note that the curve is steeper for the regular plating system (curve 1) than for the irregular plating system (curve 2). Note also that with the irregular plating system, at the high percentages of noble metal, the curve levels off indicating that an increase in the noble metal content of the bath will produce little increase in the noble metal content of the alloy.

Curve 3 represents equilibrium plating systems, and can be easily distinguished from the other two normal plating systems by the simple fact that it crosses the composition - reference line. Only at point C, where the two curves cross, will equilibrium co-deposition occur since only at that point are the two parent metals in equilibrium in the solution. Since true equilibrium co-deposition occurs only at one point, it is very difficult, in practice, to get sustained equilibrium deposition. Above, or below, point C, the deposition practice will resemble the other normal plating systems.

Another important feature of these curves is the fact that the regular and equilibrium curves each have an optimum, or limiting, bath composition. At this particular bath composition, the composition of the alloy will be 100% of the more noble metal. Any increase in the more noble metal in the bath will not result in any increase in the noble metal content in the alloy since it has already reached the maximum value.



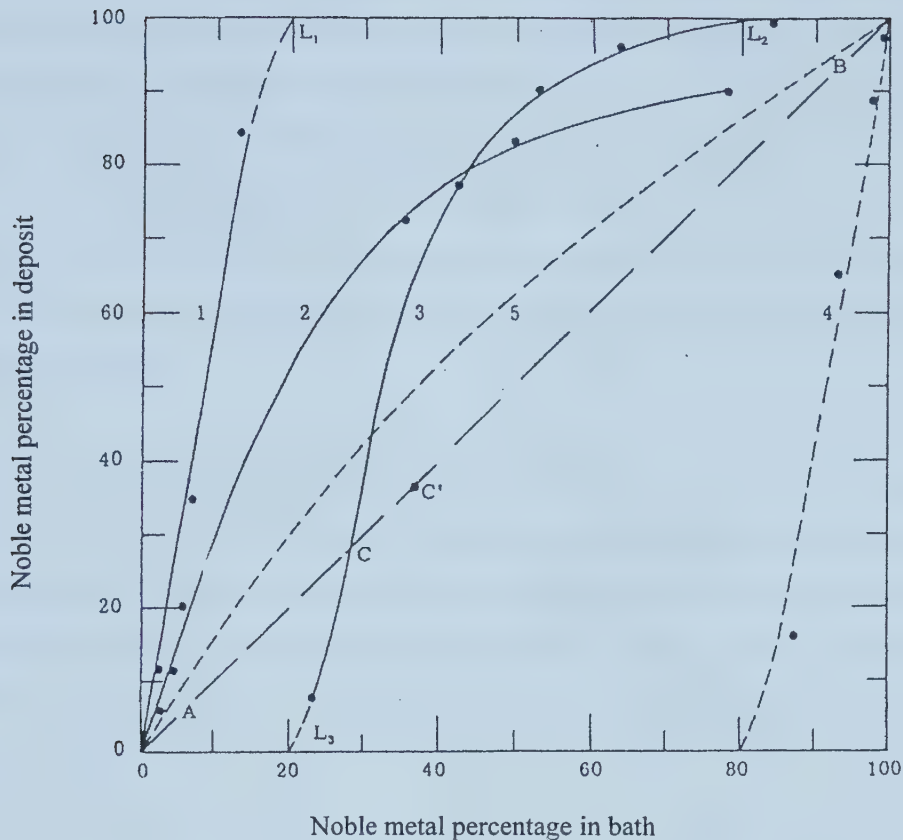


**Figure 6.** Graph showing the effects of bath composition on alloy composition for normal deposition. Curve 1 represents the Bi-Cu alloys, curve 2 represents the Cu-Zn alloys, curve 3 represents the Pb-Sn alloys, curve 4 represents the Bi-Cu curve plotted against percentage of Bi, and curve 5 represents a hypothetical curve. Line AB is the compositional reference line [Brenner, 1963]. In all cases, the copper and lead are the more noble metals.

#### 2.3.2.3.1.1.2 Abnormal Co-deposition

Figure 7 [Brenner, 1963] illustrates the alloy composition vs. bath composition for anomalous co-deposition. Note that in this instance, the composition curves for the more noble metal lie below the composition reference line. This indicates that the more noble metal does not preferentially deposit, the key feature of abnormal co-deposition.

Figure 8 [Brenner, 1963] illustrates the typical curve for induced co-deposition. Notice that unlike the normal plating, these curves do not tend towards 100% of the reluctant





element in the alloy. Instead they tend towards another, often poorly defined, limiting value that is less than 100% of the reluctant element [Brenner, 1963]. The limit of the metal deposition in the alloy must be determined experimentally for each plating system. From the curves, it appears that by increasing the metal percentage of the reluctant metal in the bath, the metal percentage of the reluctant metal in the alloy can be increased. However, it has been determined experimentally that as the reluctant metal concentration in the bath is increased without bounds, the cathode current efficiency decreases until it no longer deposits.

As well, from the graph, it seems that some of the curves lie above the composition reference line, while others lie below. This indicates that there is no tendency for the reluctant metal to act as a noble metal. As well, the reluctant metal will not enter into chemical equilibrium with the solution, and for that reason, when the composition reference line is crossed, this cannot be interpreted as equilibrium co-deposition [Brenner, 1963].



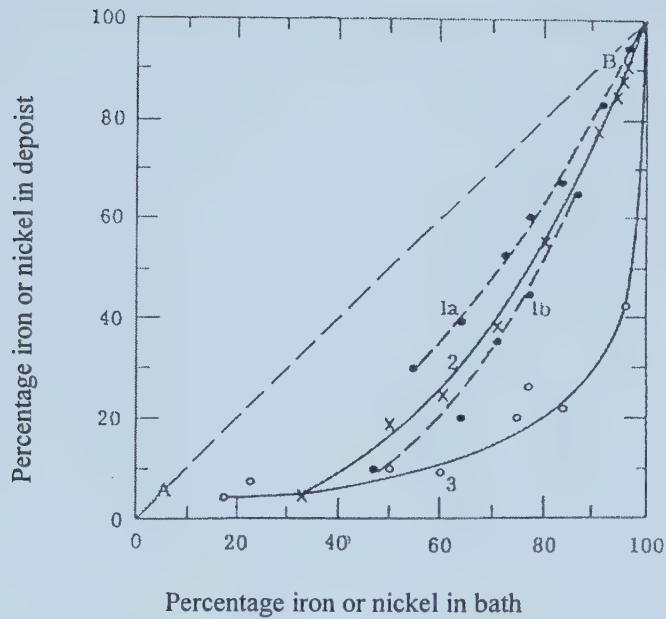


**Figure 7.** Graph showing the effects of bath composition on alloy composition for anomalous deposition. Curve 1a represents the Fe-Zn alloys deposited from a bath with 1M total metal content. Curve 1b represents Fe-Sn alloys deposited from a bath with 0.5 M total metal content. Curve 2 represents the Ni-Co alloys deposited from a bath with 0.5M total metal content. Curve 3 represents Ni-Zn alloys deposited from a bath with a variable total metal content. Line AB is the compositional reference line [Brenner, 1963].



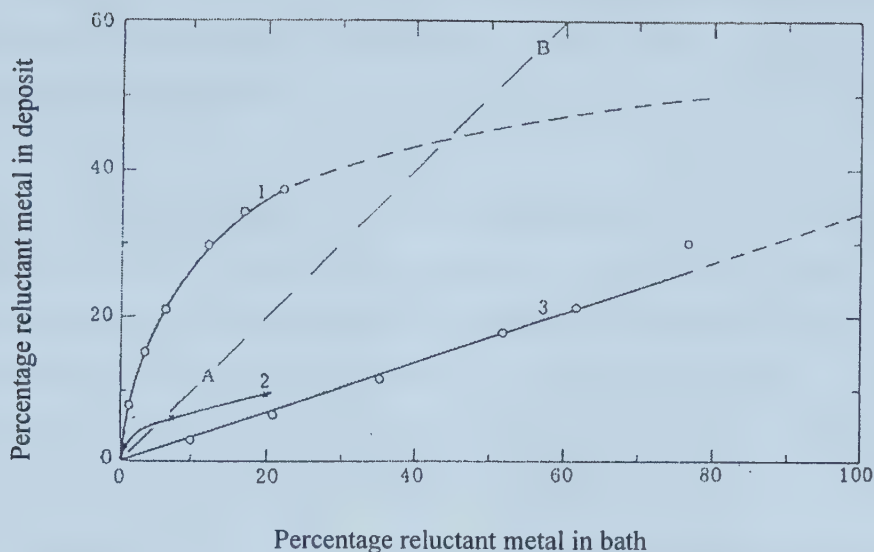


**Figure 8.** Graph showing the effects of bath composition on alloy composition for induced deposition. Curve 1 represents W-Fe alloys where W is the reluctant metal. Curve 2 represents P-Ni deposits where P is the reluctant species. Curve 3 represents Mo-Ni alloys where Mo is the reluctant metal. Line AB is the composition reference line [Brenner, 1963].

#### 2.3.2.3.1.2 Total Metal Concentration

Whereas the previous discussion concerned with the concentration ratio of the two parent metals in the solution, this section deals with the effect of increasing the overall metal content in the bath, while the metal ratio is kept the same. Unfortunately, very little work has been done in this area, and therefore, the topic will only be discussed briefly.

In a regular alloy plating system, increasing the total metal content of the bath will increase the overall percentage of the more noble metal in the alloy. This can be very easily understood if the total amount of noble metal in the bath is considered. By increasing the amount of metal in the solution without changing the ratio of the parent metals, the total amount of noble metal in the bath increases. Since the noble metal will deposit preferentially, it is consistent with the theory that the percentage of noble metal in





the alloy should also increase. It has been determined experimentally that the effects of varying the metal ratio are more pronounced than the effects of varying the total metal content of the plating bath.

Varying the total metal content of the plating solution in irregular and anomalous plating systems has very little effect on the composition of the alloy. For instance, in the co-deposition of copper-lead (most likely anomalous) an eightfold increase in the total metal concentration of the plating bath results in a decrease of the copper content in the alloy by 15% [Brenner, 1963]. This effect is similar for induced co-deposition. These discrepancies can likely be explained by considering the mechanism involved in the actual deposition process. If the process is diffusion controlled, then altering the concentration of the bath will affect the composition. If it is charge transport controlled, however, then no large effect should be expected.

#### **2.3.2.3.2 Complexing Agents**

Since complexing agents are often used to initiate co-deposition, it is important to understand their effect on the alloy composition. In fact, the effects of the complexing agent on the alloy composition are quite pronounced. Generally, when a complexing agent is added to a bath, the potentials of the parent metals are made more negative, and hence deposition is more difficult. However, if the complexing agent affects one metal more severely than the other, then the percentage of that metal in the alloy will decrease. Since a great deal of work has been done in this area, the most common plating systems will be discussed individually.

##### **2.3.2.3.2.1 Regular Co-deposition**

The effect of the complexing agent on a regular plating system is very straightforward. Figure 9 [Brenner, 1963] illustrates this with the indium-silver plating system. As the amount of free cyanide (complexing agent) is increased, the concentration of silver in the alloy is decreased. This can be easily explained by considering the effect of free complexing agent on the electrode potential of the more noble metal. The purpose of the



complexing agent is to make the electrode potential more negative, or more difficult to deposit, and since the noble metal is more greatly affected, it is expected that it would become more difficult to deposit. Thus, an increase in the amount of complexing agent should reduce the amount of the noble metal in the alloy, since the ease with which it can be plated has been reduced.

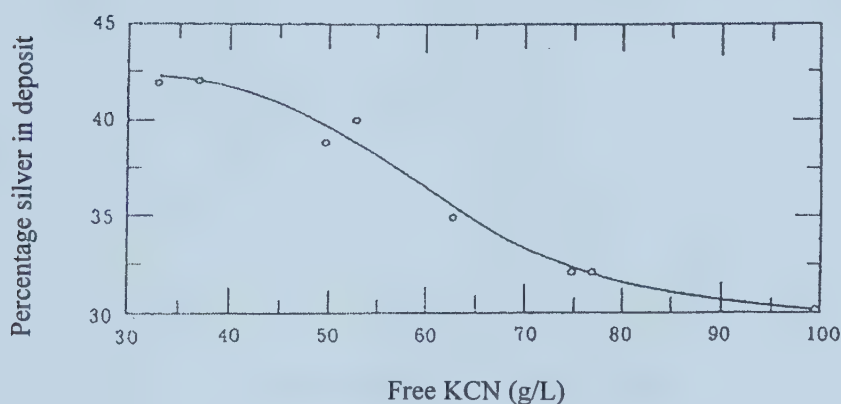


**Figure 9. Graph showing the effect of a complexing agent on alloy composition for In-Ag alloys [Brenner, 1963].**

#### **2.3.2.3.2.2 Irregular Co-deposition**

The copper-tin plating system where the copper is present as a cyanide complex and the tin as a stannate ion provides an excellent example of an irregular co-deposition. Figure 10 [Brenner, 1963] gives an illustration of the effect of free complexing agent on the amount of tin in the alloy deposit. An increase in the cyanide concentration results in an increase in the amount of tin in the alloy, while an increase in the caustic concentration results in a decrease in the amount of tin in the alloy deposit. These effects are easily explained. An increase in the cyanide content makes the copper more difficult to deposit but does not affect the tin, and hence the amount of tin in the alloy increases. An increase in the caustic content makes the tin more difficult to deposit (more negative potential),



but does not affect the copper thereby decreasing the amount of tin in the alloy as indicated by the figure. This type of plating system, however, is rare [Brenner, 1963], and often the effects of increasing the amount of complexing agent must be determined experimentally for each plating system.

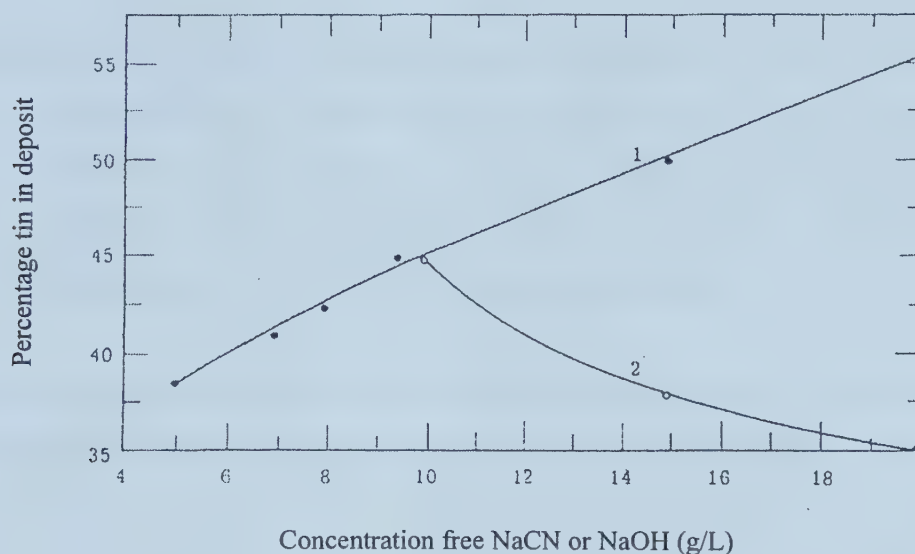


**Figure 10.** Graph showing the effects of complexing agents on alloy composition for Cu-Sn alloys. Curve 1 represents the effects of cyanide on the deposit composition. Curve 2 represents the effects of NaOH on the deposit composition[Brenner, 1963].

#### 2.3.2.3.2.3 Induced, Equilibrium, and Anomalous Co-deposition

Unlike the other two types of co-deposition previously discussed, the trends between alloy composition and complexing agent concentration are not very well defined for these three systems. The results depend almost exclusively on the interaction of the parent metals with the particular complexing agent, and for that reason, a generalization about the effects of the complexing agent on the plating systems as a whole cannot be made. The results must be determined experimentally for each plating system.

#### 2.3.2.3.3 Effect of pH

Even more so than with the complexing agents, the effects of pH on the plating bath and alloy composition are specific to the individual system. Since many plating baths are





acidic, it is important to understand the effects of changing the pH level of the bath on the composition of the alloy. However, the effects of pH have more to do with the chemical nature of the metallic ions in the bath and less to do with type of co-deposition [Brenner, 1963].

It seems that the effects of pH on the alloy composition are restricted to situations where complexing agents are used. In baths where simple ions are used, the pH has very little effect. In baths where complexing agents are used, the effect of the bath pH can be quite pronounced implying that the effects are determined by the metallic complexes in the system, and are independent of the type of plating system [Brenner, 1963].

Since the pH affects the mechanism of deposition, the mixed potential theory may be more successful in explaining the effect of pH. For instance, the effect of pH in the mass transport coupled codeposition theory was described earlier. Many metals will deposit under concurrent hydrogen evolution, which results in the consumption of protons at the cathode surface. Ultimately the change in local pH can affect the deposition rate of one of the metal components. However, the extent of the  $H^+$  depletion at the cathode surface, and therefore the extent of the effect on the metal deposition kinetics, depends on the mass transport conditions and buffering capacity of the electrolyte [Landolt, 1994]. Therefore, it is still necessary to determine the effect of the pH experimentally for the particular plating system being studied.

#### **2.3.2.3.4 Effect of Addition Agents**

Like complexing agents, addition agents are used to bring about co-deposition by altering the potentials of the parent metals, and therefore, their effect on the alloy composition must be considered. Unfortunately, like the complexing agents, the effects of the addition agent must be determined experimentally for each individual plating system. Therefore, since generalizations regarding the different plating types cannot be made, this topic will not be discussed further except to say that the effects can be quite pronounced [Brenner, 1963; Landolt, 1994].



### **2.3.2.3.5 Effect of Plating Variables on Alloy Composition**

The plating variables for alloy deposition, i.e. current density, current efficiency, temperature, and agitation, are the same as for single metal deposition. However, due to the extremely complex nature of alloy deposition, it is far more important to understand the effects of the operating variables on the alloy composition in alloy plating than in single metal deposition. Although the effects of the operating parameters do not always follow specific rules, a general discussion of their effects is required since the effects on the alloy composition are often significant.

#### **2.3.2.3.5.1 Current Density**

Current density is one of the most important operating variables, since it essentially determines the rate of metal deposition. Since the effects of current density are complex and variable, all that will be presented is a general qualitative discussion.

Brenner approaches the concept of current density from two viewpoints: electrode potential and diffusion control. For the former, it is sufficient to say that an increase in the current density of the plating system will cause the cathode potential to become more negative (or less noble) and thus more closely resemble the deposition conditions favorable to the less noble metal. This will therefore increase the proportion of the less noble metal in the alloy. Using the diffusion control approach (mass transport coupled codeposition in the mixed potential theory), the rate of metal deposition has an upper limit known as the limiting current density. At any current density, the more noble metal will be closer to its limiting current density than the less noble metal. Therefore, an increase in current density causes a larger increase in the plating rate of the less noble metal as compared with the more noble metal, resulting in a greater concentration of the less noble metal in the deposited alloy.

While this simple theory is easy to explain, and is easily applicable to regular plating, there have been instances in which the opposite relation is found to be true. Thus far,



there has been no explanation presented except to suggest that it is an artifact of poor bath control [Brenner, 1963]. There is no explanation concerning the effects of current density on the alloy composition offered by the mixed potential theory.

Using the model developed by Li et al, the effects of current density on the deposit composition can be relatively easily explained. In anomalous co-deposition, the composition for the less noble metal increases rapidly at first with an increase in current density, remains invariable for a time, and then slowly begins to drop as the current density is increased even more. According to Li's model, increasing the current density (overpotential) will favor the deposition of the less noble metal (hence the rapid increase in the alloy composition) and then transform the reaction to diffusion controlled where the subsequent evolution of hydrogen will further speed the deposition of the less noble metal. The plateau region describes the situation wherein the deposition rates of the less noble and noble metal ions are increased simultaneously (hence the constant composition) albeit by different mechanisms. The less noble metal experiences an increase in deposition rate due to increased convection mass transfer from the increased hydrogen evolution (rule 4). Simultaneously, the more noble metal experiences an increase in its deposition rate due to the increase in overpotential (rule 5). These two different mechanisms increase the deposition of both metals at the same rate accounting for the constant composition. Finally, at the extremely high current densities, the noble metal deposition process becomes diffusion limited and the overpotential and convection effects increase the deposition rate to the point where it surpasses the less noble metal's deposition rate. Thus, the proportion of the less noble metal in the alloy decreases [Li et al, 1999].

#### **2.3.2.3.5.2 Current Efficiency**

Although current efficiency is usually only considered in an economical sense, it does have a significant impact on the composition of the deposited alloy. However, cathode





current efficiency in regards to alloy plating is far more complicated than single metal plating current efficiency. Not only must the weight of the deposit and the quantity of current be considered, but the composition of the alloy must be factored in as well. The cathode current efficiency is actually the sum of the current efficiencies for the individual metals [Brenner, 1963]:

$$E_r = P_1w/(Q_1IT) + P_2w/(Q_2IT)$$

where P is the percentage by weight of the parent metal, w is the weight of each metal in the deposit, Q is the electrochemical equivalent, I is the current, and T is the plating time.

The effect of cathode current efficiency on the alloy composition is intuitively quite obvious. An increase in the cathode current efficiency of one of the parent metals at the expense of the current efficiency of the other metal results in an increase in concentration of that metal in the alloy. Likewise, in the case where the current efficiency of each of the parent metals increases or decreases by the same proportion, then there will be no change in the alloy composition [Brenner, 1963]. Thus, when alloy plating is being considered, it is important to take into account the effects of the relative current efficiencies on the composition of the alloy.

#### **2.3.2.3.5.3 Temperature**

The effects of temperature on the alloy composition are at times quite complicated since temperature will affect many aspects of the plating bath. For instance, temperature affects not only the equilibrium potentials of the parent metals, but also polarization effects, the concentration of the metal ion species at the cathode surface as a result of increased diffusion rates, and the cathode current efficiency of the system.

The Nernst equation clearly reveals the temperature dependence of the static electrode potentials for the parent metals. However, since these static potentials are weak predictive tools at best, this effect is often neglected. An increase in temperature will also decrease the polarization effects in the system thereby causing the deposition



potentials of the metals to become more noble. However, whether or not one metal is more greatly affected than the other is specific to each plating system, and so a generalization for all systems cannot be made.

In terms of ion concentration, an increase in temperature of the plating bath increases the concentration of metal ions in the cathode diffusion layer. An increase in the metal concentration at the metal-solution interface will favor the metal that is already depositing preferentially [Brenner, 1963]. Thus, this is the most important mechanism by which temperature affects the composition of the alloys. Similarly, the effect of temperature on the cathode current efficiency is also quite pronounced. For instance, in a plating system, an increase in temperature will often only change the cathode current efficiency of one of the parent metals, hence significantly altering the composition of the alloy. Ion concentration and cathode current efficiency are considered the most important mechanisms by which temperature affects the composition of the deposited alloy. However, the predominant mechanism and the subsequent effect of temperature often must be determined individually for the plating system.

For those deposition reactions that are charge transfer controlled, temperature will have a more significant effect on increasing the deposition rate since activation energies for the reactions are involved. However, those reactions that are diffusion controlled may not experience the same increase in deposition rate, unless the effects of one of the other mechanisms mentioned earlier are extremely severe [Li et al, 1999].

#### **2.3.2.3.5.4 Agitation**

The effects of agitation are perhaps the most poorly studied of all the operational variables. Although some qualitative work has been done, very little quantitative work has been done. The effects of agitation on the composition of the alloy are quite significant. Increasing the agitation of the bath will reduce the thickness of the cathode diffusion layer, and thereby change the metal ion concentrations at the cathode-solution interface. The effect of reducing the cathode diffusion layer is to increase the metal ion



concentrations near the cathode which, as indicated previously, increases the deposition rate of the metal that is already depositing preferentially [Brenner, 1963]. The magnitude of increasing the agitation depends on the specific plating system, requiring experimental work to understand the full effects.

For mass transport coupled co-deposition systems, it is expected that agitation would have a significant effect since the limiting step is mass transfer, and agitation will greatly increase the rate of mass transfer [Chen et al, 1988]. However, for the charge transfer coupled co-deposition system and the non-interactive system, the effects of agitation are not discussed [Landolt, 1994].

#### **2.3.2.4 Structure of Alloy Electrodeposits**

Beyond obtaining the desirable composition of the alloy that is being plated, it is equally important that the plated alloy layer is of the appropriate structure for its intended application. For instance, if a bright, level finish is required, then it is essential that no dendrites are present on the surface of the alloy. For this reason, it is important to understand the effects of the plating parameters on the structure of the electrodeposit. The effects of most of the bath operating variables, such as temperature, agitation, and cathode current efficiency have not been studied specifically with respect to the structure of the alloyed electrodeposit.

As mentioned earlier, one of the requirements for alloy deposition is that the two metals be able to form a solid solution. It has been determined experimentally that one of the major factors affecting the solid solubility and hence phase composition of the alloy formed is the cathode overpotential. Generally, the solubility limit of the more electronegative component will increase with an increase in the cathode overpotential [Gorbunova and Polukarov, 1969]. The major outcome of these studies concerning the structure of electrodeposited alloys is the frequency of formation of non-equilibrium phases since the solubility is shifted from its equilibrium value.





As a general experimental trend, unlimited solid solubility in the deposited alloy results in a non-uniform crystal composition. Supersaturated solid solutions usually exhibit a decrease in crystal size accompanied by a smooth, uniform surface. Equilibrium structures, those predicted by the phase diagram, have a coarser grain structure, while metastable phases not predicted by the phase diagram serve to level the surface of the deposit [Gorbunova and Polukarov, 1969]. Unfortunately, no explanation for these phenomena is offered.

## 2.4 Pulse Plating

Pulse plating builds directly on the principles of single metal plating, but with the added variable of pulsing either current or voltage [Puipe, 1986]. Pulse plating has been defined as "current/voltage interrupted electroplating" [Duva, 1984(2)]. Essentially, pulse plating can be described as applying a direct current or voltage for a specific time, and then returning to ground zero (no applied current or voltage) for another specified time period. The result is a significant improvement in deposition layer properties and greater control over the deposition process.

The pulses can be either "forward" or "reverse". A forward pulse can be considered to be the application of a cathodic current or voltage [Puipe, 1986]. Under these conditions, plating at the cathode will occur, and oxidation at the anode will occur. The reverse pulse essentially reverses the current from cathodic to anodic. Under these conditions, dissolution of metal will occur at the cathode, and reduction occurs at the anode. The major advantage of the reverse pulse is to preferentially remove material from areas on the cathode where overplating has occurred thereby reducing the amount of dendrite growth, and improving the thickness uniformity of the plated layer [Puipe, 1986].

The electrodeposition process can be done either by pulsing current or pulsing voltage. In the pulsed current mode, the reaction rate is kept constant, and the potential will vary as a function of time. Alternately, if the voltage is pulsed then the driving force of the reaction is kept constant, and the reaction rate will vary as a function of time [Puipe,



1986]. The main advantage of the voltage regulation is an increased control over the current efficiency of the deposition process.

### **2.4.1 Components**

There are three major components to pulse plating: waveform, current density, and duty cycle [Duva, 1984(1)]. The pulse plating cycle can be completely defined by these three variables.

#### **2.4.1.1 Waveform**

Four major waveforms dominate pulse plating: square, asymmetric sine, split sine, and periodic reverse square. With the asymmetric sine and periodic reverse square waveforms it is important to note that for a brief time, reverse pulsing occurs, allowing the cathode to become the anode. Figure 11 shows examples of each of the types of waveform. As expected, each waveform has its particular advantages and applications. Square waveforms can be generated at very high frequencies (up to 10kHz) and are often used when a high frequency plating cycle is desired. Asymmetric sine wave, and periodic reverse square waves can only be operated at lower frequencies (50-60 Hz). However, they are advantageous in that they allow for faster replenishment of metal ions at the cathode/electrolyte interface when the cathode becomes the anode for a short period of time during the reverse pulse [Duva, 1984(1)]. The split sine wave produces only a cathodic current like the square wave. This is generally used for situations in which the electroplated metal would readily dissolve in the electrolyte. Thus, the application of a continuous cathodic current/voltage prevents excessive metal dissolution [Duva, 1984(1)].



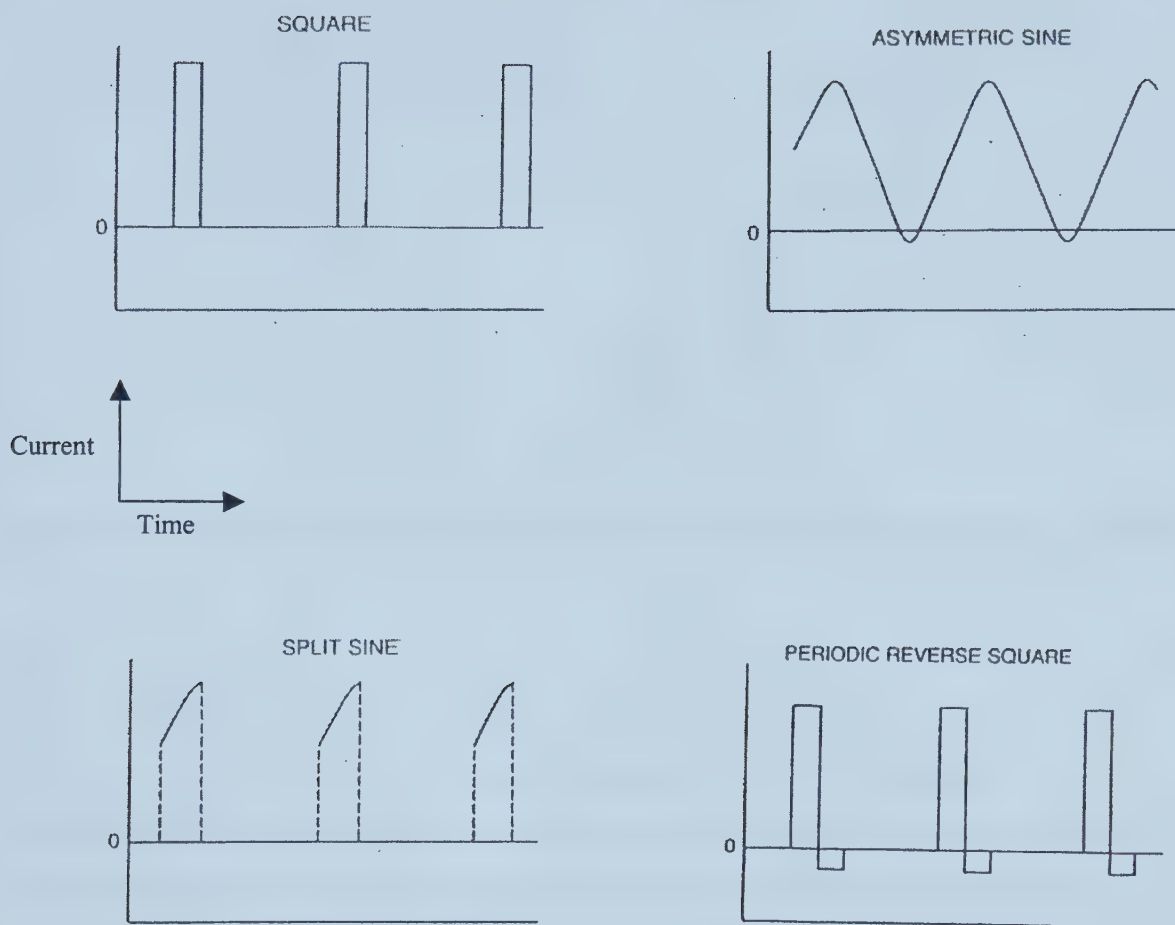


**Figure 11. Schematics of various pulsed deposition waveforms [Duva, 1984(1)].**

The four waveforms mentioned above each have a constant pulse configuration where the off-time and on-time are the same, and the peak current density is kept constant.

However, virtually any variation of the waveforms above is possible. Figure 12 shows some of the variations of the square waveform that are possible [Puipe, 1986]. Notice that the peak current density is not kept constant, nor is the off and on-time. The amount of variation that is possible in the pulsing variables allows for superior control of the deposition process and subsequent layer quality.





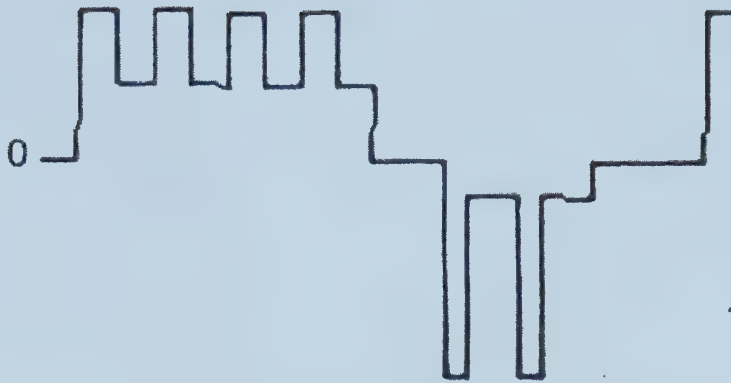


**Figure 12. Schematic representation of modified square waveforms [Puiippe, 1986].**

#### **2.4.1.2 Current Density**

Obviously, the current density is important in any plating application, however, in pulse plating it has added meaning. Since pulse plating is defined as intermittent current/voltage plating, it is important to define not only the maximum value for current density/voltage, but also the average value. Figure 13 clearly illustrates the different pulse plating parameters [Tannenberger, 1985]. The peak current density,  $j_p$ , refers to the maximum value that the current/voltage reaches while the mean current density,  $j_m$ , refers to the mean value of the current/voltage, if direct plating were used throughout the elapsed time [Tannenberger, 1985]. Generally it is the peak current density that will determine the characteristics of the deposit since that is the current that will define the deposition rate [Duva, 1984(1)].



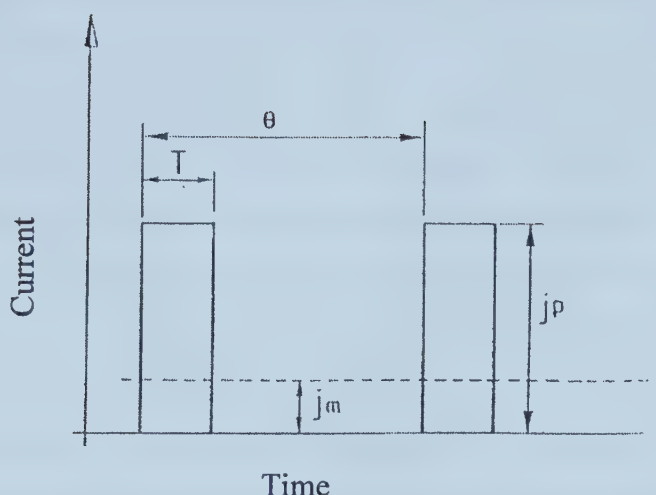


**Figure 13.** Schematic illustrating pulse plating parameters [Tannenberger, 1985].

#### 2.4.1.3 Duty Cycle

One of the most important variables in pulse plating is the duty cycle. It is defined as the ratio between the on-time and off-time of the pulse. The on-time is defined as the duration of the applied pulse. The off-time, then, is defined as the time during which there is no pulse applied at all. In the case of the pulses presented in Figure 11, the duty cycle is constant. However, in the pulse cycle presented in Figure 12 the duty cycle is not necessarily constant. Obviously the duty cycle will affect many aspects of the deposit since it will determine how often the cathode is active [Duva, 1984(1)].

#### 2.4.2 Electrical Double Layer-Capacitance Effects

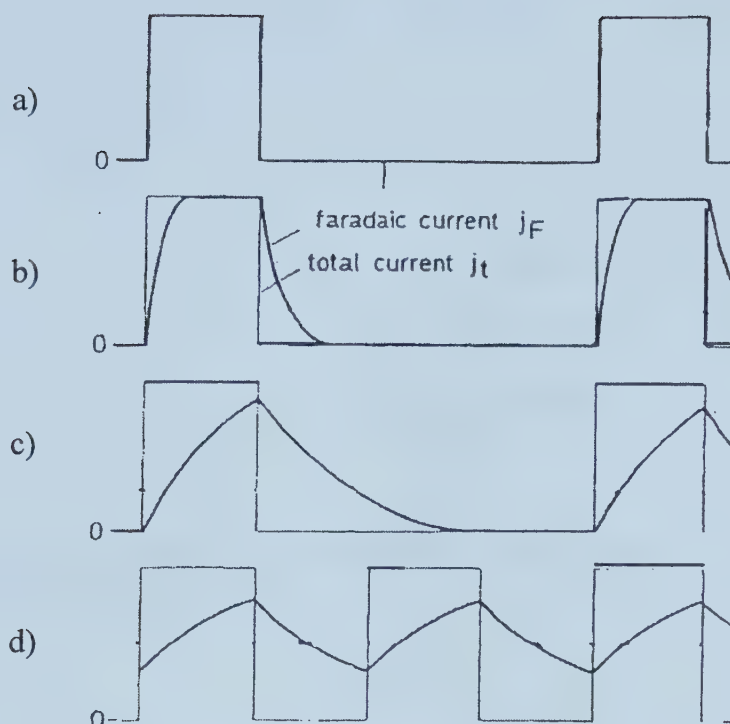
Understanding the influence of the capacitance nature of the electrical double layer on the nature of the pulse is extremely important. For instance, if the charging time of the layer is much larger than the on-time of the pulse, the current pulse will be strongly distorted. Similarly, if the layer discharge is longer than the off-time of the pulse, the pulsed current essentially becomes a direct current situation [Duva, 1984(1); Puippe, 1986(2)]. The charging and discharging times of the electrical layer are a function of the exchange current density, capacitance, and pulse current density and are therefore unique to each plating system.



Figure 14 illustrates situations where the capacitance of the double layer affects the pulsing action [Ibl, 1980]. The thin line represents the applied pulse current, and the thicker line represents the faradaic current which is the part of the current that corresponds to metal deposition. At the very beginning of the pulse, the whole current is used to charge the double layer, and hence no deposition takes place (faradaic current is zero). However, as the electrical layer becomes charged, the potential becomes more negative, and the faradaic current will increase eventually reaching the value of the pulse followed by a termination of the pulse and discharging of the electrical layer. If the charging and discharging time is negligible compared to the length of the pulse, then the situation in Figure 14a will occur where the faradaic current mimics almost exactly the applied pulse. If the charging/discharging time is comparable, but still smaller than the applied pulse, the situation in Figure 14b will occur. However, if the charging/discharging time is larger than the applied pulse current, then the faradaic current will never reach the value of the applied pulse current as illustrated in Figures 14c,d [Ibl, 1980; Puippe, 1986(2)]. Thus it is extremely important in pulse plating to understand the capacitance nature of the electrical double layer in order to ensure that the current pulses are not too severely distorted as in the last two cases.







**Figure 14. Schematics showing the influence of the capacitance of the electrical double layer on the pulsed current [Ibl, 1980].**

### 2.4.3 Cathode Diffusion Layer-Mass Transport Effects

One of the major differences that arises from pulsed plating is the existence of two separate diffusion layers if a short pulse duration is used [Puipe, 1986]. Figure 15 is a schematic of the typical double diffusion layer. In the layer immediate to the cathode, the concentration of metal ions pulsates at the frequency of the applied pulsed current. The concentration decreases during the pulses since the metal ions are being deposited, and then "relaxes" in the interval between the pulses since plating has stopped [Puipe, 1986]. If the pulse duration is quite short, then this layer will be quite thin, and will not have convection controlled mass transport. This means that the supply of metal ions must be replenished through a diffusion process from the solution bulk. This creates the second stationary diffusion layer to transport ions from the bulk electrolyte to the pulsating diffusion layer. This layer is generally the same thickness as the diffusion layer that exists under direct plating conditions.



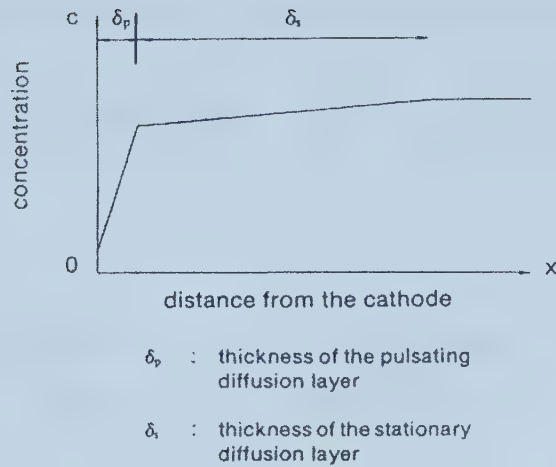


**Figure 15. Schematic showing the concentration profile for the two diffusion layers in pulsed deposition [Puipe, 1986].**

#### 2.4.3.1 Pulsating Diffusion Layer

Fick's first law can be used to describe any flux density due to a concentration gradient. Thus, if the concentration profile of the pulsating diffusion layer is approximated as a straight line as indicated in the figure, then the flux density of the cations in the pulsating layer during a pulse,  $N_p$ , can be described by the following equation [Ibl, 1980].

$$N_p = D (c'_e - c_e) / \delta_p$$

where  $c'_e$  is the concentration at the pulsating diffusion layer boundary,  $c_e$  is the concentration at the cathode surface, and  $D$  is the diffusivity. This expression, however, is derived based on 100% current efficiency.

Similarly, the pulse current density can be described by the following equation [Ibl, 1980].

$$j_p = zFD (c'_e - c_e) / \delta_p$$



Notice that the current density during a pulse is directly proportional to the concentration gradient during the pulse.

The thickness of the pulsating diffusion layer is approximated by the following equation.

$$\delta_p = (2DT)^{1/2}$$

where T is the pulse length. Notice that the thickness of the diffusion layer is independent of both the concentrations and the pulse current density.

#### 2.4.3.2 Stationary Diffusion Layer

As with the pulsating diffusion layer, the flux of cations through the stationary diffusion layer can be described by Fick's first law.

$$N_s = D(c_o - c'_e) / \delta_s$$

where  $c_o$  describes the concentration of the metal ion in the bulk electrolyte. This results in an average current density of :

$$j_s = zFD (c_o - c'_e) / \delta_s$$

Notice that the average current depends only on the concentration gradient in the outer diffusion layer [Ibl, 1980].

#### 2.4.3.3 Limiting Currents

Since there are two distinct diffusion layers, there also exist two distinct limiting currents in the pulse plating system [Puipe, 1986; Ibl, 1980; Landolt, 1986(2)]. The first is the limiting pulse current density. This situation arises when the cationic concentration in the pulsating diffusion layer becomes depleted. This directly reduces the metal deposition rate at the cathode. The other limiting current is the average limiting current density. This limiting current arises as a result of the depletion of cationic concentration in the





stationary diffusion layer. This indirectly influences the deposition rate by reducing the interfacial concentration of ions,  $c_e$ , and therefore reducing the cationic concentration in the pulsating diffusion layer [Puipe, 1986].

The presence of a limiting pulse current density gives rise to a maximum possible practical pulse duration. Any pulse time beyond this value would deplete the pulsating diffusion layer to the point where plating would not occur [Puipe, 1986]. This maximum pulse duration is called the transition time,  $\tau$ , and describes the situation wherein the interfacial ion concentration,  $c_e$ , drops to zero.

#### **2.4.4 Kinetic Effects**

It has been determined experimentally that the deposition rate during on-time for pulsed deposition can be increased considerably from the deposition rate in direct current plating [Puipe, 1986]. This effect has been attributed to the kinetics of the competitive reactions at the cathode surface. Pulsed electrodeposition affects the reaction kinetics in two major ways. The first is that the abrupt changes in applied current density that occur at the beginning and end of each pulse cause a change in the state of the electrical double layer. Secondly, the change in the surface concentration of the metal ion also influences the kinetics of the plating system [Cheh, 1986].

##### **2.4.4.1 Electrical Double Layer Effect**

As discussed earlier, pulsed deposition has a significant effect on the electrical double layer. The total applied current for the transient pulsed process is equal to the sum of the faradic and nonfaradic currents. The nonfaradic current is used to charge and discharge the electrical double layer while the faradic current is responsible for the deposition process and therefore controls the reaction rate. Hence, the kinetics of the reaction are controlled by the magnitude of the faradic current [Cheh, 1986]. Consider a plating process that involves more than one reaction, as is often the case. The faradic current now becomes the sum of the partial currents of each of the reactions. This results in a



time variable total faradic current since the individual partial currents will change as the individual ion concentrations change due to deposition. This in turn produces a time variable electrode potential, which in turn affects the current efficiency of the deposition process [Cheh, 1986].

#### **2.4.4.2 Surface Concentration Effect**

The deposition rate of any metal, in any plating system depends on the surface concentration of the reacting species. For a deposition process with a single reaction, the variation of surface ion concentration leads to a time-dependant overpotential for the entire deposition process [Cheh, 1986]. Unfortunately, the specifics of the mechanism involved are not discussed by Cheh.

#### **2.4.5 Alloy Pulse Plating**

Pulsed alloy deposition is simply a combination of alloy plating technology and pulse plating technology. The major advantage of pulsed deposition of alloys is the possibility of maintaining the composition of the deposit closer to that of the plating solution [Avila, 1986]. Similarly, it provides increased control over the deposition process, which is critical in alloy deposition in order to obtain the desired composition.

##### **2.4.5.1 Prediction of Pulsed Alloy Composition**

Several theoretical models have been developed to describe the effect of pulse parameters on the composition of the alloy. However, they were developed to explain a particular plating system and therefore are not applicable to other systems. Beyond this, the electrical double layer effects were not considered, and codeposition reactions were assumed to be independent. Essentially, the models serve only as successful qualitative predictors.

However, Sanchez et al, have developed an empirical model based on the silver-gold alloy plating system [Sanchez et al, 1997]. Using statistically designed experiments, a relationship between the pulse plating parameters and the chemical composition of the



alloy was derived. Their experimental work showed only one transition time that is due to the simultaneous co-deposition of the gold and silver. Since pulse plating is being studied, the final composition of the alloy will be a function of the pulse plating parameters mentioned earlier;  $j_p$ ,  $t_{on}$ , and  $t_{off}$ . Other factors such as temperature and electrode rotation rate are kept constant during the model derivation. As well,  $j_{lim,t}$  is used as the maximum value for  $j_p$  in order to avoid the electrolysis of water, and a minimum value of  $t_{on}$  was selected to reduced the double layer charging effect [Sanchez et al, 1997].

A quadratic model with centered variables of the following form is used to describe the composition of the alloy in terms of the three plating variables.

$$\begin{aligned} \text{mole percent Au} = & b_0 + b_1(j_p - j_{p,a}) + b_2(t_{off} - t_{off,a}) + b_3(t_{on} - t_{on,a}) + b_4(j_p - j_{p,a})(t_{off} - t_{off,a}) \\ & b_5(j_p - j_{p,a})(t_{on} - t_{on,a}) + b_6(t_{off} - t_{off,a})(t_{on} - t_{on,a}) + b_7(j_p - j_{p,a})^2 + \\ & b_8(t_{off} - t_{off,a})^2 + b_9(t_{on} - t_{on,a})^2 \end{aligned}$$

where  $b_i$  are the coefficients of the model, and  $x_{,a} = (x_{max} - x_{min})/2$ .

For the gold-silver alloy, the coefficients for co-deposition under diffusion controlled conditions were found to be 63.24, 1.38, -7.74, 13.44, 7.41, -0.09, 14.41, -19.38 for  $b_0$ - $b_3$  and  $b_6$ - $b_9$ . This gives an adjusted correlation coefficient of 0.98 suggesting excellent statistical fit of the model to the experimental data. For the gold-silver alloys under activation controlled co-deposition, the coefficients for the model are 41.8, 2.98, -3.85, 9.5, 1.48, -15.13 for  $b_0$ - $b_3$ ,  $b_5$ , and  $b_8$  [Sanchez et al, 1997].

Since this method involves statistical experimentation, it should be possible to apply it to other alloy systems in order to quantitatively predict the composition of the alloy.

However, if the temperature or rotation speed of the plating system is changed, then this model must be revised to include those variables.





#### **2.4.5.2 Gold Alloy Pulse Plating**

Pulsed deposition of gold alloys favors a low bulk and contact resistance deposit with high density and a relatively good ductility [Fluehmann, 1980]. Much of the original work done regarding DC gold alloy deposition is based on cyanide based plating systems. These systems generally consist of potassium gold cyanide and an organic buffer in the presence of small amounts of cobalt or nickel to act as a brightening agent. It has also been found experimentally that pulse plating gold alloys reduces the inclusion content of the deposit [Knoedler, 1986; Fluehmann, 1980].

### **2.5 Electrocrystallization**

Since the electrodeposition process is much different than any other metal production technique, it is important to understand the process of electrocrystallization and the resulting final structure of the deposit since that will determine many of the physical properties.

Generally, when a metal is deposited, it will try, if possible, to copy the structure of the substrate on to which it is being deposited. This involves epitaxy where crystal planes and directions are parallel in the deposit and the substrate. This is most often achieved when the crystal structure of the two materials is the same and the difference in lattice parameters is not great [Weil, 1984]. However, even if this is not the case, epitaxy can still occur to some small degree. The first layer of atoms on the substrate will stretch or compress in order to approximate the same interatomic spacing of the substrate. This leads to a residual stress immediately adjacent to the substrate. However, as the layer continues to grow, it will assume its own equilibrium interatomic spacing and relieve the residual stresses by introducing edge dislocations into the deposit [Weil, 1984].

The actual mechanism of epitaxial growth of an electrodeposited metal requires atoms attaching themselves onto a suitable site on the substrate. These sites are termed kink sites [Weil, 1984]. Metal atoms will either be deposited on the surface of the substrate



and then diffuse to the kink sites or they will be deposited directly on the kink site and incorporated into the growing lattice immediately. Thus pure epitaxial growth occurs by a lateral spreading of one-atom-high layers. If the substrate is almost completely covered with foreign material then epitaxial deposition is not possible [Barcelo et al, 1998; Dini, 1993]. In most plating situations, the presence of foreign substances, addition agents etc., for the most part prevent this type of lateral spreading. Instead, bunching, which are steps several atom layers high, will occur resulting in the presence of crystallites on the growth surface. Obviously, the greater the number of foreign substances, the greater the number of crystallites. As the crystallites coalesce, twins and dislocations often form. As a result, electrodeposited metal has more dislocations and twins than thermally formed metals [Weil, 1984].

These general trends are all explained in the electrocrystallization theory. Generally, electrocrystallization is more difficult to explain than physical crystallization since it must take into account the charge transfer to a more or less solvated ion, the very high electric field at the electrode-solution interface ( $>10^7 \text{ Vcm}^{-1}$ ), and the presence of adsorbed molecules and ions at the surface of the electrode [Winand, 1994]. Thus, electrocrystallization is typically described by two parameters: apparent cathodic current density and inhibition intensity. The apparent cathodic current density is used as a means of describing the cathodic overvoltage, which controls charge transfer, diffusion, reaction rates, and crystallization. The inhibition intensity is a qualitative measure of the effect of molecules in the solution that are different from the depositing ion. These inhibitors tend to adsorb on active sites, slowing the cathodic process. More importantly, however, inhibitors virtually eliminate the possibility of growth through screw dislocations. The easiest growth mechanism observed during physical crystallization is the growth of a layer through the rotational growth of a screw dislocation. However, since screw dislocation sites are typically blocked by adsorbates during electrocrystallization, the primary growth mechanisms are one and two dimensional nucleation mechanisms. Two-dimensional nucleation is the generation of a new plane at the crystal surface and corresponds to a vertical growth mechanism. One-dimensional nucleation is the generation of a new row at the crystal surface and results in a lateral growth. Thus, with



electrocrystallization, there is a competition between the vertical and lateral growth mechanisms since the activity of screw dislocations has been compromised.

The type of nucleation (one-dimensional or two-dimensional) that occurs during a deposition process depends on the amount of inhibition and the cathodic current density during the plating. Generally, at a constant level of inhibition, as the current density increases, the amount of lateral growth, or one-dimensional nucleation, decreases. The result is a deposit with a finer grain size due to the increase in nucleation events; and as the current density continues to increase, whiskers, prismatic crystals, dendrites, and powder deposits are successively obtained [Winand, 1994]. In fact, at high enough current density, the lateral growth of the layer is almost completely retarded in favor of two-dimensional nucleation or vertical growth. At constant current density, as the inhibition intensity of the system increases, the amount of lateral growth increases resulting in a denser, more coherent structure. At extremely low inhibition and current density, there is insufficient energy for either two or one-dimensional nucleation and the only way for nucleation to occur is through an active screw dislocation. Similarly, at very high inhibition and current density, three-dimensional nucleation will occur in the solution giving rise to a powder, rather than a coherent layer. These trends are illustrated schematically in Figure 16 .





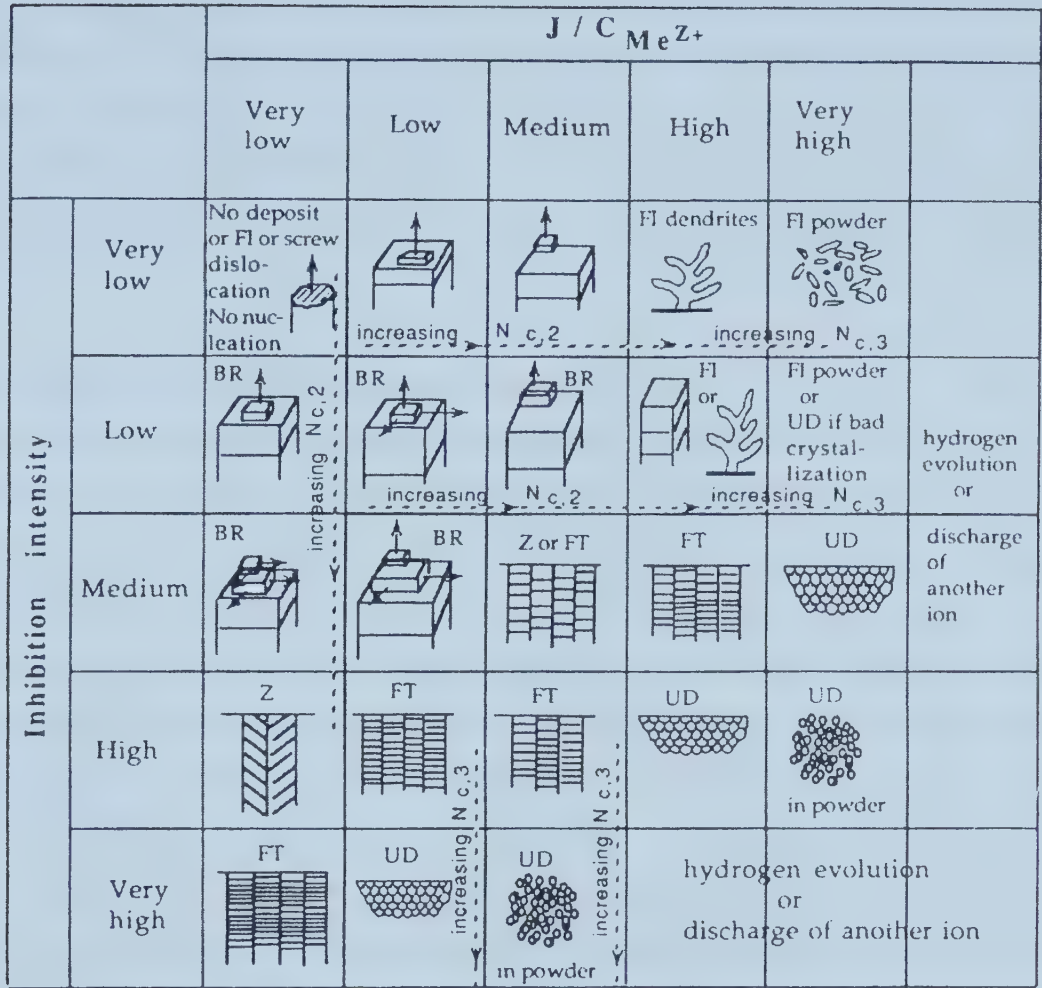


**Figure 16. Schematic diagram of different types of polycrystalline deposits as a function of current density and inhibition intensity [Winand, 1994].**

The five major types of growth illustrated in the diagram are field orientated isolated crystals (FI), basis-oriented reproduction type (BR), twinning intermediate type (Z), field orientated texture type (FT), and un-orientated dispersion type (UD). FI is usually observed at low inhibition. BR is typically observed at moderate inhibition and/or current density. The third type (Z) is considered an intermediate between BR and FT. FT is observed at strong inhibition and/or current density and is characterized by a large number of elongated crystals perpendicular to the substrate, but unlike FI, will form a





coherent deposit. The final type (UD) is obtained at very high levels of inhibition and/or current density. It typically contains a large number of small crystals, forming a coherent deposit. Unfortunately, there are no values for the axes of Figure 16. As a result, each system must be characterized separately through the use of metallographic, SEM and TEM techniques to obtain a clear understanding of the type of growth that is occurring.

### **2.5.1 Effects of Pulse Deposition on Crystal Growth**

The crystallization process, as mentioned earlier is the process of incorporating atoms into the growing lattice on the surface of the cathode. High surface diffusion rates, low adatom populations, and low overpotential (low current density) will enhance the growth of already existing crystals while low surface diffusion rates, high populations of adatoms, and high overpotentials (high current density) will favor nucleation of new crystal grains [Puipe, 1986]. In pulse plating, the maximum current density is usually higher than for DC plating, therefore there is increased tendency for nucleation. The result is a finer grain structure than would be obtained with DC plating. In practice, the only variable that is easily manipulated is the overpotential, and therefore, plating at higher current densities is often required in order to achieve grain refinement [Puipe, 1986(3)]. Copper, for instance, shows a refinement in grain size due to an increase in the pulse current density.

The effects of the other plating parameters such as on and off time are more vague. At times, an increase in off-time will result in a finer grain structure, while at other times, the increase in off-time will result in a larger grain structure [Puipe, 1986(3)]. It is suggested that the larger grain structure is a result of a grain growth process that occurs when there is no applied current or voltage. Thus, it is proposed that the finer grain structure is a result of the blocking of growth centers on the cathode as a result of an inhibiting species. This will prevent grain growth from occurring during the off-time and a finer grain structure will be retained [Puipe, 1986(3)]. The effects of on-time are even more uncertain, and no generalized trend has been developed yet. Since one of the defining factors regarding electrocrystallization (nucleation or growth) is the population



of adatoms at the surface of the deposit, it has been suggested by Puiippe that the number of coulombs per pulse is also an important factor in determining the grain size.

## **2.6 Gold-Tin Solder Deposition**

Because the quality of the solder joint produced with solder preforms is often insufficient, it was desirable to find a new method of producing the Au/Sn eutectic solder. This resulted in the development of thin film techniques for solder deposition. Such techniques offer reduced oxide content, improved thickness uniformity, and improved solder alignment, through the use of masking techniques as compared with the preforms. The solder can be deposited either sequentially or co-deposited.

### **2.6.1 Sequential Deposition**

The traditional high-vacuum based techniques such as evaporation and sputtering have been used to sequentially deposit Au/Sn alloys with great success. Sequential evaporation and sputtering have been used successfully in the past to produce a eutectic solder layer [Katz et al, 94].

The technique entails depositing a layer of pure gold on top of a layer of pure Sn. Then, a reflow is typically used to allow the Au and Sn to diffuse together to form the eutectic phase that is used as a solder. However, because of the fast diffusion characteristics, a complete reflow is not always necessary. One of the major disadvantages of sequential deposition is oxidation. Although the gold layer will not oxidize, the tin layer will oxidize during deposition and during the reflow and diffusion steps. This oxide layer will ultimately disrupt the bonding ability of the solder resulting in failed or poor quality bonding surfaces. Also detrimental to bonding is the inhomogeneous solder layer that results from this technique. During reflow, the tin is first to melt, and then the gold will slowly dissolve into the molten tin layer. During this time, however, the Sn and Au will also form ternary intermetallic compounds with the diffusion barrier materials (either Pt or Ni), which will continue to coarsen during the reflow period due to intergranular diffusion of the Sn and Au [Lee et al, 1992]. This results in a local depletion of Sn in the Sn/Au interface. As seen in the gold/tin phase diagram (Figure 1), any deviation from the



eutectic composition results in a significant increase in the freezing temperature resulting in local freezing of the solder layer. As a result, when the solder layer finally freezes, there is significant inhomogeneity in terms of both composition and morphology ultimately degrading the ability of the solder to bond properly.

As an alternative to the traditional high vacuum based deposition procedures for sequential deposition, electrodeposition offers all the advantages of evaporation techniques in terms of layer uniformity, reduced oxide content, and solder alignment, but with a significantly reduced capital cost for the equipment as there is no need for a high vacuum.

### **2.6.2 Co-deposition**

Because of the many problems associated with sequential deposition, it is more desirable to co-deposit the solder. The major advantage of co-deposition is the elimination of a post-deposition reflow, which will help reduce the oxidation of the tin and void formation. Co-evaporation of the solder has been done successfully by Ivey in 1998 using a combination of e-beam evaporation for the Au and thermal evaporation for the Sn. One of the problems with this technique is that additional Sn had to be deposited in order to compensate for the Sn that is lost during the evaporation process. As a result, the films produced were typically off-eutectic in composition. In addition, temperatures during the deposition process often exceeded 200°C which resulted in lift-off problems and photoresist sagging. In order to combat the heating issue, the deposition was done with intermittent cooling. This resulted in the oxidation of the tin at the surface of the solder layer and ultimately an inhomogeneous layer composition. The solder layer was bonded successfully, but it is desirable to develop a method of co-deposition that is faster with fewer oxidation and photoresist issues.

#### **2.6.2.1 Co-electrodeposition**

As an alternative to co-evaporation, co-electrodeposition has been proved possible for the Au/Sn solder. Two major plating baths that have been developed recently for depositing





the gold-tin eutectic alloy; one is based on a cyanide stabilizing system, and one is based on a chloride stabilizing system.

### 2.6.2.2 Cyanide System

A cyanide based plating bath was developed by Holmbrom et al in order to deposit the eutectic gold-tin alloy. Table 4 describes the chemical make-up of the solution, and Table 5 describes the operating conditions used in the deposition process including the optimum conditions found for this particular bath [Holmbrom et al, 1998]. In this work, DC plating was used to deposit the alloy rather than pulsed deposition.

**Table 4. Electrolyte composition for gold-tin deposition [Holmbrom et al, 1998].**

<i>Bath Constituent</i>	<i>Concentration Range (g/L)</i>	<i>Optimal Concentration (g/L)</i>
$\text{Au}(\text{CN})^-$	0.5-15	2
$\text{SnO}_3^-$	5-30	20
$\text{PO}_4^{3-}$	20-50	40
$\text{CO}_3^{2-}$	10-30	20
$\text{CN}^-$	20-50	40
Proprietary additive	20-100 ppm	60 ppm
pH	10-11	10.5

**Table 5. Operating conditions for Au-Sn alloy plating chemistry [Holmbrom et al, 1998].**

	<i>Range</i>	<i>Optimal</i>
<i>Temperature</i>	40-50°C	45°C
<i>Current Density</i>	5-15 mA/cm <sup>2</sup>	8 mA/cm <sup>2</sup>
<i>Agitation</i>	5-10 cm/s	7.5 cm/s
<i>Current Efficiency</i>	40-70%	55%
<i>Plating rate</i>	6-11 µm/hr	9 µm/hr



In addition to selecting the optimal conditions for deposition, the effects of the various operating parameters, such as temperature, current density, and agitation, on the composition of the alloy were also studied. An increase in the concentration of the gold ions results in a decrease in the concentration of the Sn in the film. An increase in Sn content in the alloy accompanies a decrease in solution agitation, and an increase in the temperature of the plating bath results in a reduction of the Sn content of the alloy [Holmbrom et al, 1998].

These effects are explained by some simple electrochemistry. The gold ions are the more noble of the two ions in the solution, and therefore tend to deposit preferentially. Indeed, in order for the Sn to begin plating, the diffusion limiting current of the gold must first be exceeded. Since alloy deposition must occur with the Au at its diffusion limiting current, only the Sn partial current will be affected by any changes in the applied current. Au deposition will therefore be favored when its diffusion limiting current is increased by an increase in solution temperature or solution agitation [Holmbrom et al 1998]. In addition, increasing the concentration of gold ions in the solution will obviously result in more gold reduction at the cathode accounting for the decrease in Sn content of the plated alloy.

This plating bath has produced films at the eutectic composition consisting of the two eutectic phases,  $\text{Au}_5\text{Sn}$  and  $\text{AuSn}$ . In addition, it can have a relatively high deposition current, up to  $15 \text{ mA/cm}^2$ , giving it the advantage of a relatively fast deposition rate. The major disadvantage of this plating system is the use of cyanide as a gold stabilizing agent. Because it carries so many environmental concerns with it in terms of waste disposal, it is unlikely that this system could be commercialized on a large scale. In addition, the  $\text{CN}^-$  based plating solutions, because of their alkaline nature, are often incompatible with photoresists causing them to lift off the wafer allowing deposition to occur underneath the resist.



### 2.6.2.3 Chloride System

As an alternative to the cyanide stabilized system, Sun and Ivey developed a chloride based plating bath for co-depositing the eutectic gold-tin alloy. The composition of the most stable plating bath is listed in Table 6.

**Table 6. Chemical composition of chloride based plating bath [Sun and Ivey, 1999].**

<i>Chemical</i>	<i>Concentration (g/L)</i>
ammonium citrate	200
KAuCl <sub>4</sub>	5
Na <sub>2</sub> SO <sub>3</sub>	60
l-ascorbic acid	15
SnCl <sub>2</sub> ·2H <sub>2</sub> O	5

The advantage of this bath is that unlike the cyanide based system, the chloride based system is thought to be compatible with photoresists that are used in patterning the semiconductor wafers because of its neutral pH. Thus, there will not be any problems with resist lifting and deposition occurring under the resist layer.

Polarization tests were used to determine the effects of the bath additives on cathodic polarization. The ammonium citrate, primarily added to prevent the hydrolysis of the gold and to act as a solution buffer, had little effect on cathode polarization with respect to the deposition of both the gold and tin. However, the sodium sulphite, added to stabilize the gold, results in a dramatic shift of the cathode potential to more negative values for the gold, essentially reducing the ease of gold plating. However, the addition of the sulphite results in a higher cathodic potential for the Sn as well as increasing its limiting current density, thereby increasing the ease with which the Sn can be deposited [Sun and Ivey, 1999]. Thus, the sulfite ion acts to retard the deposition of the Au while improving the deposition of the Sn, allowing both metals to deposit simultaneously. As mentioned in the theory of alloy plating, it is desirable to select bath additives that will





increase the plating potential of the less noble metal relative to the more noble metal thus enabling a more equal deposition process.

The plating operating parameters were also optimized in this study. An on-time of 2ms and an off-time of 8ms was found to give the densest structure with the finest grain size and smoothest deposit. In addition, it was found that any off-time greater than 4ms was sufficient to reverse any ion depletion effects near the cathode surface. Figure 17 shows the effects of the average current density on the concentration of Sn in the subsequent alloy deposit using a 2ms on-time and 8ms off-time. Note that the concentration of Sn in the alloy is higher with pulsed current than with direct current. The shape of the curve can be explained quite easily. Brenner has already explained the initial increase in Sn content that occurs as a result of the increase in current density. Any increase in the current density of the plating system will cause the cathode potential to become more negative (or less noble) and thus more closely resemble the deposition conditions favorable to the less noble metal. This will therefore increase the proportion of the less noble metal in the alloy. The decrease in Sn content that occurs at the higher current densities is a result of the competing hydrogen evolution reaction [Sun and Ivey, 1999].

The pulsed deposition process typically yields a finer grain structure than the DC plating process as predicted by the theory. Figure 18 clearly shows the trend in refining the grain structure from the DC plating [Sun and Ivey, 1999]. Also apparent is a coarser microstructure at the higher current densities. There is no sufficient explanation given for the coarser microstructure as a result of increasing the PC current density. According to the theory of pulse plating, an increase in current density should result in a finer grain structure. However, as indicated earlier, a larger off-time may provide sufficient time and energy for recrystallization to occur. Unfortunately, in this instance, the on-time and off-time are kept constant. What is more likely is that the features in the plan-views do not represent the true grain size.





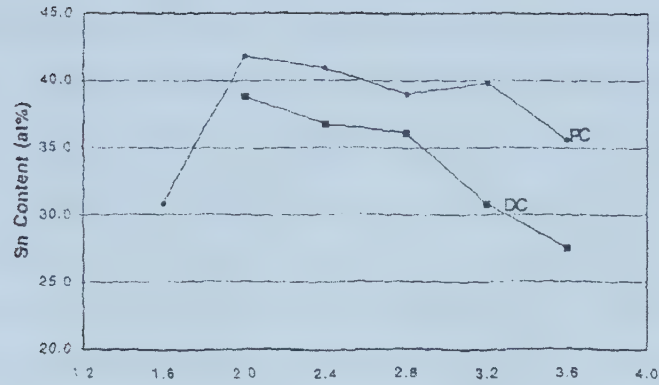


Figure 17. Effect of current density on the alloy composition [Sun and Ivey, 1999].

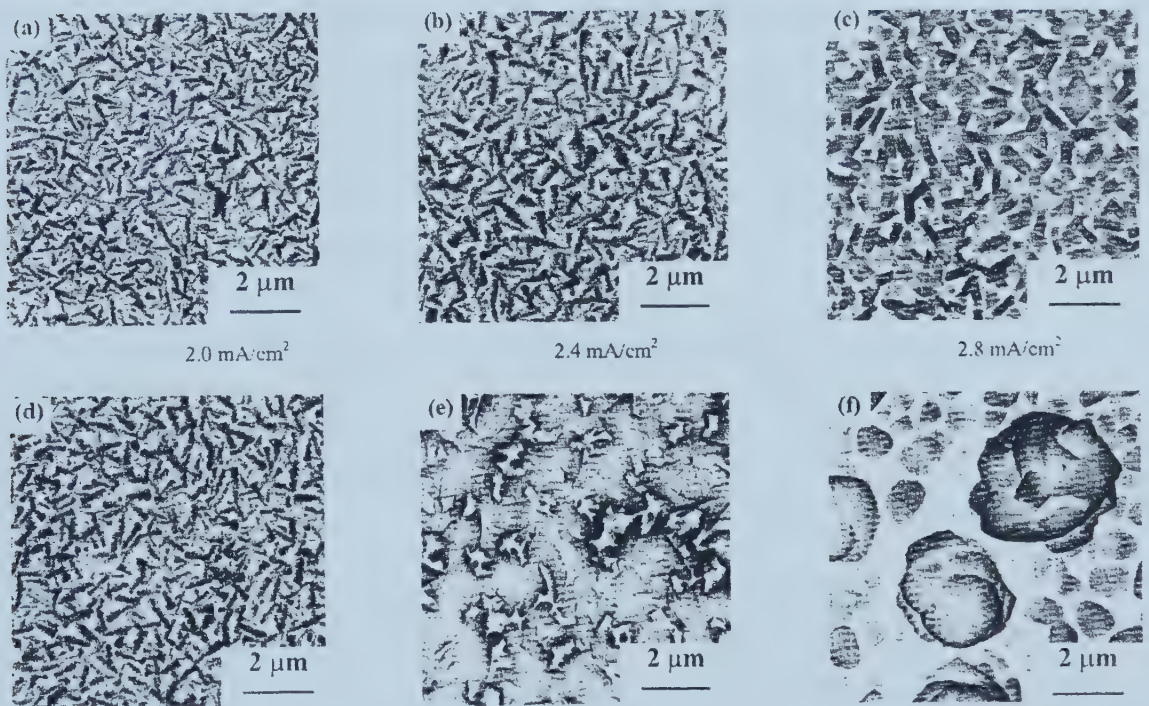


Figure 18. Micrographs showing the effects of current density on the grain size of the deposits. a), b) and c) are pulsed current deposits; d), e), and f) are direct current deposits [Sun and Ivey, 1999].



Subsequent work on this particular plating system was carried out by Doesburg and Ivey in 2000. Ethylenediamine (EDA) was added to the existing plating solution given in Table 6 to improve the overall stability of the solution. It was found that the addition of EDA in a 0.01M concentration was optimal for increasing the stability of the solution (from 16 to 18 days) and the deposition rate. As an undesirable side effect, the roughness of the deposit was greatly increased compared to deposits made from solutions containing no EDA. Deposits produced between current densities of 1.2 and 3.2 mA/cm<sup>2</sup> had a columnar, field oriented texture structure (large numbers of grains elongated perpendicular to the cathode surface), which then changed to an unoriented dispersion structure (large number of fine crystals).

The addition of EDA to the solution also adjusted the composition of the deposited alloy. While Sun and Ivey located a plateau at 37 at%Sn, Doesburg and Ivey found that the plateau was consistent at 50at%Sn corresponding to the deposition of the AuSn phase (Figure 19). What is left to accomplish with the Sun and Ivey plating solution is to consistently produce the eutectic composition. Neither Sun nor Doesburg consistently produced the eutectic composition.

The advantage of co-deposition over co-evaporation is that there is no high vacuum requirement resulting in significantly reduced capital costs. In addition, there should be limited interference with the photoresist.



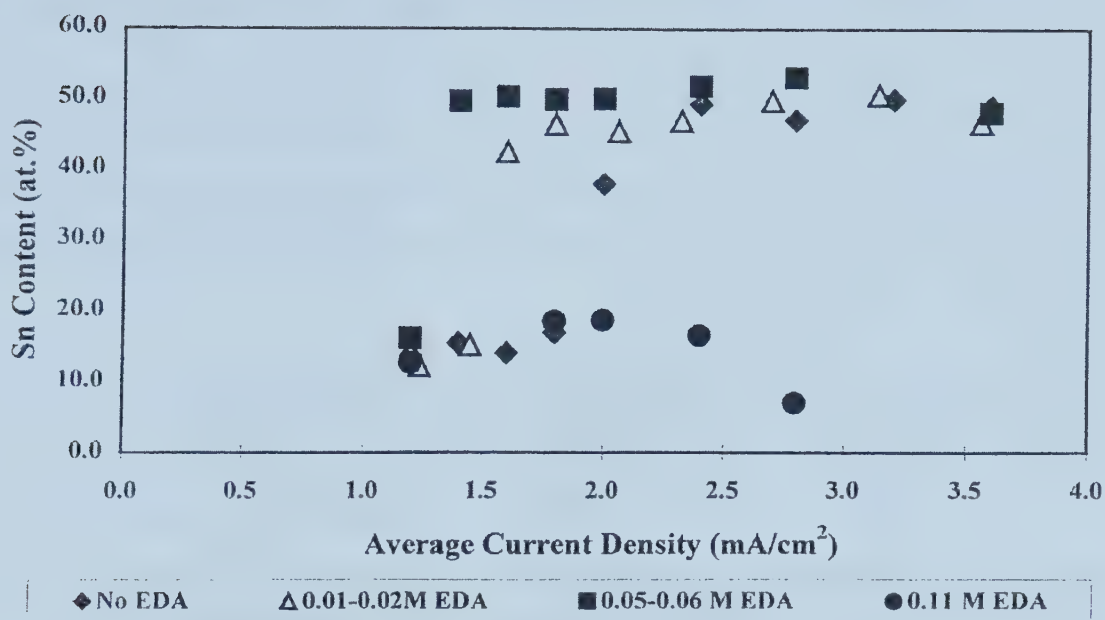


**Figure 19. Deposit composition for solutions containing 5g/L KAuCl<sub>4</sub> and 5g/L SnCl<sub>2</sub>·2H<sub>2</sub>O with various ethylenediamine concentrations [Doesburg and Ivey, 2000].**





### 3 Experimental Methods

#### 3.1 Solution Preparation

The composition of the solution that was used to deposit the Au/Sn alloy films is listed in Table 7. De-ionized water was used as the solvent.

**Table 7 Composition of plating solution for Au/Sn Alloy plating**

<i>Chemical</i>	<i>Molecular Weight</i>	<i>Concentration (g/L)</i>
(tri)-ammonium citrate	243.22	200
KAuCl <sub>4</sub>	377.88	5
sodium sulfite	126.04	60
l-ascorbic acid	176.12	15
SnCl <sub>2</sub> ·2H <sub>2</sub> O	225.63	5

The following procedure was used to produce a 30 mL quantity of the plating solution useful for 6-8 deposits of 2-3 micron thickness. The pH of the solution is around 5-6.

1. 6 grams of ammonium citrate was added to a clean, dry beaker.
2. Approximately 23 mL of de-ionized water was then added to the beaker and mixed until the ammonium citrate was completely dissolved. The solution was colorless.
3. 0.15 grams of the KAuCl<sub>4</sub> was added to the ammonium citrate and de-ionized water solution. It was mixed until the gold salt had completely dissolved into solution. The solution was a deep golden yellow, but not cloudy.
4. 1.8 grams of sodium sulfite was added to the solution and mixed until it completely dissolved. The solution rested for approximately 15 minutes until it had lightened to a pale yellow. The solution was not cloudy.
5. 0.45 grams of l-ascorbic acid was added to the solution and mixed until it completely dissolved.
6. 0.15 grams of SnCl<sub>2</sub>·2H<sub>2</sub>O was then added to the solution and mixed until it was completely dissolved as well.
7. When required, sufficient de-ionized water was added to produce 30 mL of solution.



6. 0.15 grams of  $\text{SnCl}_2 \cdot 2\text{H}_2\text{O}$  was then added to the solution and mixed until it was completely dissolved as well.
7. When required, sufficient de-ionized water was added to produce 30 mL of solution.

## 3.2 Plating Experiments

### 3.2.1 Wafer Preparation

The deposition substrate was pieces of metallized Si or InP wafer with 25 nm of sputtered Ti adhesion layer followed by 250 nm of either sputtered gold or platinum. The purpose of the gold or platinum was to act as a seed layer for deposition by providing the necessary conducting surface. Stop-off lacquer was applied to the back and front surfaces of the wafer to prevent deposition. On the front side of the wafer, however, two areas of the seed layer were left exposed. The first was at the top of the wafer and served as the contact area for electrically connecting the sample to the power supply. The second area left exposed was of a known area and was used as the deposition surface. Figure 20 is a schematic representation of the front surface of the prepared metallized wafer. Generally the plating area was not in excess of  $1\text{cm}^2$ .

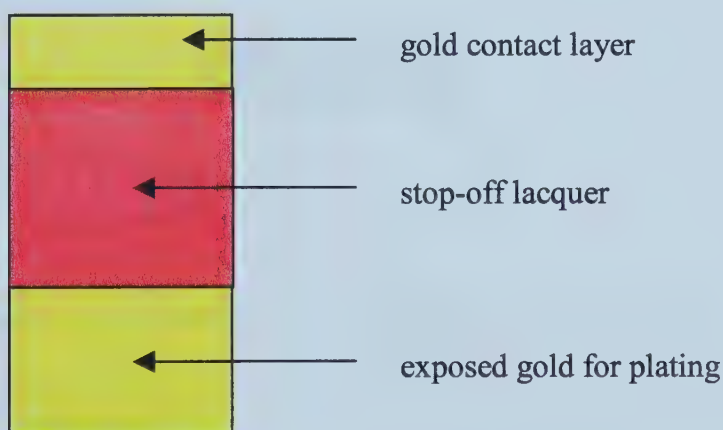


**Figure 20. Schematic of plating wafer preparation.**



### 3.2.2 Plating Power Supply

A Dynatronix DuPR 10-0.1-0.3 pulse plating power supply was used for all the depositions. It has a maximum current rating of 100mA average current and 300mA peak current. Based on previous work [Sun and Ivey, 1999; Doesburg and Ivey, 2000] a forward direction time of 10ms was selected with a forward on-time of 2ms and a forward off-time of 8ms. No reverse pulse was employed. This resulted in a 20% forward duty cycle for plating. Typical deposition currents for this particular solution were between 5 and 10mA of peak current based on the area used. Plating times were usually between 1.5 to 2 hours to ensure a sufficiently thick deposit ( $>1.5\ \mu\text{m}$ ) for composition analysis. Figure 21 is a schematic of the experimental set-up. The oscilloscope, in conjunction with a  $50\Omega$  resistor, was used to set and monitor the peak current applied to the wafer in order to increase the accuracy of the applied current density. The metallized wafer was the cathode, and a piece of platinum foil acted as the anode.

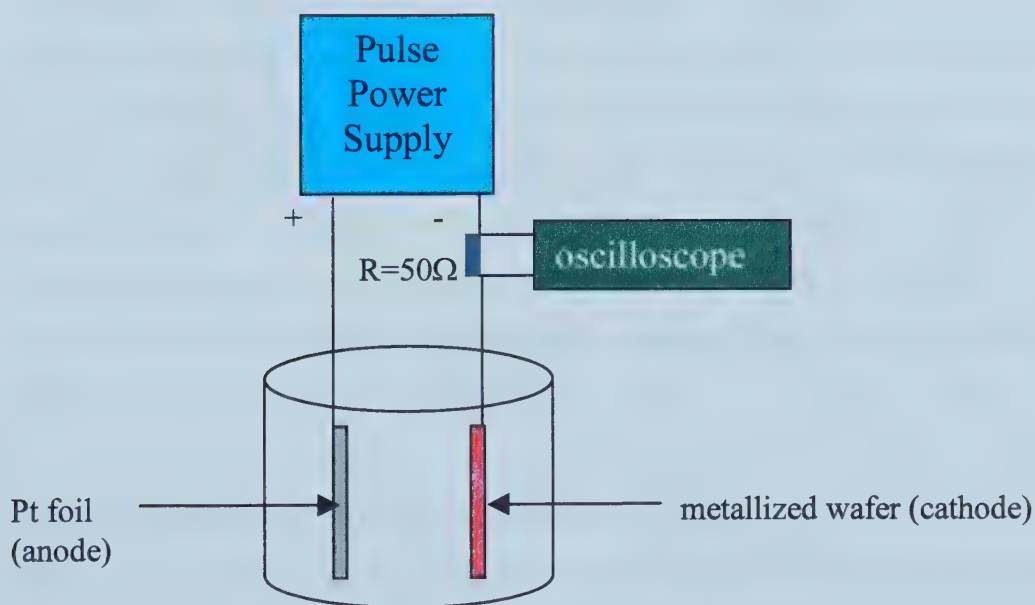


**Figure 21. Schematic diagram of experimental plating set-up.**

At the cathode, two simultaneous reductions of the gold and tin complexes to their corresponding metals is occurring. At the anode, there is either the oxidation of the tin



complex from a  $2^+$  to  $4^+$  valence state, or the oxidation of water. Most likely, a competition between the two oxidation reduction reactions is occurring.

### 3.2.3 Multi-Layer Plating

For multi-layer plating, two specific current densities were selected for deposition. The rationale for this is presented in the Results and Discussion section. The two current densities were then cycled to produce the separate phase layers; thickness and composition control were achieved by adjusting the plating time used for each phase.

### 3.2.4 Solution Stability

Previous stability tests were based on observation of the solution in a closed container and the stability time was based on a visual change in the solution [Sun and Ivey, 1999; Doesburg and Ivey, 2000]. This type of testing, however, is not accurate as the destabilization process may not be instantaneous, but may occur in several stages some of which may not produce a visual change in the bath, but compromise its performance nevertheless. A series of baths were made and aged to the appropriate number of hours (from 0 to 72 hours) and then used to deposit a single film. One deposition was made every 24 hours in order to mark the effects of time on the composition of the deposited film. It is reasonable to assume that any change that affects the bath chemistry will manifest itself in a change in the composition of the deposited alloy layer. All depositions for the stability testing were done at  $3 \text{ mA/cm}^2$  for 90 minutes. A single deposition was made from each aged bath in order to eliminate the possibility of any effects that may arise from ion depletion.

## 3.3 Scanning Electron Microscopy (SEM)

Initial imaging of all the solder layers was done using a Hitachi H2700 scanning electron microscope (SEM) with a Link eXL ultra-thin window (UTW) energy dispersive x-ray (EDX) analysis system, using a thermionic emission tungsten (W) filament. Images were typically taken at 20kV. Additional images (mostly cross-sectional) were taken using a JEOL-JSM 6302 FXV field emission SEM. An accelerating voltage of 5kV was used.





Compositional analysis of the solder layers was done in the Hitachi H2700 SEM at 20kV at a working distance of 17cm with a count rate of 3500 counts/second. Pure gold and tin standards were applied in order to obtain accurate quantitative results to within 2at%.

No sample preparation was required for imaging in the SEM. Wafers were simply cleaved to the appropriate size, and placed flat on a pin mount to ensure the surface was perpendicular to the incident electron beam for the compositional analysis.

### **3.4 Transmission Electron Microscopy (TEM)**

Imaging was also done using a JEOL EM 2010 transmission electron microscope (TEM) with a Noran UTW Ge-x-ray detector EDX system for compositional analysis. Cross-section and plan view samples were analyzed using a 200kV electron beam. Crystal structure analysis was done using electron diffraction patterns.

TEM sample preparation consisted of the traditional grinding, dimpling, and ion milling technique for Si and InP based materials. A plan view sample was made by grinding from the backside of the wafer to a 250  $\mu\text{m}$  thickness. The sample was dimpled, again on the backside, until a small hole appeared in the center. The plan view sample was then mounted deposit side down onto a copper ring to provide reinforcement. The sample was sputtered in a Gatan model 600 Dual Ion Mill using argon as the source gas. The sample was sputtered on one side only at a gun angle of  $15^\circ$  for 15 minutes using a gun current of 0.5mA and 4kV energy. The gun angle was then lowered to  $13^\circ$  and the sample was sputtered for another 10 minutes at a current of 0.3mA and energy of 3kV.

Cross-section samples were made using the following procedure. Two pieces of equal size were first cleaved from the sample. The two pieces, with deposit surfaces facing each other, were glued together. Scrap Si pieces were used as supports on either side of the glued samples to build a raft structure. The raft was then ground on the flat surface, with the wafer pieces on edge, to a thickness of 200  $\mu\text{m}$  after which a 3 mm disk was



machined from the raft with the sample interface centered in the disk. The disk was dimpled on both sides until optical transparency was reached ( $\sim 30\ \mu\text{m}$ ) at the centre. The sample was sputtered from both sides at a gun angle of  $15^\circ$  with a current of 0.5mA per gun at 4kV until perforation. At this time, the gun angle was lowered to  $13^\circ$ , the current to 0.3mA per gun, and the energy to 3kV. Sputtering was continued for 40 minutes, or until a smooth edge at the hole was formed. For the cross-section sample, the hole must cross the sample interface to allow imaging of the deposit. All sputtering was done on the cold stage where the samples were cooled to liquid nitrogen temperatures prior to sputtering. This was done so that all materials would sputter at a similar rate.

### **3.5 X-Ray Diffraction Analysis**

X-Ray diffraction (XRD) phase analysis was done using a Rigaku Rotaflex rotating anode diffractometer with a thin film camera attachment. The filament voltage and current were set at 40kV and 110mA respectively. The sample was scanned between  $10^\circ$  and  $90^\circ$  at a rate of  $1^\circ/\text{min}$  using an x-ray incidence angle of  $3^\circ$  to ensure no substrate was sampled. A blank wafer (prior to deposition) was run for background signal comparison and elimination. In some cases Ti/Pt metallized wafers instead of Ti/Au metallized wafers were used for deposition so that it could be determined whether or not metallic gold was being plated in addition to the gold/tin compounds.



## 4 Results and Discussion

### 4.1 Bath Stability

Work by Doesburg and Ivey revealed that the addition of EDA (ethylenediamine) to the plating solution improved the stability of the bath from roughly 16 days with no EDA added to 22 days with the addition of 0.05-0.06 M EDA. However, these solution stability experiments were based on a visual change in the solution, either a color change or the presence of a precipitate. What was not examined was the possibility of a non-visual change within the solution that would signal the start of bath de-stabilization. Continued testing of the solution indicated that the actual solution stability was significantly less than 16 days, indicating a non-visual change is occurring within the solution that ultimately compromises its performance. It was found that after 3 or more days, deposits produced at identical conditions contained significantly less tin [Private communication, 2000]. At identical deposition conditions, the composition of the layer should have remained constant unless there was a change in the chemical make-up of the solution. The change in composition with time indicates that the bath was de-stabilizing despite there being no visual cues to this effect. In addition, it means that the practical life of the solution was reduced to less than three days. Because the EDA does not noticeably improve bath stability, it was determined to be an unnecessary addition and was therefore not used in the subsequent work.

Because the lifetime of the solution with EDA was found to be much shorter than previously anticipated, it was also likely that the stability of the bath without EDA would also be substantially less than the previously reported 16 days. Using plating reproducibility over time as a method of determining a non-visual bath change, the practical stability of the solution with no added EDA was found to be < 48 hours as opposed to the 16 days reported previously (Figure 22). If there were no chemical changes occurring within the solution, then the composition of the alloy film should have remained constant at 50at%Sn since all of the plating parameters were constant. The decrease in the Sn composition of the film at 48 hours indicated that some changes had occurred within the bath, although they were not accompanied by any visual change in





the solution. Unfortunately, the result was that the solution with no EDA was only suitable for use for 24 hours instead of the previously cited 16 days. This is a significant obstacle for any potential commercial application of the solution.

The plan view SEM images of the deposits produced from the aging baths (Figure 23) also appeared to support the trend seen in Figure 22. As the bath aged, the composition of the deposited layer changed, and the surface of the deposit became rougher. The deposits produced at 0 and 24 hours revealed a similar, fairly smooth surface. However, at 48 and 72 hours, when the bath began to first exhibit de-stabilization according to Figure 22, the surface became much rougher, and the deposit was no longer as dense and coherent. Instead, it exhibited a fairly porous structure with a large number of voids. At 96 hours, although the film was not as porous, it appeared to have degenerated into a poor quality film. It is possible that these trends in the film structure are related to the slow decomposition of the bath although the effect is clearly not linear.



**Figure 22. Graph of film composition vs. time for deposition at 3 mA/cm<sup>2</sup> for 90 minutes.**



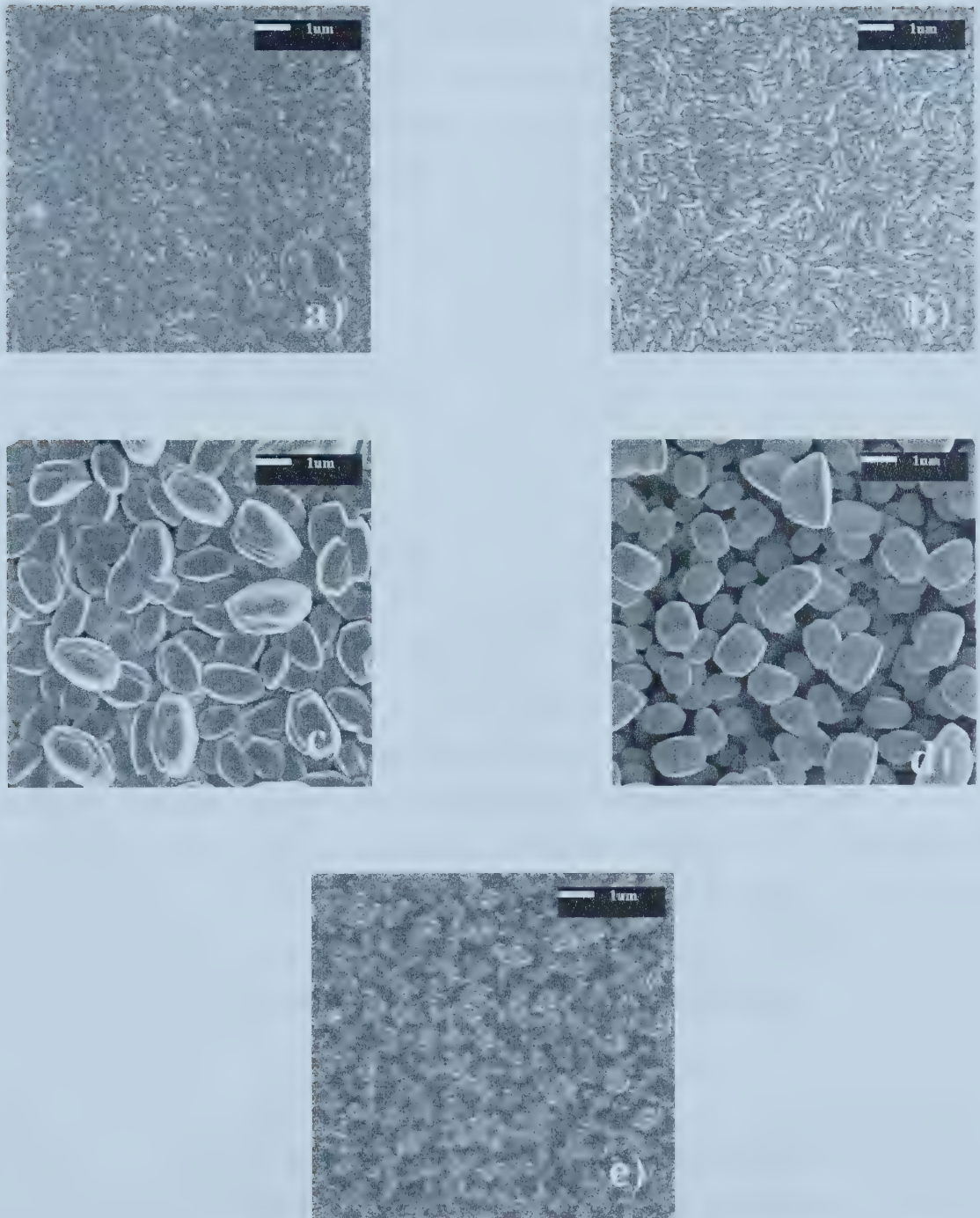
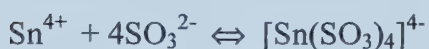


**Figure 23.** SEM secondary electron plan view images of solder layer at a) 0 hours; b) 24 hours; c) 48 hours; d) 72 hours; e) 96 hours.



The change that most likely occurred at 24 hours and accounted for the change in composition with time was the de-complexation of the tin. Even though the tin was added to the solution in the form of a chloride ion, it has been suggested that the sulfite will act as a complexing agent for the tin as well as the gold [Sun and Ivey, 1999]. The following reactions give the possible tin complexes that would form in the presence of the sulfite ion according to the specific coordination of the  $\text{Sn}^{2+}$  and  $\text{Sn}^{4+}$  ions [Perrin, 1964].



The decrease in the amount of tin in the deposit with time suggests that the tin is becoming more difficult to reduce from the solution. Previous work [Sun and Ivey, 1999] indicated that the addition of sulfite to the solution made the Sn easier to reduce. Thus, retardation in the deposition of the Sn suggests that the nature of the Sn complex has changed such that it has impaired the tin's ability to be reduced. Although this mechanism has not been verified, it is the most likely cause since a complete decomposition of the bath was not observed. The lack of visual evidence indicates that only a subtle chemical change has occurred affecting only the tin. Thus, the solution can only be used for 24 hours in order to ensure that the beginning of bath de-stabilization does not adversely affect the composition of the deposited alloy layer.

## 4.2 Current Density/Composition Relationship

Because the composition of the deposited film in alloy electrodeposition is heavily dependent on the current density that is used for deposition, it is necessary to completely define this relationship. In addition, it is important to have a firm grasp on the types of alloys that can be produced using this method: solid solutions with impurity levels of Sn, or actual alloy compounds with significant Sn content.





Previous work on this solution has failed to produce either consistent or complete results further emphasizing the need to establish the dependence. For instance, the results obtained by Sun and Ivey in 1999 are not consistent with the results obtained by Doesburg and Ivey in 2000. Doesburg and Ivey reported a plateau occurring at 50at%Sn (Figure 19), while Sun and Ivey reported a completely different curve with a plateau occurring at approximately 40at%Sn (Figure 17) for the solution without EDA. In addition, the results from Doesburg and Ivey do not completely identify the effects of the lower current densities on the composition of the deposited film.

In order to complete the curve, a range of current densities was sampled in order to determine the effect of current density on the composition of the alloy (Figure 24).

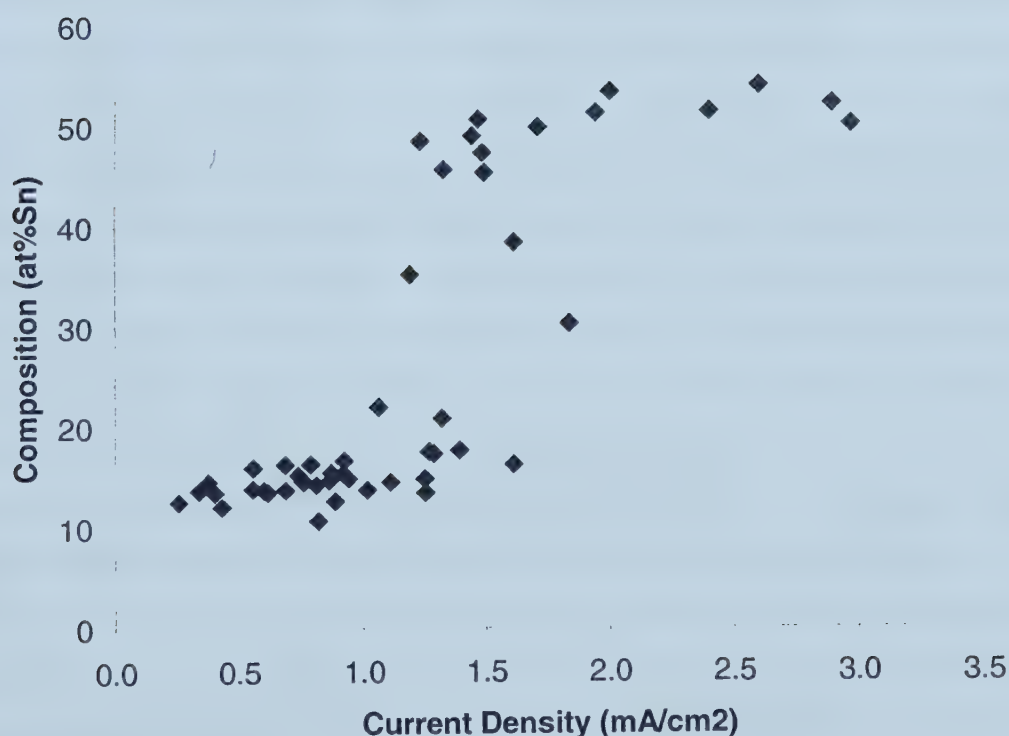


**Figure 24. Graph of current density vs. film composition.**





The results at higher current density agree with the results obtained by Doesburg and Ivey where a plateau at 50at%Sn was found for the current density range from 2.5 to 3.5 mA/cm<sup>2</sup>. Building on this work, the compositional plateau at 50 at% Sn has been extended back from 2.5 to ~2 mA/cm<sup>2</sup>. A lower compositional plateau was also established at an average Sn composition of 15 at% Sn extending up to ~1mA/cm<sup>2</sup>. Between 1mA/cm<sup>2</sup> and 2mA/cm<sup>2</sup> there is a transition region where the composition of the film is not dependent on the current density. The error bars for the measurement are roughly the size of the individual points on the graph.

The type of curve seen in Figure 24 is typical of a normal deposition process as defined by Brenner. Normal deposition refers to the process where the more noble metal, in this case gold, tends to deposit preferentially. This can be seen clearly from the higher gold content relative to the tin at lower current densities indicating that gold is depositing preferentially. As the current density increases, the amount of the less noble metal, tin, increases in the deposit. This type of behavior is typical of the regular co-deposition process, which is a sub-set of normal deposition. Regular co-deposition is controlled by diffusion phenomena. As a result, at any current density, the more noble metal will be closer to its limiting current density than the less noble metal. Therefore, increasing the current density causes a larger increase in the plating rate of the less noble metal (tin) as compared with the more noble metal (gold), resulting in a greater concentration of the less noble metal in the deposited alloy. This trend describes exactly the behavior seen in Figure 24. The advantage is that now knowing that the deposition process is controlled by diffusion, the effects of other variables can be extrapolated. For instance, anything that increases the amount of tin in the diffusion layer will increase the amount of tin in the final deposit. Thus, increasing the total metal content of the bath, increasing the bath temperature, and increasing the agitation of the bath system should all increase the concentration of the more noble metal ion (Au) in the diffusion layer, and thereby increase the percentage of the more noble metal in the deposit.

The results indicate that alloys containing 15 or 50 at%Sn can be easily produced. However, outside of these limits, it is not possible to obtain a suitable deposit with this



solution. At current densities much higher than  $3 \text{ mA/cm}^2$ , the competing hydrogen reduction reaction will prevent the deposition of a coherent layer. At current densities much lower than  $0.26 \text{ mA/cm}^2$ , there is insufficient energy available to overcome the threshold energy required for reduction at the cathode. In addition, in the transition region between 1 and  $2 \text{ mA/cm}^2$ , there is no visible relationship between the current density and the film composition, which would allow for reproducible deposition in that range. Thus, the composition of the deposited films seems to be limited to two compositions: 15 and 50 at%Sn.

### 4.3 X-Ray Diffraction Analysis

Since two plateaus exist, it is realistic to assume that within each plateau, a single phase is being deposited accounting for the constant Sn composition. XRD analysis was performed on several samples in order to identify the phases present and also to validate the EDX analysis. The deposition was carried out on Pt seeded wafers in order to eliminate any confusion with regard to possible metallic gold deposition. According to the phase diagram (Figure 1), the most likely phase to be produced at 50 at%Sn is the AuSn,  $\delta$ , phase. Similarly, the most likely phase to be produced at 15 at%Sn is the  $\text{Au}_5\text{Sn}$  phase. Any deposit with an intermediate composition should be a two-phase structure according to the phase diagram. The results of the XRD work are summarized in Figure 25. Note that the upper and lower plateaus are indeed single-phase regions of AuSn and  $\text{Au}_5\text{Sn}$  respectively. In the transition region, where the composition is intermediate between 15 and 50 at%Sn, the structure is two-phase with both AuSn and  $\text{Au}_5\text{Sn}$  present. Figure 26 gives an example spectrum for each region illustrated in Figure 25.

Unfortunately, XRD analysis could not distinguish between the ordered and disordered forms of  $\text{Au}_5\text{Sn}$ . As seen in Figure 26a, the distinguishing lines between the ordered and disordered phase are not present. Thus, the only conclusion that can be drawn from the XRD analysis is that  $\text{Au}_5\text{Sn}$  is being deposited, although the form cannot be specified.



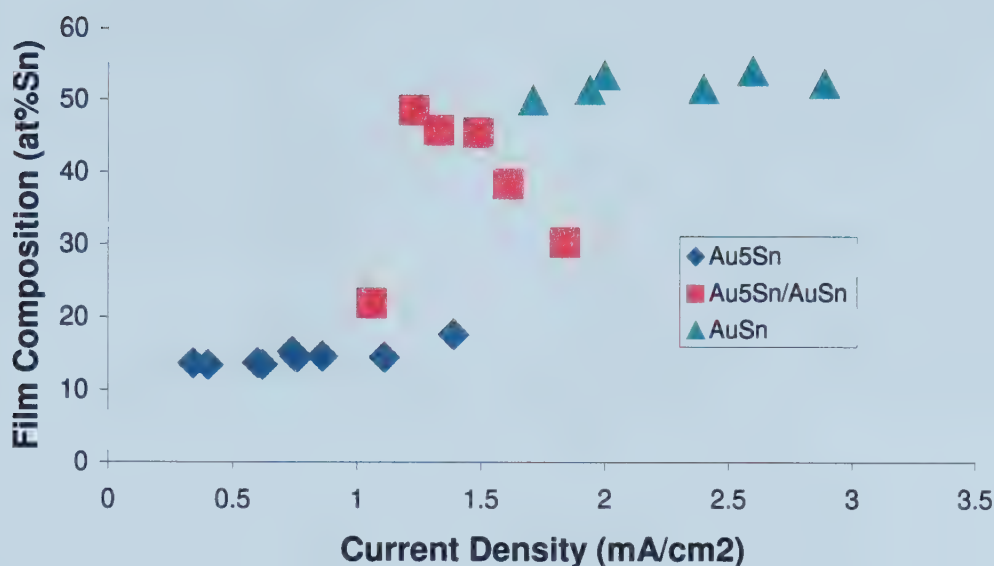


**Figure 25. Plot of current density vs. film composition showing phase analysis.**

Recalling the curve shown in Figure 24, there is a significant amount of scatter in the lower plateau. Since the disordered Au<sub>5</sub>Sn phase has a larger homogeneity range than the ordered intermetallic (a line compound), it is suspected that the disordered phase is being deposited as opposed to the ordered compound accounting for the scatter in the data. In addition, in electrodeposition it is not uncommon for a non-equilibrium phase to be deposited, further supporting the supposition that the disordered phase is being deposited.

The phase analysis serves to further define the limits of each plateau area. It can be seen very clearly from Figure 25 that the minimum current density required for the deposition of the AuSn phase only is 2mA/cm<sup>2</sup>. The maximum current density for deposition of Au<sub>5</sub>Sn only is 1mA/cm<sup>2</sup>.





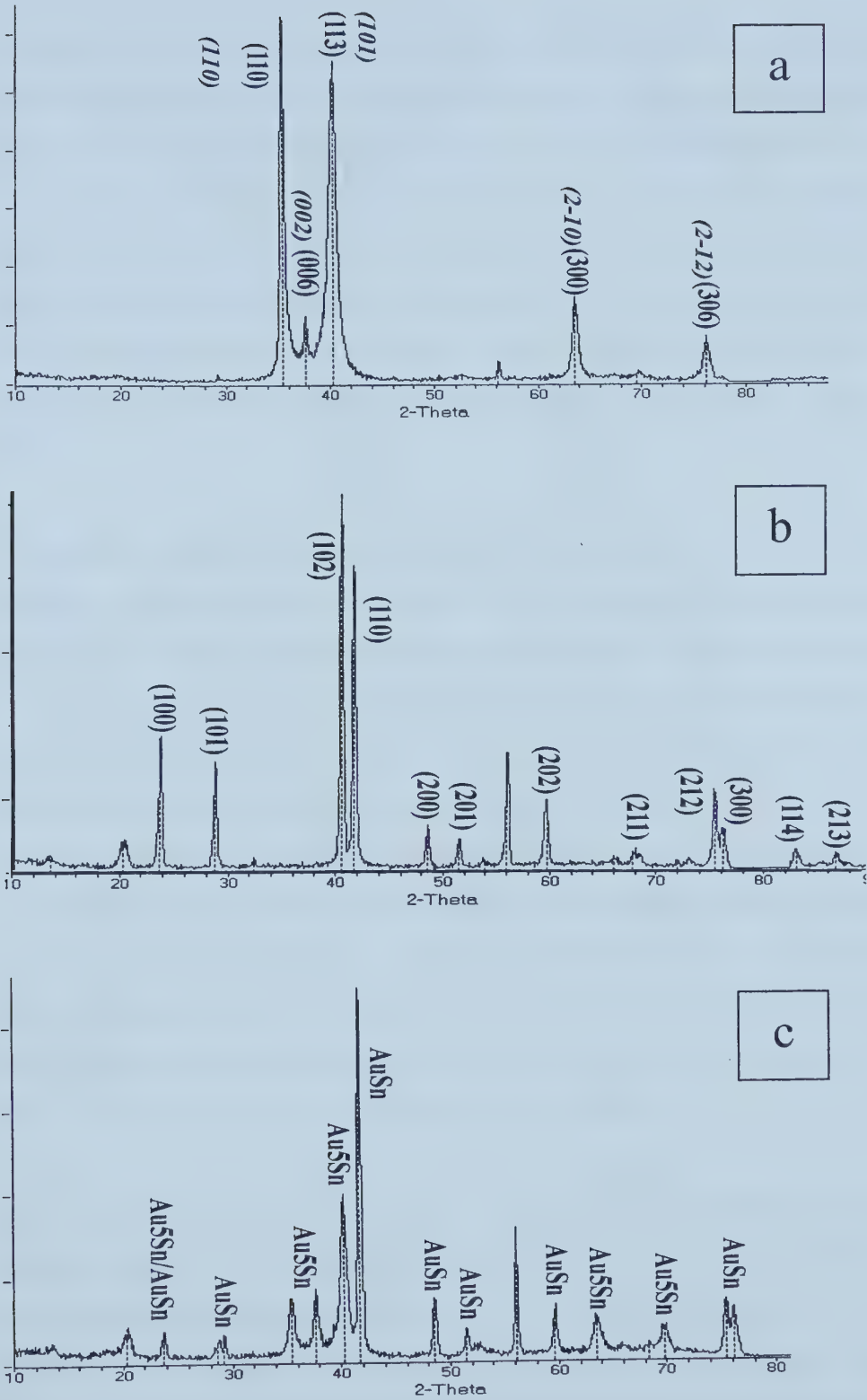


Figure 26. XRD pattern from (a) Au<sub>5</sub>Sn ordered phase in bold and Au<sub>5</sub>Sn disordered in italics, (b) AuSn phase, and (c) mixed phase (AuSn/Au<sub>5</sub>Sn) sample.



Although the increase in the amount of the less-noble metal (Sn) in the deposit with increasing current density is explained by the regular plating system definition, the shape of the curve, with two plateau regions, is not explained by this definition. The trend shown in Figure 25 mirrors the Au/Sn phase diagram; a multi-phase region bound on either boundary by the corresponding single-phase regions. However, what is not apparent is the reason the single-phase regions are so extensive with a smaller, almost random two-phase region. What would be more typical would be having the two defined plateaus, but with a smooth transition region where transition from  $\text{Au}_5\text{Sn}$  to  $\text{AuSn}$  is linear.

It is possible to explain the shape of the curve in this manner. At the lower current densities, or lower applied overpotentials, the Au, tending to reduce more easily than the Sn, will be in greater concentration on the wafer surface. Since a greater concentration of Au is depositing compared with Sn, the formation of the Au-rich compound,  $\text{Au}_5\text{Sn}$ , occurs. As the current density increases, the overpotential of both the Sn and the Au increases as well. At higher current densities,  $2\text{--}3\text{ mA/cm}^2$ , it is assumed that the reduction of Au ions has reached its limiting current density and is therefore reacting on the surface at a constant rate. The increase in overpotential, however, increases the deposition of Sn and since the Au deposition remains fixed, the Sn/Au ratio on the wafer surface increases. As a result,  $\text{Au}_5\text{Sn}$  is no longer the preferred phase for deposition. The next possible phase for deposition, as seen from the Au/Sn phase diagram in Figure 1, is  $\text{AuSn}$ . This results in the  $\text{AuSn}$  plateau seen in Figures 25.

The two-phase transition region represents an intermediate condition to the two cases discussed above. Local variations in current density may favour nucleation of one phase over the other, resulting in the formation of both phases. It is possible that local variations in microstructure, protrusions for example, may provide a sufficient local increase in overpotential causing  $\text{AuSn}$  to become the more favorable compound for deposition in those regions. However, in areas where the overpotential is not increased by the film morphology, the ratio of ions reacting at the wafer surface will remain more



conductive for depositing  $\text{Au}_5\text{Sn}$ . As a result, it becomes possible to deposit both phases in this transition region. Because of the significant element of randomness associated with the effects of these local variations in current density, there is no real relationship between the film composition and the current density in this region.

## 4.4 Eutectic Alloy Deposition

The determination of the two-phase plateaus, the  $\delta$  phase at 50 at%Sn and the  $\xi$  or  $\xi'$  phase at 15 at%Sn means that the appropriate combination of these phases will result in a structure with an overall composition between 15 at% and 50 at%. Having already established that the two phases of the eutectic structure can be deposited individually, the next step is to deposit them one on top of the other to form a structure with the eutectic composition (30at%Sn). The final composition of the structure will depend on the relative amounts of the  $\delta$  and  $\xi$  phases.

### 4.4.1 Deposition Rate

In order to determine the thickness of each layer that is required to produce the eutectic composition, some understanding of the deposition rate of each phase is required. Since deposition rate is dependent on the current density used for deposition, a specific deposition rate calculation must be made for each current density investigated. The deposition rate is estimated using the time required for plating, and the subsequent thickness of the plated layer. The thickness of each deposit is measured from the cross-section FE-SEM image using an average of 10 measurements.

The two current densities that were studied were  $0.8 \text{ mA/cm}^2$  and  $2.4 \text{ mA/cm}^2$  because these two current densities were selected for use in the multi-layer deposition process.  $2.4 \text{ mA/cm}^2$  was selected as the deposition current for the AuSn phase because it is well within the upper plateau to give a relatively high deposition rate, but still produces a dense, coherent layer.  $0.8 \text{ mA/cm}^2$  was chosen as the current density for depositing the  $\text{Au}_5\text{Sn}$  phase because it is well within the lower plateau, but is near the maximum current density and will therefore exhibit a more rapid deposition rate than the other possible deposition currents in the lower plateau.



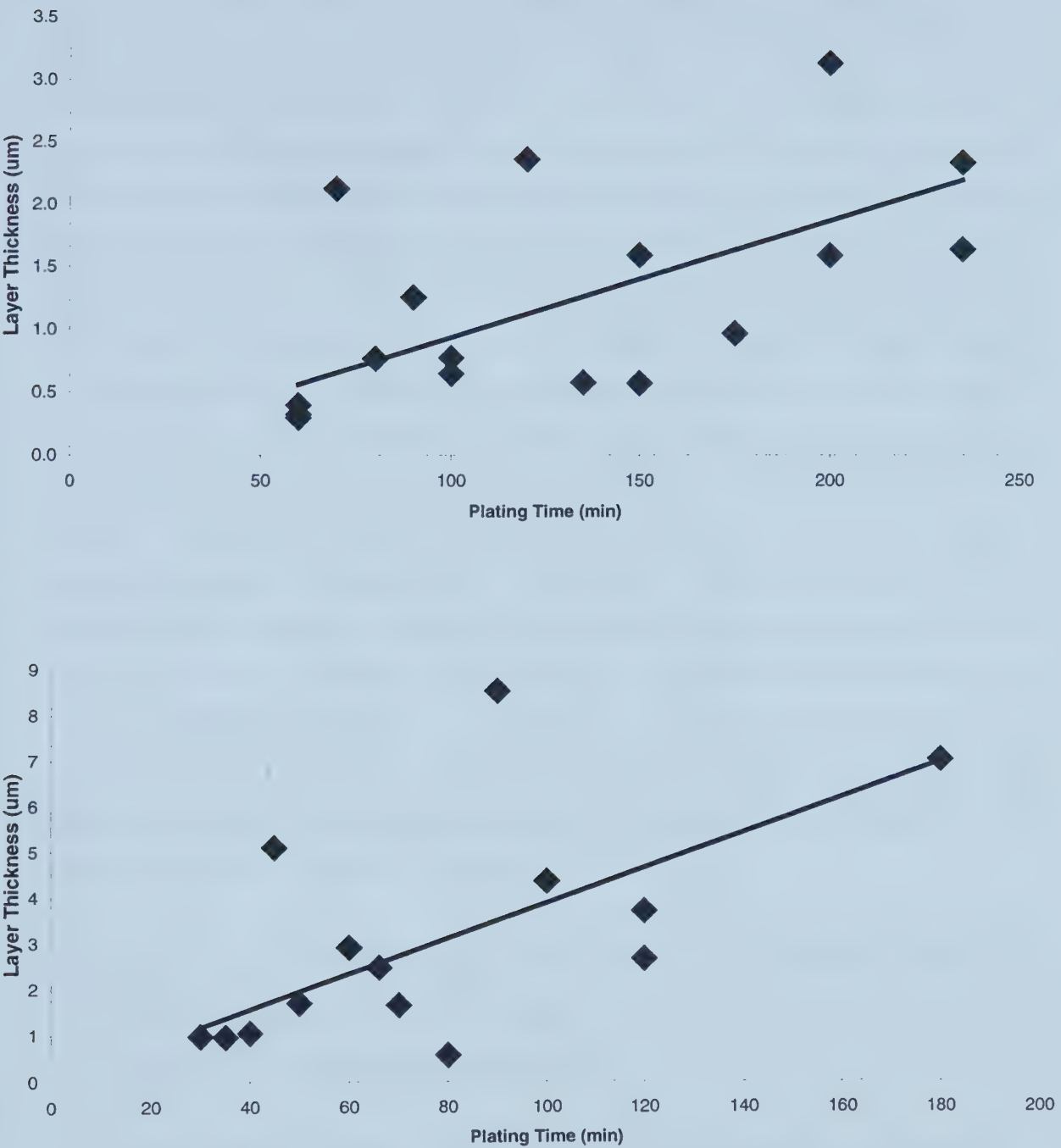


Figure 27. Deposition rate data for a) 0.8mA/cm<sup>2</sup> and b) 2.4 mA/cm<sup>2</sup>.





What is obvious from both deposition rate graphs is that there is a significant amount of scatter in the data. There are numerous possible reasons for this amount of scatter: errors in measuring the thickness of the layer, errors in setting the deposition current density, and errors in calculating the deposition area will all contribute to the overall uncertainty of the deposition rate. However, all of these errors combined will still not account for the significant scatter. Perhaps a better explanation for the scatter seen in Figure 27 is that fresh solutions were not prepared for each deposition. Since one bath was typically used to produce several deposits, it is possible that ion depletion issues led to larger variations in deposition rate than is normal. There is also some dependence of deposition rate on the quality of the surface. For instance, if there is high inhibition in the solution, then nucleation will be retarded and the deposition rate will slow. Thus, it is possible that during the depositions, the inhibition was not constant, resulting in severely scattered deposition rate data. This explanation is quite plausible if one considers the nature of inhibition in alloy deposition. The individual metal ions often act as inhibitors for each other; Au inhibiting Sn and vice versa. As a result, it is possible that a solution that was previously used for two depositions at  $0.8\text{mA/cm}^2$  would then produce a film at  $2.4\text{mA/cm}^2$  at a slightly different deposition rate than if the solution were fresh because of the differences in inhibition due to changes in the Sn concentration. This effect may account for some of the scatter in the data.

Assuming a linear growth rate, the expected thickness of a layer deposited at  $0.8\text{mA/cm}^2$  and  $2.4\text{mA/cm}^2$  are given by the following equations. Note that an intercept of 0 has been imposed during the least squares regression.

$$\text{Au}_5\text{Sn thickness } (\mu\text{m}) = 0.0091 * \text{plating time (min)} \quad \text{for deposition at } 0.8\text{mA/cm}^2$$

$$\text{AuSn thickness } (\mu\text{m}) = 0.0326 * \text{plating time (min)} \quad \text{for deposition at } 2.4\text{mA/cm}^2$$

Although the fit is quite poor, the  $R^2$  values for the  $0.8$  and  $2.4 \text{ mA/cm}^2$  are  $0.32$  and  $0.33$  respectively, the linear assumption is valid. Faraday's Law describes the relationship



between the oxidation or reduction rate and the current density according to the following relationship.

$$R = i/nF$$

where  $R$  is the rate of oxidation or reduction,  $i$  is the exchange current density,  $n$  is the amount of charge transferred, and  $F$  is Faraday's constant.

The rate of reduction/oxidation is akin to the mass deposition rate and thus this law describes the mass deposition rate as being directly proportional to the current density. Since each graph is for a fixed current density, 0.8 or 2.4 mA/cm<sup>2</sup>, the mass deposition rate must also be fixed. With a constant deposition rate, the thickness of the deposit must vary linearly with the plating time.

The deposition rate data for each phase was then used to calculate the approximate time of deposition required for each phase in order to produce the desired average composition during multi-layer deposition.

For instance, if the Au<sub>5</sub>Sn phase is plated four times as long as the AuSn phase is deposited, then the overall composition of the sample will be near the eutectic 30at%Sn. Assuming that the films are deposited with their bulk density, then the densities of the Au<sub>5</sub>Sn and AuSn phases are 17.081g/cm<sup>3</sup> and 11.74g/cm<sup>3</sup> respectively. Assuming a total deposition time of 120 minutes, the AuSn phase will be deposited for 24 minutes, and the Au<sub>5</sub>Sn phase for 96 minutes in keeping with the four to one ratio. The thickness of each layer is therefore estimated to be:

$$\text{AuSn thickness} = 0.033 \times 24 = 0.78 \mu\text{m}$$

$$\text{Au}_5\text{Sn thickness} = 0.0091 \times 96 = 0.87 \mu\text{m}$$

Assuming a constant cross-sectional area of 1 cm<sup>2</sup> for the deposition, the total amount of each element in the AuSn and Au<sub>5</sub>Sn phases is calculated in the following manner.



$$\text{Total mass AuSn} = 7.8 \times 10^{-5} \text{ cm} \times 1 \text{ cm}^2 \times 11.74 \text{ g/cm}^3 = 9.2 \times 10^{-4} \text{ g AuSn}$$

$$\text{Total mass Sn in AuSn} = 9.2 \times 10^{-4} \text{ g AuSn} \times 0.37 = 3.4 \times 10^{-4} \text{ g Sn}$$

$$\text{Total mass Au in AuSn} = 9.2 \times 10^{-4} \text{ g AuSn} \times 0.63 = 5.8 \times 10^{-4} \text{ g Au}$$

$$\text{Total mass Au}_5\text{Sn} = 8.7 \times 10^{-5} \times 1 \text{ cm}^2 \times 17.081 \text{ g/cm}^3 = 1.49 \times 10^{-3} \text{ g Au}_5\text{Sn}$$

$$\text{Total mass Sn in Au}_5\text{Sn} = 1.49 \times 10^{-3} \text{ g Au}_5\text{Sn} \times 0.10 = 1.5 \times 10^{-4} \text{ g Sn}$$

$$\text{Total mass Au in Au}_5\text{Sn} = 1.49 \times 10^{-3} \text{ g Au}_5\text{Sn} \times 0.90 = 1.34 \times 10^{-3} \text{ g Au}$$

$$\text{Total Sn in deposit} = 3.4 \times 10^{-4} \text{ g} + 1.5 \times 10^{-4} \text{ g} = 4.9 \times 10^{-4} \text{ g Sn}$$

$$\text{Total weight in deposit} = 9.2 \times 10^{-4} \text{ g} + 14.9 \times 10^{-4} \text{ g} = 2.41 \times 10^{-3} \text{ g Sn and Au}$$

$$\text{Wt\% Sn} = \frac{0.00049}{0.00241} \times 100\% = 20\text{wt\%Sn} = 30\text{at\%Sn}$$

#### 4.4.2 Multi-Layer Deposition

The first attempt at mixed phase plating was done with two individual phase layers in order to assess the viability of this technique. This step was necessary to ensure that the two phases were compatible in a multi-layer structure. The typical results of the two-layer phase structure are shown in Figure 28. Notice that there is excellent adhesion of the AuSn phase to the gold seed layer and along the interface between the AuSn and Au<sub>5</sub>Sn phases. A lack of voids is important when the application of these alloys is considered. Excessive voiding in a structure that ultimately is being designed for soldering purposes may reduce the quality of the solder bond.

Although the overall composition of the structure illustrated in Figure 28 may be that of the eutectic, and may melt at the eutectic temperature, it is not ideal for soldering applications. Because each phase exists as a separate, thick layer, the sample will have to be held above the eutectic temperature for a longer time than if the layers were thinner in order for the solder to melt completely because the diffusion distances are so large. Typically, it is desirable to minimize sample heating in order to prevent any other





unwanted reactions within the structure from occurring. As a result, a more integrated structure with thinner layers that will melt quicker is more desirable in soldering applications.

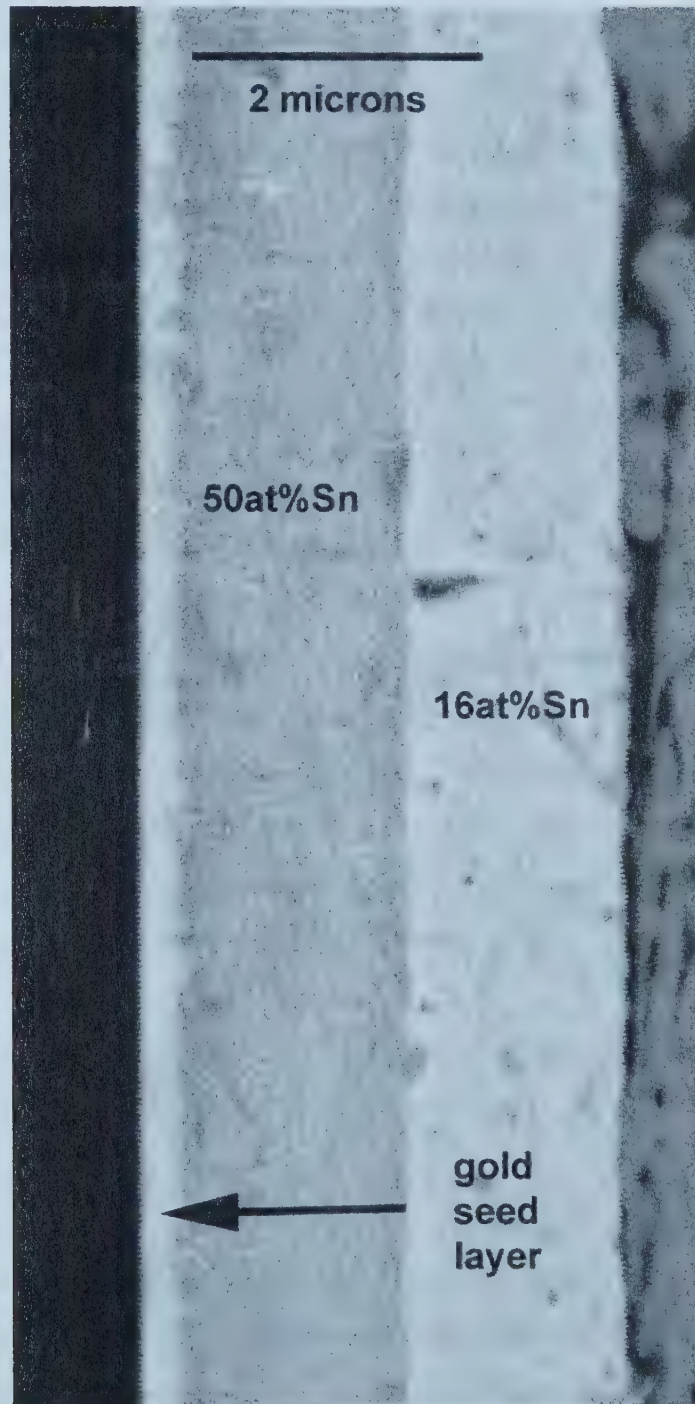


**Figure 28. SEM backscattered electron (BSE) image of a two-layer cross-section.**



The next step in producing a viable solder layer with both eutectic composition and properties is to significantly reduce the thickness of each layer and increase the number of layers in order to produce a more integrated structure. Using  $2.4\text{mA/cm}^2$  and  $0.8\text{mA/cm}^2$  as the current densities for deposition of the AuSn and Au<sub>5</sub>Sn phases respectively, composite multi-phase layers were produced with finer and finer alternating layers of each phase. The deposition time for the Au<sub>5</sub>Sn phase was four times the length of the deposition time for the AuSn phase according to previous calculations to ensure a value close to the eutectic was obtained. The goal is to produce a structure with very fine alternating layers of each phase so that a two-dimensional eutectic structure can be formed. If the layers of each phase are fine enough, then the structure should exhibit a similar melting temperature as the actual eutectic. Figure 29 shows images of three such structures. As with the two-layer structure in Figure 28, the adhesion to the substrate and between the two phases is excellent showing no signs of voiding or lifting. The two different phase layers can be seen clearly because of the atomic number contrast in the backscattered images (Fig 29a and b). The Au<sub>5</sub>Sn phase appears brighter because of the higher gold content. Note also that the apparent “waviness” of the layers in Figure 29 a and b is an artifact of the backscatter detector. The images were taken at the limits of the detector’s resolution, which manifests itself in the appearance of “wavy” lines. In Figure 29c, there is no atomic number contrast, but the phases can be distinguished from each other by their different fracture behaviors resulting in a different surface texture.

The overall composition is 30 at%Sn, 26 at%Sn, and 35at%Sn for the deposits in Figure 29a, b, and c respectively. These values are exactly, or very close to, the eutectic composition of 30 at%Sn. These results indicate that it is possible to produce a eutectic solder layer directly on the substrate using this multi-layer technique. In addition, by adjusting the thickness of the individual layers, it is possible to produce a multi-layer structure with a composition anywhere between 15 and 50at%Sn simply by alternating the current pulses. Thus, this process can be adjusted for the individual substrate. For instance, during reflow, the gold seed layer will typically diffuse into the solder layer. As a result, the composition of the deposit must be adjusted to take into account the



chemistry of the seed layer. If the gold seed layer is very thick, then a hyper-eutectic structure will have to be deposited. The multi-layer composite structure easily allows for this type of flexibility in a commercial setting.

Having successfully produced the eutectic composition, it is important to verify that it possesses a similar melting point. To this end, a sample like the one seen in Figure 29b was heated in a hot-plate annealing furnace set at 400°C under a forming gas environment (95%N<sub>2</sub>/5%H<sub>2</sub>), melted and then cooled. Although 400°C is significantly above the melting temperature of the actual eutectic at 280°C, the actual specimen temperature is approximately 300°C. The 100°C difference accounts for the temperature gradient through the thickness of the sample from the hot plate quartz surface to the solder deposit. The resulting sample looked like a typical eutectic structure with the interspersed lamella of each phase as seen in Figure 30.





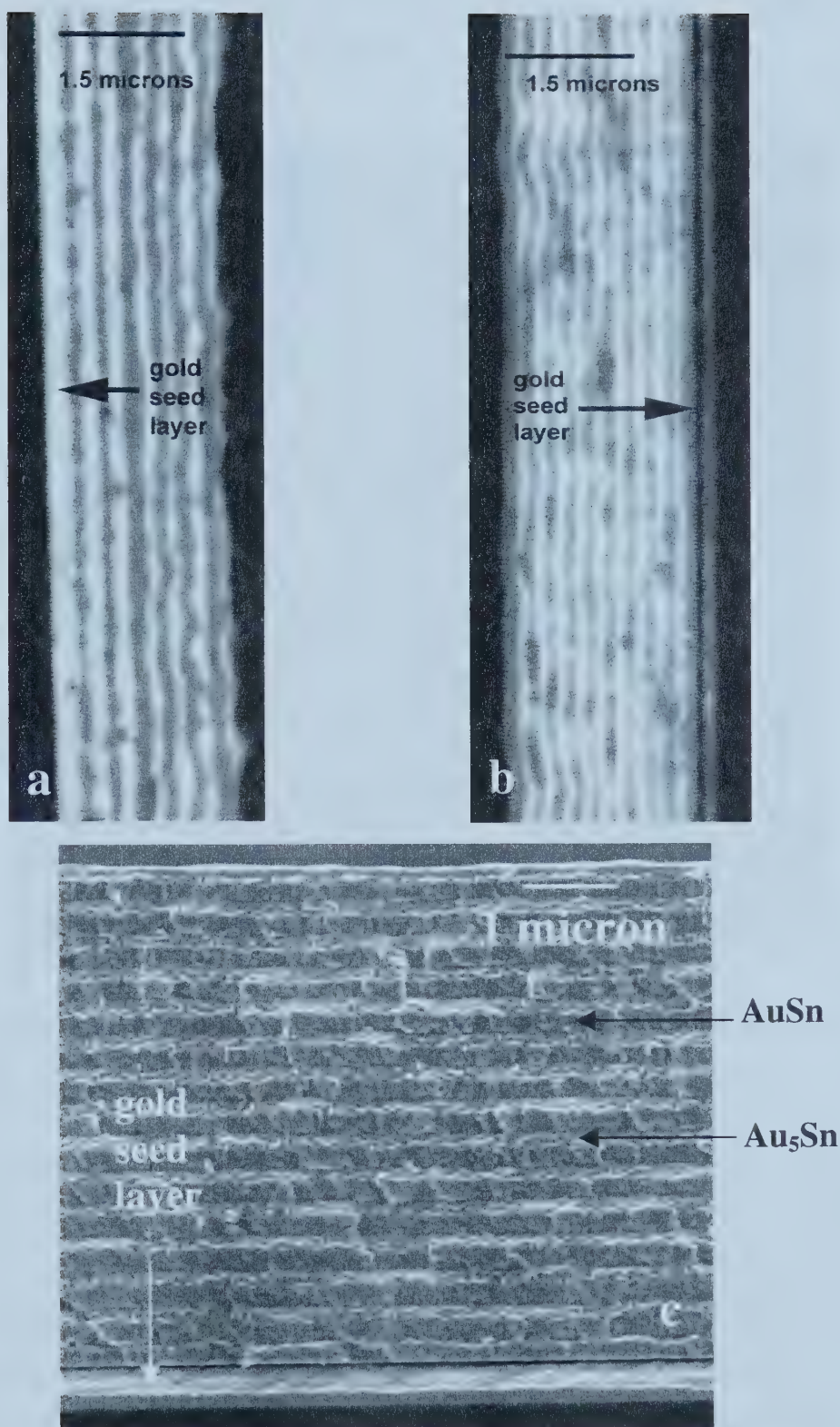


**Figure 29.** a) and b) SEM BSE cross-section images of a multi-layer deposit: a)  $2.4\text{mA}/\text{cm}^2$  for 5 minutes;  $0.8\text{mA}/\text{cm}^2$  for 20 minutes and b)  $2.4\text{mA}/\text{cm}^2$  for 2.5 minutes;  $0.8\text{mA}/\text{cm}^2$  for 10 minutes. c) FE-SE SEM image showing multi-layers deposited at  $2.4\text{mA}/\text{cm}^2$  for 5 minutes;  $0.8\text{mA}/\text{cm}^2$  for 21 minutes.





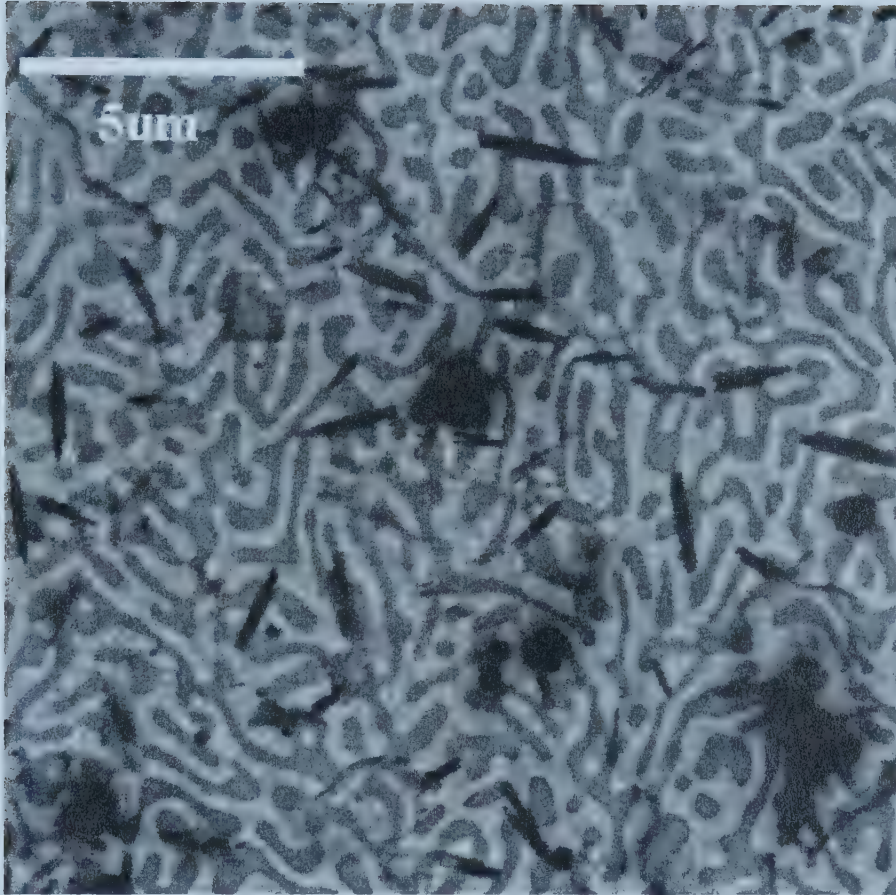


**Figure 30. SEM BSE plan view image of composite multi-layer post melting.**

Again, the lighter phase corresponds to the  $\text{Au}_5\text{Sn}$ , while the darker phase corresponds to  $\text{AuSn}$ . The voids that are seen in Figure 30 are typical of any sample that has been reflowed. There is always material shrinkage during solidification upon cooling after reflow, and the voids simply arise out of an insufficient quantity of material to cover the entire wafer surface. It is advantageous to have the sample melt near the eutectic temperature and cool to form a typical eutectic structure, however, more testing is required to ensure that the solder will provide a good bond. The results suggest that the multi-layer structure is an effective method for producing the eutectic solder.



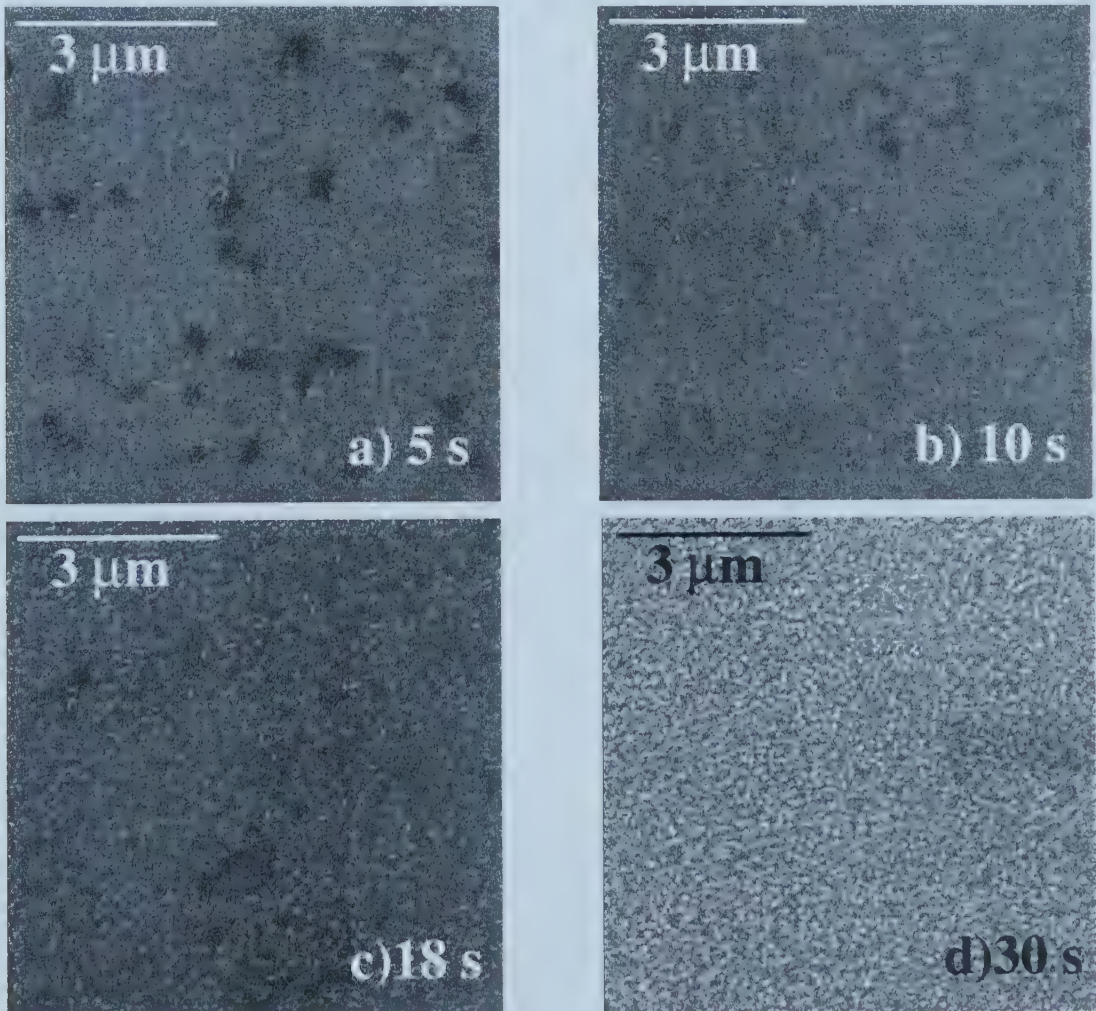
## 4.5 Phase Morphology and Film Growth Mechanism

When suggesting a composite multi-phase layer structure for depositing the eutectic Au/Sn solder onto carrier substrates, the individual morphology of each phase becomes important to the success of the structure. The ultimate goal is to produce a multi-layer structure that is so well interspersed that it behaves as if it were a “natural” eutectic. In order to accomplish this, and produce an optimized composite layer, it is necessary to study and understand individual phase formation and morphology. This information will ultimately define the physical limits of the multi-phase composite structure.

### 4.5.1 AuSn

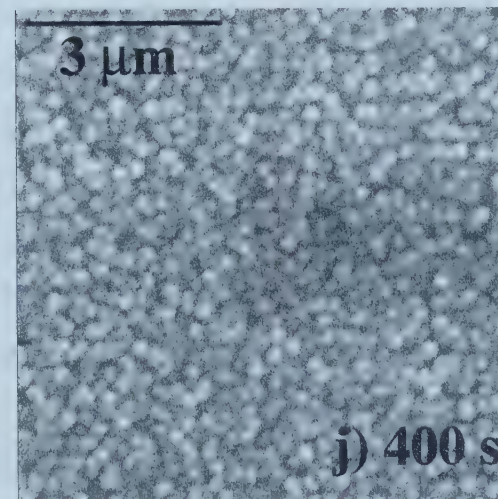
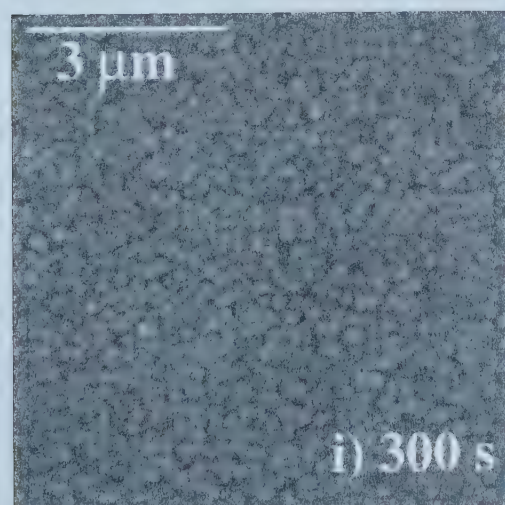
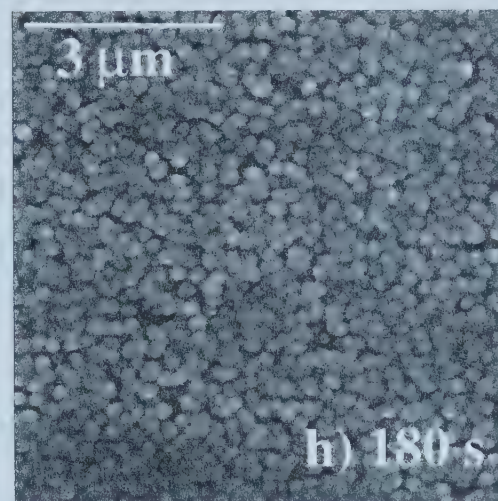
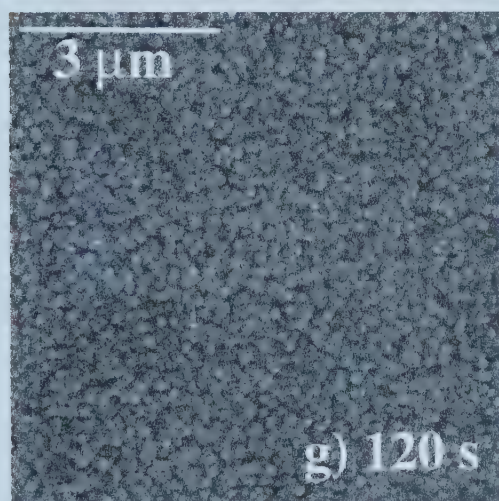
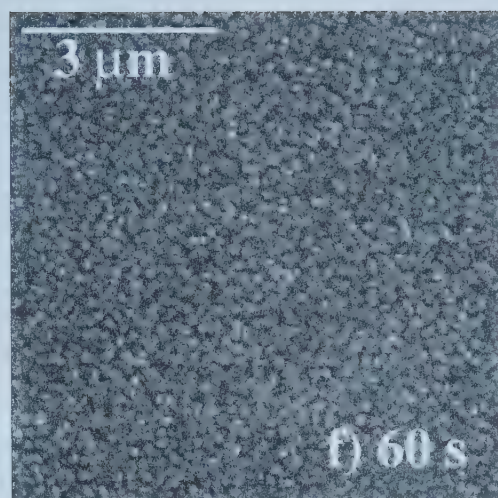
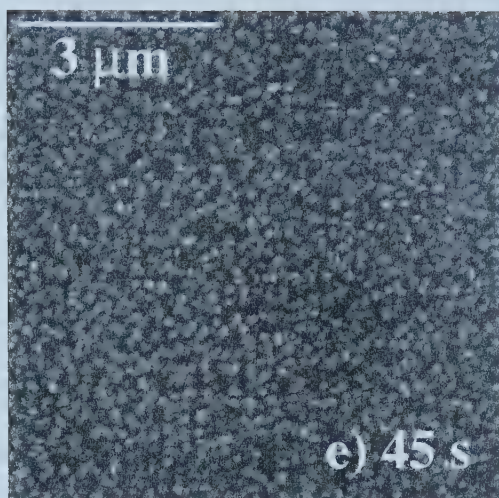
#### 4.5.1.1 Film Growth Mechanism-Imaging

The nucleation and growth process for the AuSn film is illustrated in the sequence of images presented in Figure 31.













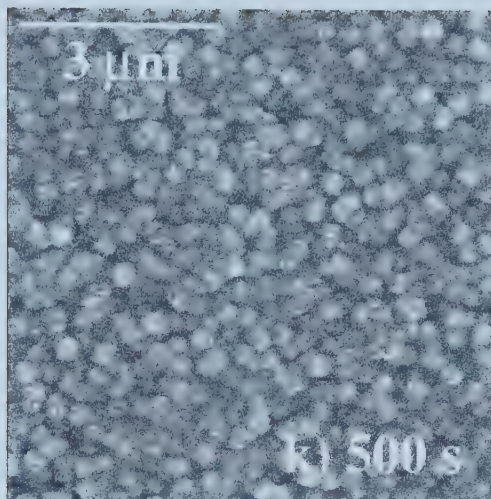


**Figure 31. Film growth progression of AuSn phase. Depositions were done at  $2.4\text{mA}/\text{cm}^2$  using a pulsed current with an on-time of 2ms and an off-time of 8ms.**

From the images, it is clear that the first particles form on the surface of the substrate at approximately 10 seconds. It is possible that prior to 10 seconds, no nuclei have formed yet, or there are nuclei present on the substrate surface which cannot be resolved by the SEM. By 30 s the substrate surface has been completely covered. From this point on, the deposited film becomes increasingly denser eventually filling in some of the voided areas that are still present at 180s. This type of growth mechanism, early surface coverage followed by densification, is typical of a growth controlled deposition process.

One of the defining features of a growth controlled deposition process is visible in Figure 31 c-j. This sequence of images reveals a continuous nucleation mechanism that results in fast surface coverage because of the presence of many small particles on the surface. This type of electrocrystallization process is typical of a higher current density deposit where the lateral growth of the film is almost completely eliminated in favor of the two-dimensional nucleation or vertical growth step [Winand, 1994]. Thus, as time progresses, and the initial layer surface has been deposited (30s), nucleation will continue in a vertical direction building up the thickness of the deposit. Because there is almost no lateral growth, there is little chance for the individual nuclei to grow together. Instead, because nucleation is so rapid, new particles will form in the spaces between existing



nuclei. The lack of lateral growth often results in voiding between existing particles as seen at 120 and 180 seconds, when nucleation within the existing voids does not occur.

For instance, in Figure 31 h, i and j, significant time has passed, but the individual diameter of each particle has not grown significantly. This effect is a result of the dominance of the two-dimensional nucleation step. Increased nucleation events result in smaller particles stacking on top of each other and forming within existing spaces between the individual particles. Thus, the growth of each particle is restricted by the presence of another particle directly adjacent to it resulting in a situation where new particles are easily produced, but the individual size of the particles cannot fluctuate greatly. Eventually, as deposition continues, the surface of the deposit begins to smooth, and the voids are slowly filled. However, because of the ease of nucleation, the surface will remain rough as compared with a lower current density deposit and film formation will be growth controlled.

The SEM plan and cross-sectional images (Figure 32) of a full thickness deposit further reinforce the typical high current density deposition mechanism that is described by electrocrystallization theory [Winand, 1994] and witnessed in the SEM nucleation work (Figure 31). The cross-sectional image of the AuSn deposit, because of the brittle fracture, clearly reveals the prevailing growth mechanism. Directly on top of the seed layer is an area made up of many small particles that are nucleating simultaneously or in short succession and stacking one on top of the other. At a certain thickness, the texture of the deposit changes and becomes more columnar. The change in texture corresponds to the formation of field-oriented crystals or a field texture structure as described by the electrocrystallization theory [Winand, 1994]. The reason for the formation of this type of structure is that a preferred growth direction has been established and it is beneficial, from an energetic point of view, to continue to nucleate along that particular direction resulting in the formation of the orientated columns that grow out of a sub-layer of equiaxed particles.



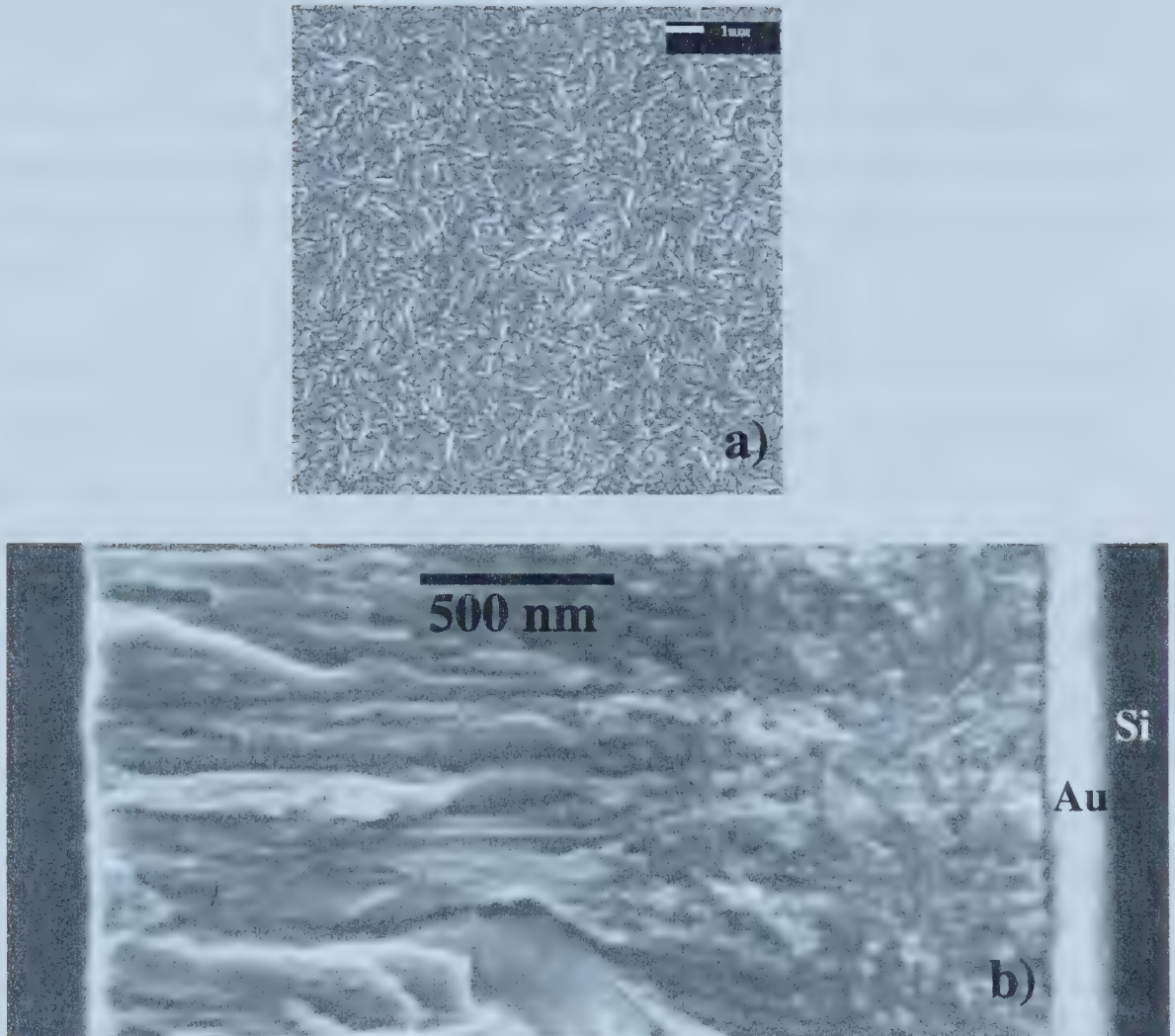


**Figure 32. SEM SE images of AuSn deposit a) plan view and b) cross-sectional view.**

What is interesting to observe is that despite the initial appearance of some voiding in Figure 31h, the cross-section image reveals a dense and coherent structure with minimal voiding. This is very important when considering that the ultimate goal is to produce a layer of solder, and any voids will ultimately degrade the quality of the solder bond.

The surface topography observed in the plan view image is a direct result of the formation of a field-texture or field-orientated crystal structure. The discrete features on



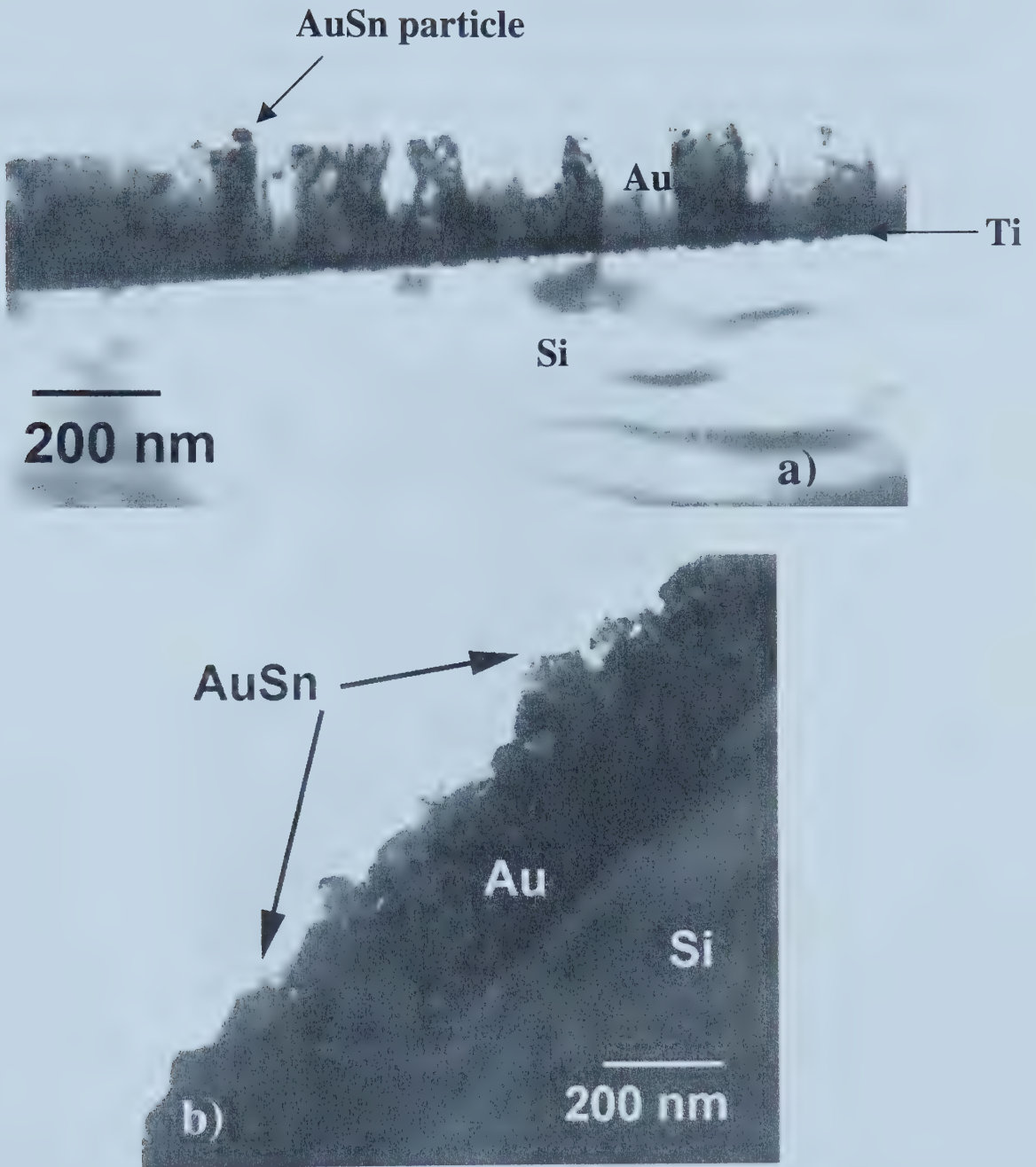




the plan view that appear at first to be individual grains are actually just a surface texture. The rough looking surface is a result of the individual columns of the deposit, which are themselves made up of many grains, protruding on the surface creating the appearance of grains. Thus, it is impossible to gain an accurate estimation of the relative grain size of the deposit by simply looking at the SEM plan view image since the grain structure is not visible.

A TEM investigation of the AuSn deposit was undertaken in order to verify the results obtained with the SEM. The two cross-sectional images (Figure 33) reveal a similar structure to the one observed in the SEM nucleation work. At 18 seconds, discrete particles, comparable in size to those in the corresponding SEM images, are visible on the surface of the seed layer, and later at 120 seconds, it is apparent that a continuous, multi-grained layer has formed along the surface of the substrate. The formation of voids along the interface between the solder and the gold seed layer at 120 seconds may have two causes. The first may be that the high current density used for the deposition does not allow for sufficient lateral coverage of the substrate. What is more likely is that the voids are Kirkendall voids. The Au/Sn diffusion system is one of the most rapid solid-state systems known to exist, exhibiting significant diffusion even at room temperatures [Gregersen et al, 1981]. Because the seed layer is gold, it is probable that during sample preparation some of the gold from the seed layer and some of the tin from the solder diffused across the interface because of the large concentration gradient across the interface. The result is the formation of Kirkendall voids because of the huge disparity in the respective diffusivities of each individual metal (Table 2). This phenomenon will be discussed in more detail in later sections.

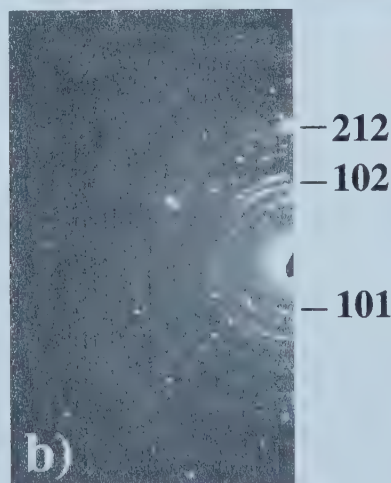
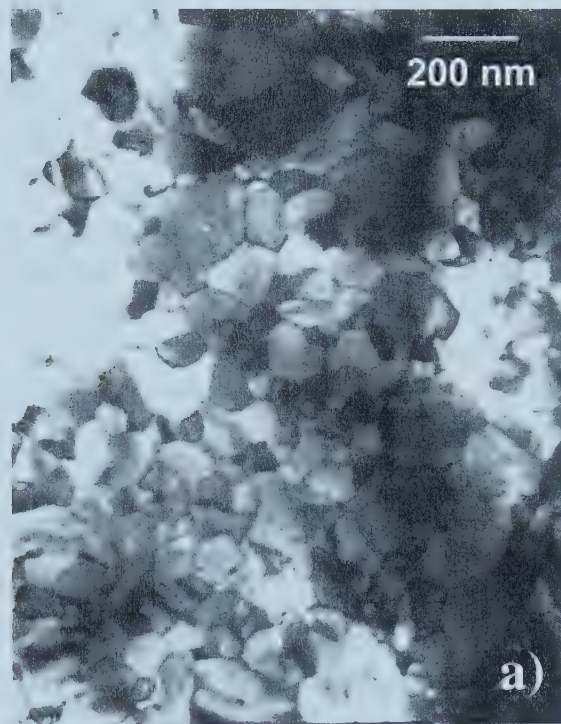




**Figure 33.** TEM cross-section bright field images of AuSn deposit at a)18s and b)120s.



The TEM plan view image (Figure 34) of a final deposit that is several microns thick reveals the true grain size of the AuSn phase that was not visible in the SEM plan view. Although it is somewhat variable in the image, the average grain diameter is on the order of 50-75 nm. This is significantly smaller than the apparent grain diameter in Figure 32a further verifying the presence of field orientated crystals in the deposit and the resulting surface topography that they produce. The fine grain size is a result of the high current density used for deposition. With a high current density, there is a significant amount of nucleation and limited growth resulting in a fine-grained deposit. The diffraction pattern and EDX spectrum simply verify the presence of the AuSn phase in the plan view image.







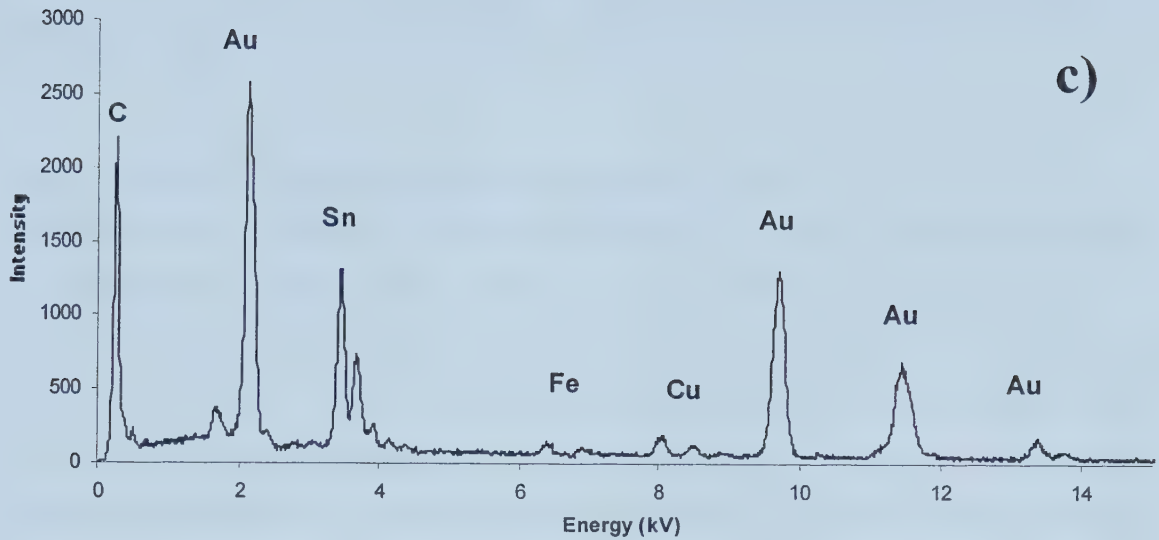


**Figure 34. a) Plan view TEM bright field image of AuSn, b) diffraction pattern showing the  $\delta$  phase, and c) EDX spectrum confirming the composition of AuSn.**

The presence of the Cu peak in the EDX spectrum is due to the copper ring used to stabilize the plan view sample, the Fe peak is an artifact from the microscope column, and the C peak is a result of beam contamination.

Various EDX spectra, like the one seen in Figure 34 c, were used to calculate the average Cliff-Lorimer or k factor that describes the relationship between the intensity of an element peak and the concentration (C) of the element in the sample according to the following equation.

$$C_{\text{Sn}}/C_{\text{Au}} = k I_{\text{Sn}}/I_{\text{Au}}$$

where intensity (I) is described as the background subtracted area beneath the peak of the same family (K, L or M).

The average intensity beneath the Sn L-peaks for three samples was 9450 counts/second  $\pm$  3% and the average intensity of the Au L-peaks was 17750 counts/second  $\pm$  2%.



Knowing that the concentration ratio of tin to gold in the AuSn compound is one to one, then the average  $k$  value for this system is calculated to be  $1.9 \pm 5\%$ .

#### 4.5.1.2 Film Growth Mechanism-Compositional Analysis

Once the growth mechanism of the AuSn film has been studied, it must be verified that the AuSn phase is nucleating and growing. Compositional analysis was attempted through a combination of diffraction and EDX analysis of the same TEM cross-sections that were made to study the nucleation and growth of the phase. When compared with the standard diffraction pattern and EDX spectrum (Figure 34 b, c), it was apparent that the AuSn phase was not forming. Diffraction patterns (e.g. Figure 35) were indexed as gold and EDX spectra (e.g. Figure 36) confirmed that there was very little tin during the initial phases of growth. Both the diffraction patterns and EDX spectra were taken from the sample illustrated in Figure 33b.

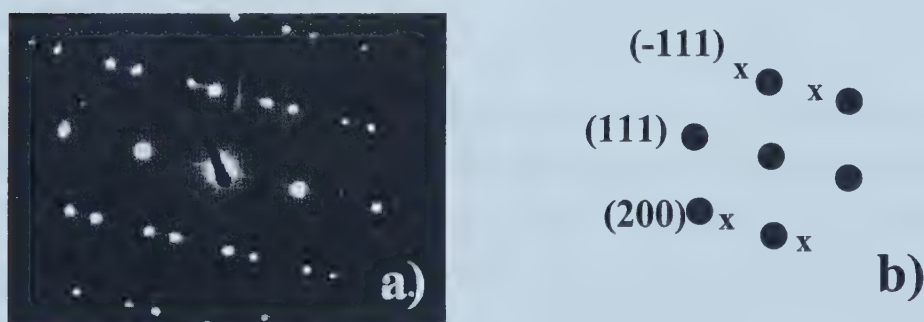


**Figure 35. a) Diffraction pattern from a solder layer grain which was indexed as gold (b). The zone axis was indexed as  $[01-1]$ . The extra spots (denoted by x's) are due to twinning of the Au grain. The twin plane is  $(111)$ .**



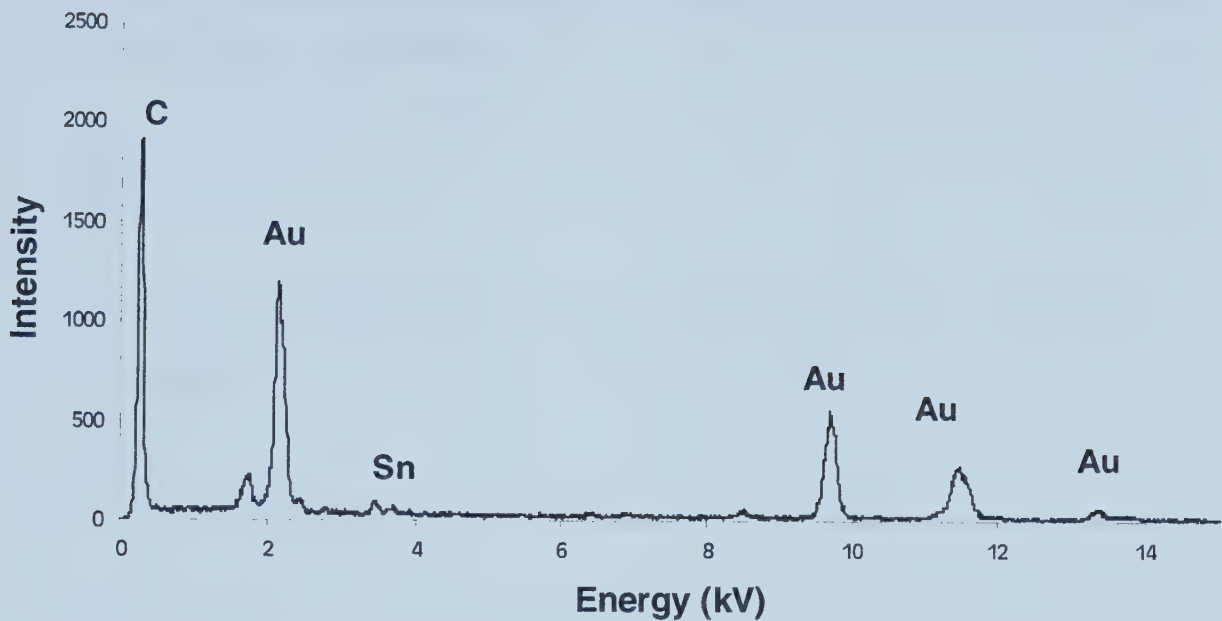


**Figure 36. EDX spectrum from the grain in Figure 35.**

The combination of the diffraction pattern and EDX spectrum suggests that a deposit of significantly less Sn than the AuSn phase is forming. It seems unlikely that a gold solid-solution would be nucleated initially only to transform to AuSn at a later time. However, the presence of large Kirkendall voids in the TEM cross-sectional images suggests that perhaps there is diffusion of tin out of the solder layer into the gold seed layer resulting in an erroneously low tin composition in the deposited layer. Using the k-value calculated from the AuSn standard EDX spectrum, it is possible to calculate the concentration of tin in the solder layer of the TEM specimen's by calculating the area underneath the tin and gold peaks. Table 8 gives the area intensities for the solder layer.

**Table 8. Intensity calculations from EDX spectra of solder layer.**

<i>Peak</i>	<i>Counts</i>
Sn L-peak	1198 +/- 9%
Au L-peak	12480 +/- 3%





Using the values listed in Table 8, the ratio of tin to gold in the layers can be calculated according to the following formula:

$$\frac{C_{Sn}}{C_{Au}} \equiv k \frac{I_{Sn}}{I_{Au}}$$

Because gold/tin is a binary system, the individual composition can be calculated according to:

$$C_{Sn} + C_{Au} = 100\%$$

For the solder layer, the ratio of compositions is:

$$C_{Sn}/C_{Au} = 1.88 \cdot (1198)/(12480) = 0.18 \pm 17\%$$

This ratio results in a 15at%Sn composition and an 85at%Au composition.

What is unusual is that the diffraction pattern in Figure 35 indicates the presence of gold, but the EDX pattern suggests that the composition is nearer to the Au<sub>5</sub>Sn phase. It is probable that the diffraction pattern is for a solid solution of tin in gold, but as indicated in the phase diagram (Figure 1) the maximum solubility of tin in gold is 6.6 at%Sn. However, the significant error associated with the EDX analysis ( $\pm 17\%$ ) explains the discrepancy between the diffraction pattern and EDX analysis.

This type of problem should not be entirely unexpected since the diffusion rates of Au and Sn in the Au/Sn diffusion system are quite rapid even at room temperature. If diffusion is occurring into the gold seed layer, then not only is a lower tin value expected in the solder layer, but a noticeable tin peak should be present in the gold seed layer as well. Figure 37 is an EDX spectrum from the gold seed layer directly beneath the solder layer from which the spectrum in Figure 36 was taken. Although quite small, there is a tin peak present in the gold seed layer verifying that the tin is diffusing out of the deposit.



The reason for the very small peak is that the concentration of the tin, once dissolved into the gold seed layer, is very dilute. Table 9 lists the area intensities for the gold seed layer spectrum from which the composition of the layer can be calculated.

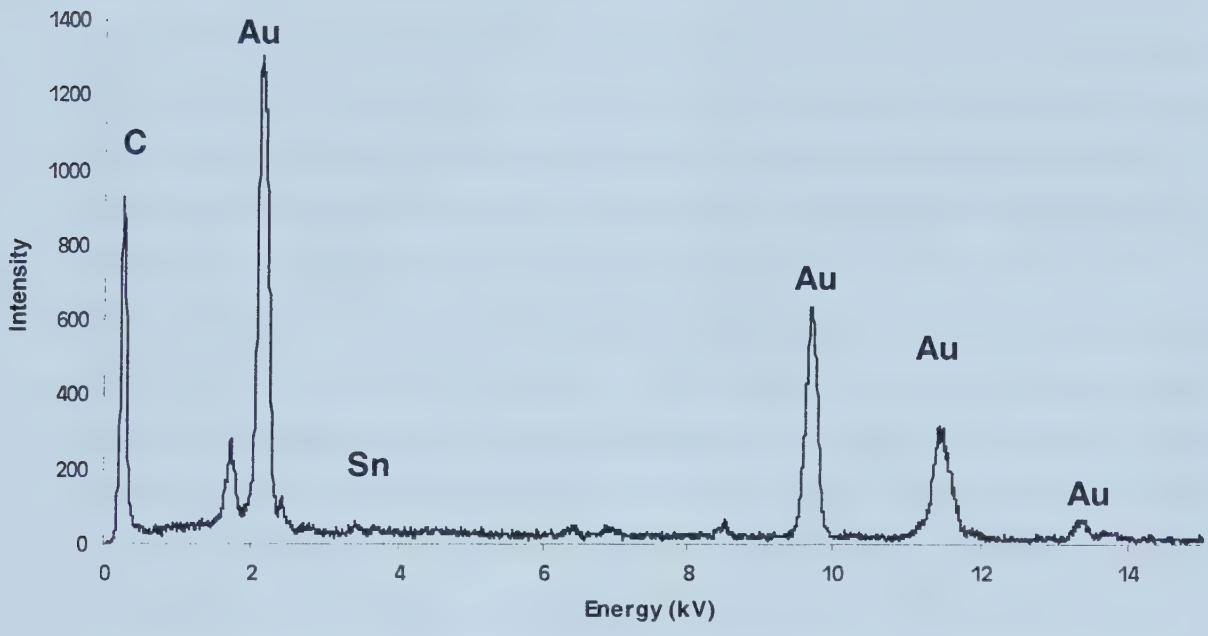


**Figure 37.** EDS spectrum from gold seed layer directly beneath the solder layer.

**Table 9.** Intensity calculations from EDX spectrum of gold seed layer.

<i>Peak</i>	<i>Counts</i>
Sn L-peak	702 +/- 11%
Au L-peak	27968 +/- 2%

For the gold seed layer, the ratio of compositions is:

$$C_{Sn}/C_{Au} = 1.88 \cdot (702)/(27968) = 0.05 \text{ +/- } 18\%$$

The corresponding tin concentration is 5at%Sn with 95at%Au in the gold seed layer. This result indicates that there is indeed a significant amount of tin in the gold seed layer



lending some credibility to the suggestion that the tin is diffusing out of the deposit into the seed layer.

The most likely explanation for the loss of tin is diffusion during sample preparation. Because XRD and SEM EDX analysis of full thickness samples that had been sitting at room temperature for several months still indicated the presence of the expected phases, it is clear that the problem arises as a result of the TEM sample preparation method. Even though the samples are cooled to liquid nitrogen temperatures during sputtering, it is possible that the ion beam provides enough local heating to cause significant tin diffusion. However, plan view TEM images of the AuSn revealed the appropriate phase and composition for the 50at%Sn deposit. The problem is either somehow associated with the cross-section sample preparation method only or a gold solid solution is indeed nucleating first and then slowly changing to the AuSn phase at a given thickness. What is possible is that in the cross-section samples the ratio of gold-seed layer to deposit is much larger than with the plan view sample, which enhances diffusion in the cross-section during sputtering. As well, in the cross-section image, the deposit is directly adjacent to the large gold layer whereas with the plan view, the deposit is far more isolated from the gold-seed layer, which may account for the apparent lack of diffusion in the plan view samples during sputtering. Unfortunately, none of this can be verified using the TEM, since it is impossible to make a sample without encountering the same diffusion issues that are the cause of tin depletion.

As a result of the problems associated with compositional analysis of the nucleating layers in the TEM, XRD was employed to determine which phase or phases formed during the initial deposition process. Pt seeded wafers were used, instead of Au, since Au was one of the possible nucleating phases. The samples were scanned in the diffractometer immediately after deposition in order to minimize diffusion into the solder layer. The results of several overlaid spectra are shown in Figure 38. Although the peaks are weak, the presence of AuSn is clearly visible as early as 18s. The weakness of the AuSn peaks is attributed to the lack of material on the surface of the substrate. The Pt peaks that are present in all spectra are simply background peaks from the Pt seed layer.





As the surface coverage of AuSn increases, the intensity of the seed layer peaks decreases since less of the layer is exposed for sampling. The XRD results, therefore, confirm that TEM sample preparation caused the erroneous TEM results, and that AuSn is indeed the nucleating and growing phase.

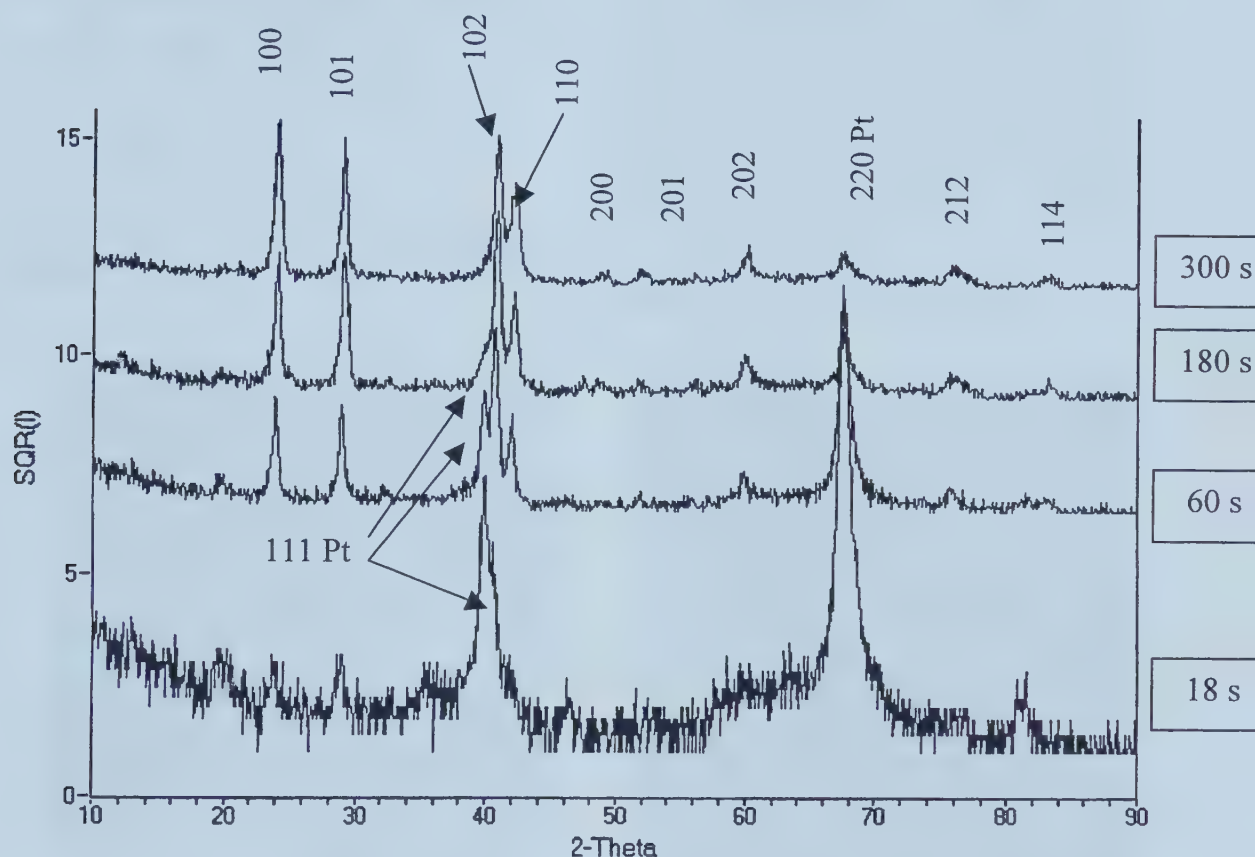


**Figure 38.** XRD spectra from deposits done for 18, 60, 180, and 300 seconds.

Ultimately it is extremely important for the AuSn phase to nucleate and grow as opposed to nucleating another phase with a later transformation to AuSn. The composite multi-layer method for producing the eutectic solder alloy has certain restrictions. Among them is a minimum plating time for each phase layer in order to produce a continuous, uniform film on the surface of the substrate. It is important for the layer to be continuous and uniform to reduce the possibility of voiding or poor adhesion with the next layer.

However, if the deposition of AuSn were to start as a solid solution of gold and tin and then later transform to the AuSn phase, the minimum thickness requirement would then

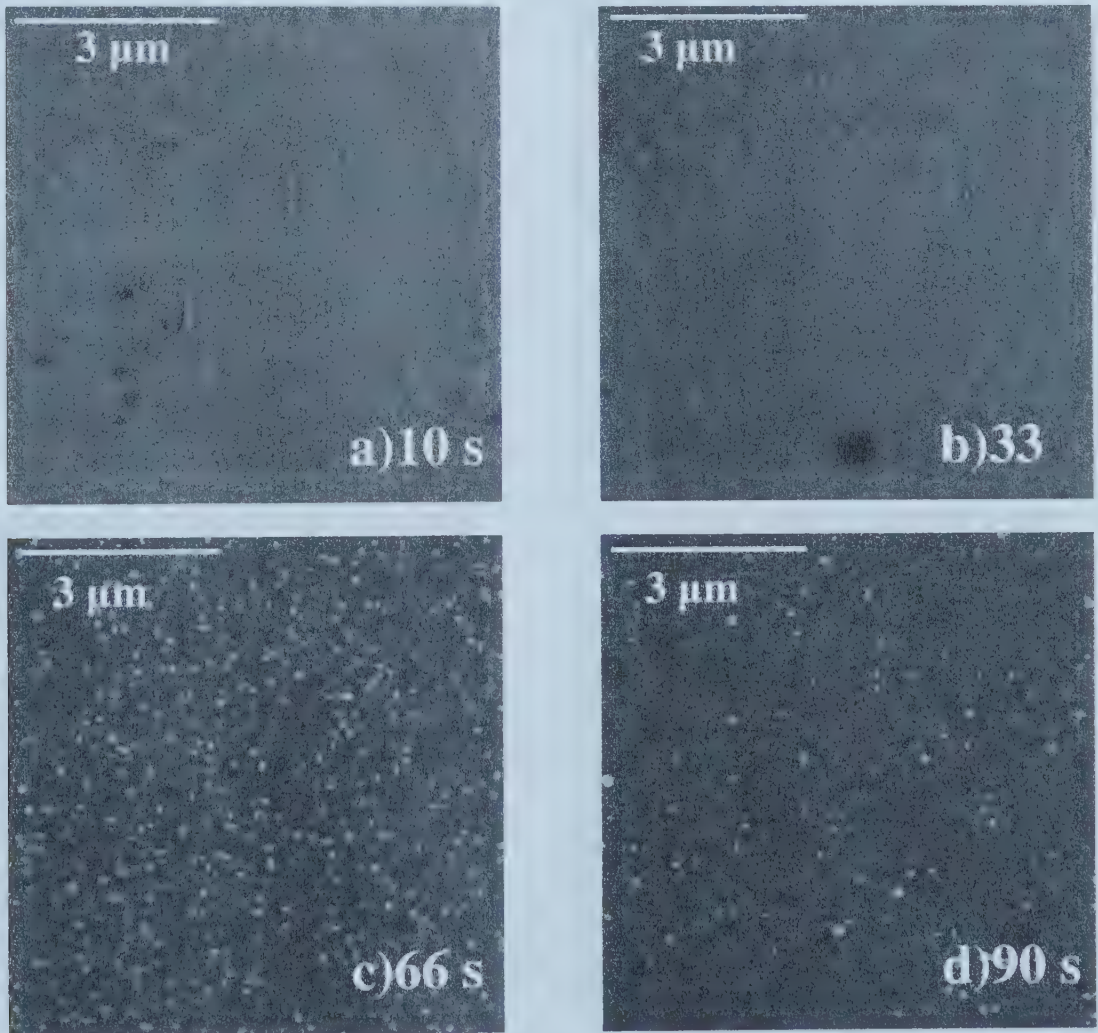


be dependent not only on complete surface coverage, but also on obtaining a film with the appropriate overall composition (50at%Sn) which would be much more difficult to determine. The advantage of having the AuSn phase deposit immediately is that the minimum thickness requirement depends only on good surface coverage. From Figure 31, it appears that any time over 60 seconds would be sufficient for producing a continuous, uniform layer.

#### 4.5.2 Au<sub>5</sub>Sn

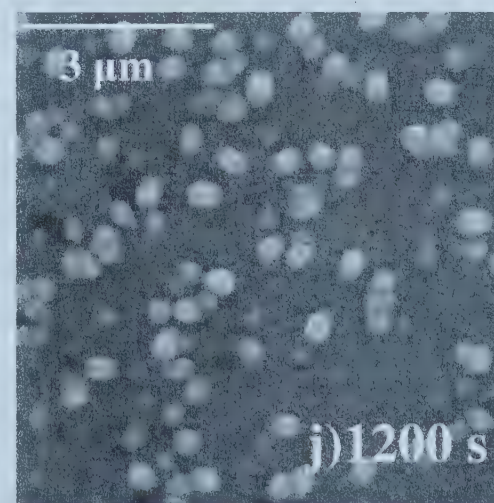
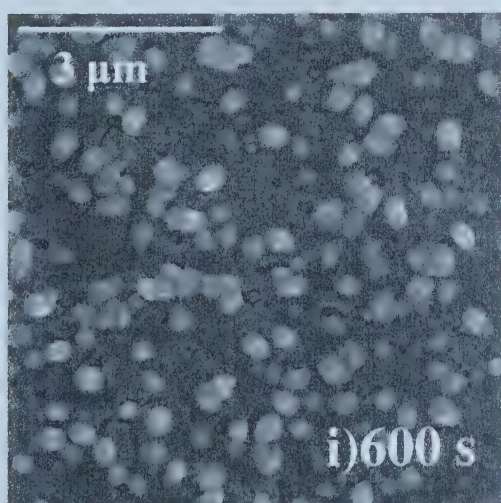
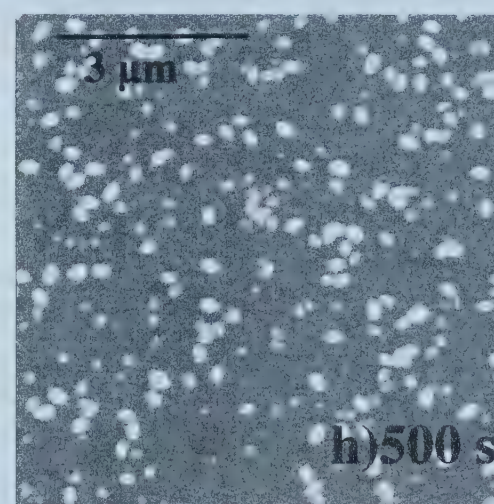
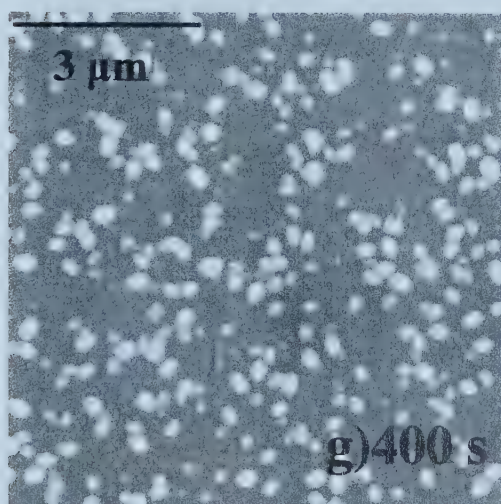
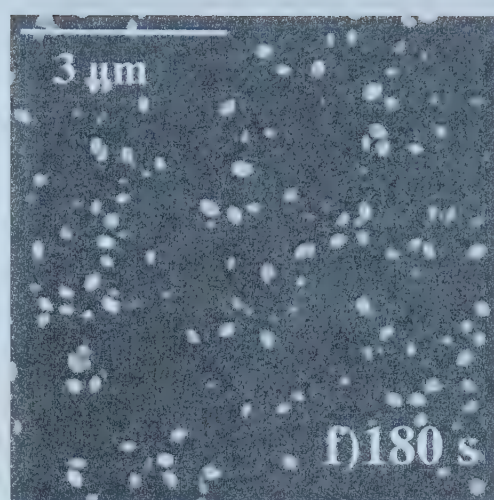
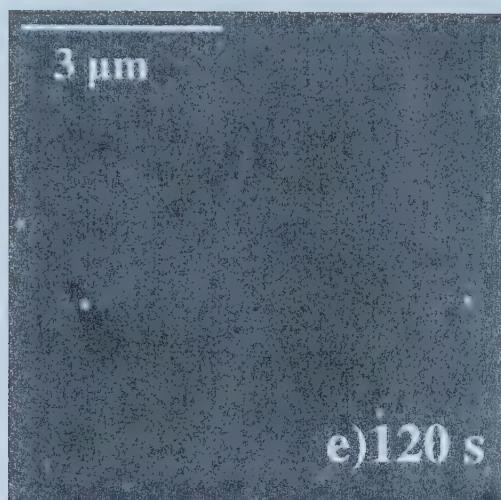
##### 4.5.2.1 Film Growth Mechanism-Imaging

Similar to Figure 31, the sequence of images in Figure 39 clearly illustrates the nucleation and growth process of the Au<sub>5</sub>Sn film.













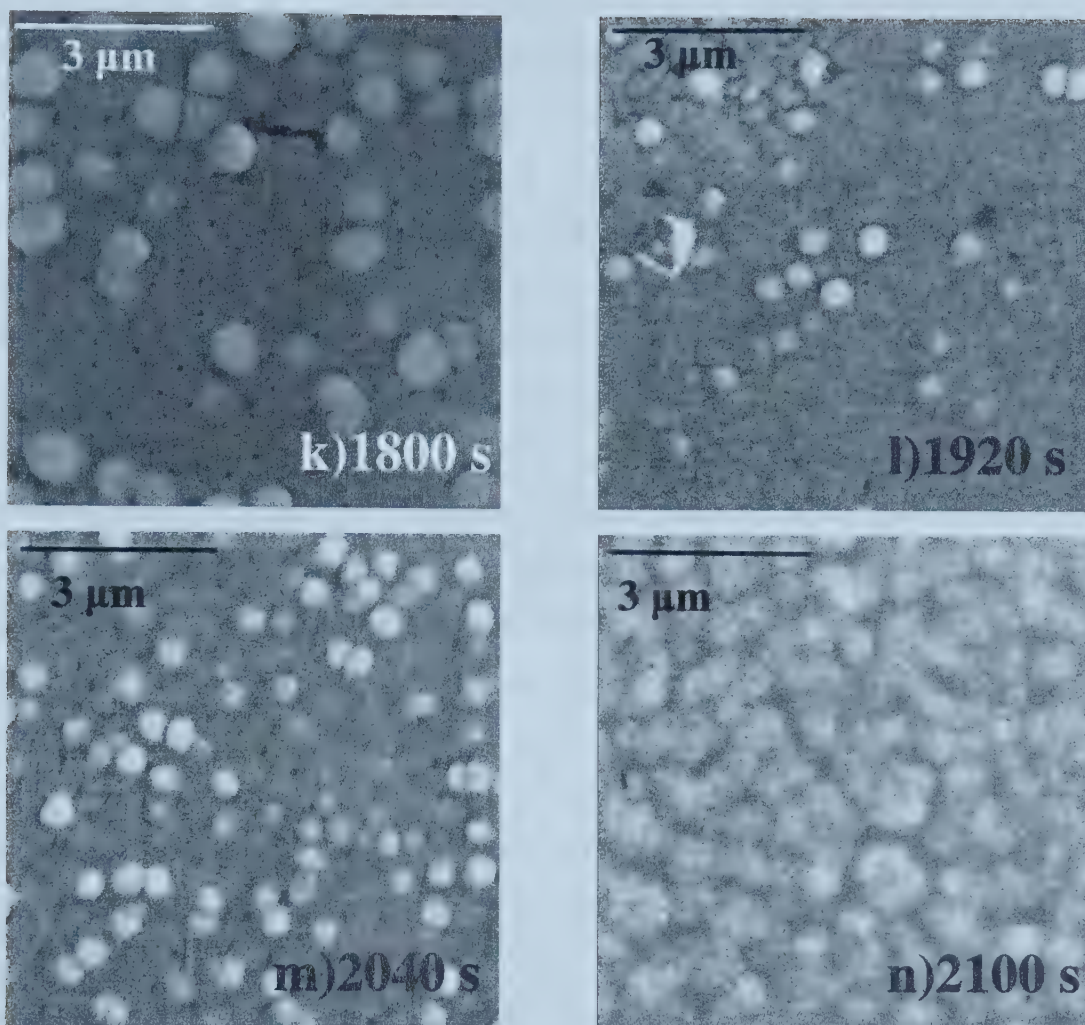


**Figure 39. SE SEM images showing film growth progression of  $\text{Au}_5\text{Sn}$  phase. Depositions were done at  $0.8\text{mA}/\text{cm}^2$  using a pulsed current with an on-time of 2ms and an off-time of 8ms**

At 66 seconds, the first particles are visible on the surface of the substrate. Prior to 66 seconds, there are no particles present, due either to a lack of nucleation or small nuclei are un-resolvable by the microscope. The particles are fairly uniform in size, submicron, and well dispersed over the surface of the substrate. However, at 90 and 120 seconds, it seems as if the number of particles on the surface diminishes and then increases again at 180 seconds. A possible reason for this is the statistical nature of nucleation. Since nucleation is heavily dependent on the substrate surface, it will not occur at the exact same moment on each wafer resulting in some small inconsistencies in the sequence. As



a result, the images do not represent an exact chronology, but they do adequately represent the general trend.

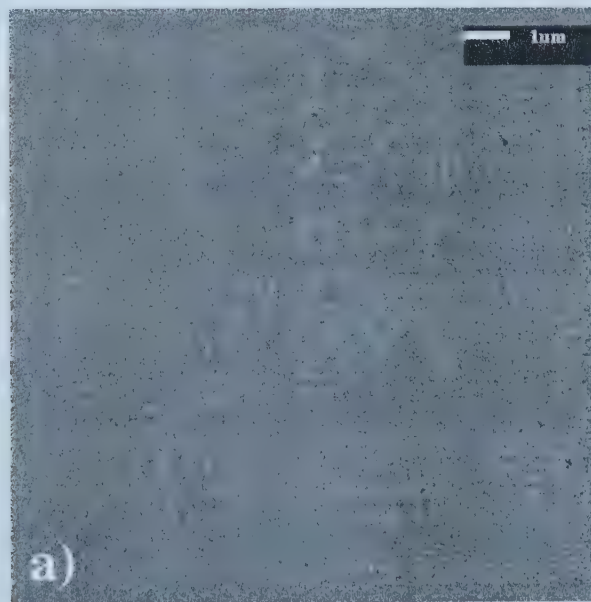
The trend that can be drawn from the series of images, in particular, those for 66s, 180s, and 400s, is that the actual number of nuclei on the surface does not increase as it did for the growth of AuSn. Instead, the size of the individual nuclei increases suggesting the dominance of lateral growth. At 600s, a continuous sub-layer has formed, with larger particles protruding from the surface of this continuous layer. As time progresses, the protruding particles spread laterally as the sub-layer grows vertically towards the protruding particles creating a smoothing effect. This mechanism is evident in the final two images at 2040 s and 2100 s where the deposit smoothes out significantly due to the competing mechanisms of vertical sub-layer growth and lateral spreading of the protruding particles.

This type of formation mechanism, nucleation controlled growth, is typical of the low current density deposition process described by electrocrystallization theory [Winand, 1994]. Low current density deposition processes result in a dense coherent structure with the lateral growth mechanism, or repeatable step, being dominant over the two-dimensional nucleation step, or vertical growth. This type of formation mechanism is evident in the images of Figure 39. With a dominant lateral growth mechanism, small nuclei will form on the surface of the substrate and instead of new nuclei forming continuously as was the case with AuSn growth, the existing nuclei will continue to grow. This results in the gradual coarsening of the initial nuclei and their ultimate agglomeration into a continuous layer because of the dominance of lateral growth. The result is the formation of a continuous under-layer with the remnants of particles protruding from the continuous matrix. Ultimately, as the lateral growth mechanism is dominant, a gradual leveling of the deposit will be seen to the point where it becomes flat. The leveling is a result of the limited two-dimensional nucleation events, and the dominance of the repeatable step, which tends to complete a layer of atoms before starting the next. This type of behavior is clearly evident in Figure 39 from the formation



of the initial nuclei, to their coarsening and agglomeration, and the ultimate formation of a continuous layer that tends to flatten with increasing time.

Figure 40 are typical SEM plan view and cross-section images for a several micron thick deposit of  $\text{Au}_5\text{Sn}$ . Note that in the cross-sectional image, it is difficult to glean any valuable information concerning structure because of the ductile fracture surface that forms upon cleaving. However, what is evident is that the deposit is both dense and coherent as predicted by electrocrystallization theory [Winand, 1994]. In addition, the plan view image of the sample confirms that the film formation is lateral growth dominated because of the topographically smooth surface. As mentioned previously, the final structure for a low current density deposit should be topographically smooth because of the limited two-dimensional nucleation events, which prevent a rough surface from forming. Typically, the dominance of the repeatable step will result in the completion of full layers giving a smooth surface finish.









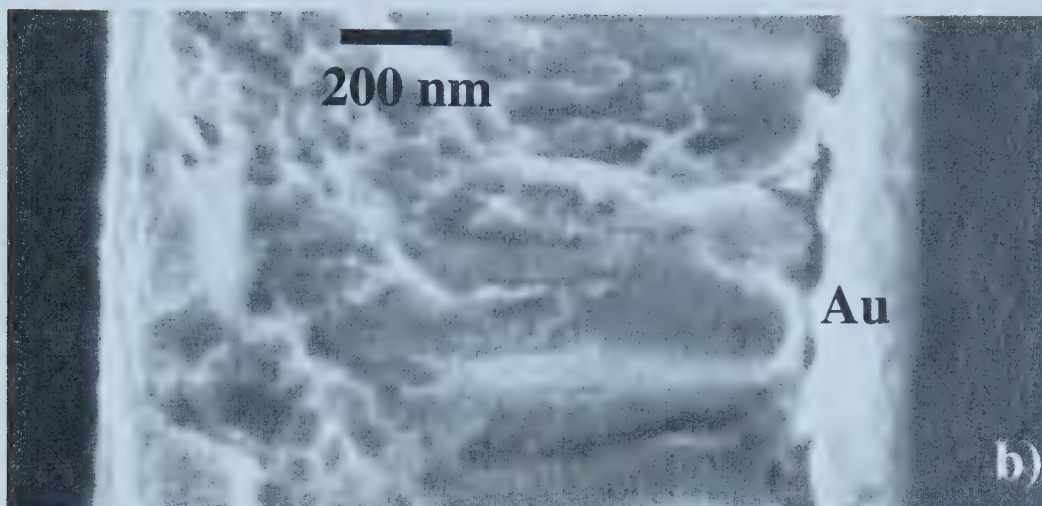


**Figure 40. SEM SE images of  $\text{Au}_5\text{Sn}$  deposit a) plan view b) cross-sectional view**

As a check on the conclusions drawn from the SEM results, TEM investigation of the nucleation and growth mechanism was undertaken partly to verify the mechanism, and partly to verify the composition of the deposit through EDX and diffraction pattern techniques.

The cross-sectional images shown in Figure 41 confirm the results that were obtained with the SEM. At 66 seconds, individual, discrete particles are visible on the surface of the gold seed layer. It does not appear as if the particles are multi-grain at this point, although they are slightly over 100 nm in diameter. The image of the deposit at 1200 seconds clearly reveals a multi-grain structure with an average grain diameter of roughly 200nm. This is further confirmation that the particles at 100nm would not likely be multi-grain. In addition, this image at 1200 seconds reveals the typical growth mechanism of the low current density deposit that was previously discussed. A continuous layer is clearly visible making up a background matrix. Rising above this matrix, is a larger particle. Due to non-uniform sputtering effects, it is possible that the height of the protruding particle above the background matrix is slightly exaggerated, but



it is clear that there is a continuous layer with several protruding particles that were first observed in the SEM plan views (Figure 39j).

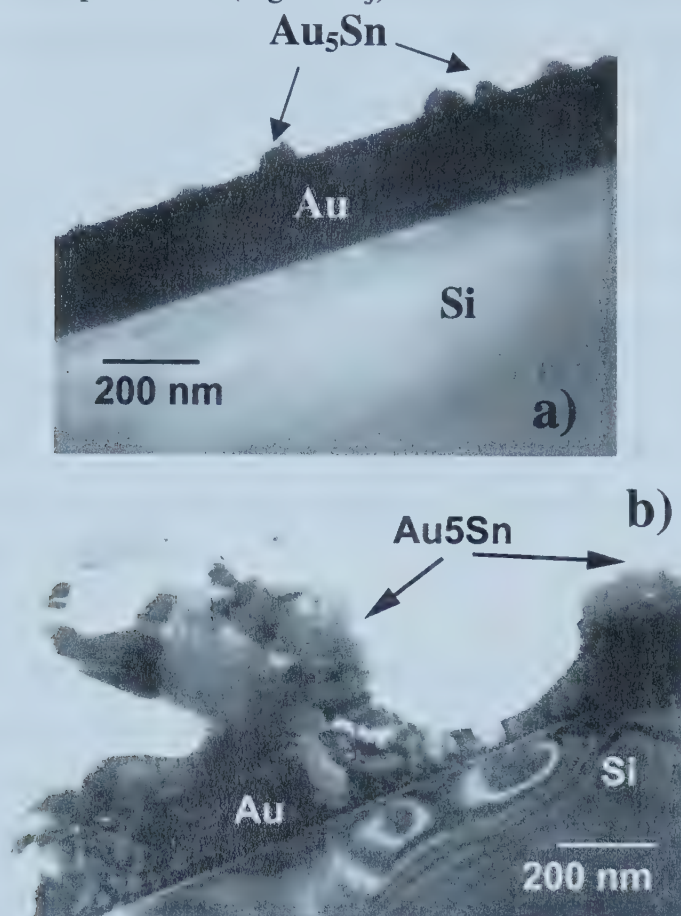


**Figure 41.** TEM cross-section images of solder layer at a) 66s and b) 1200s.

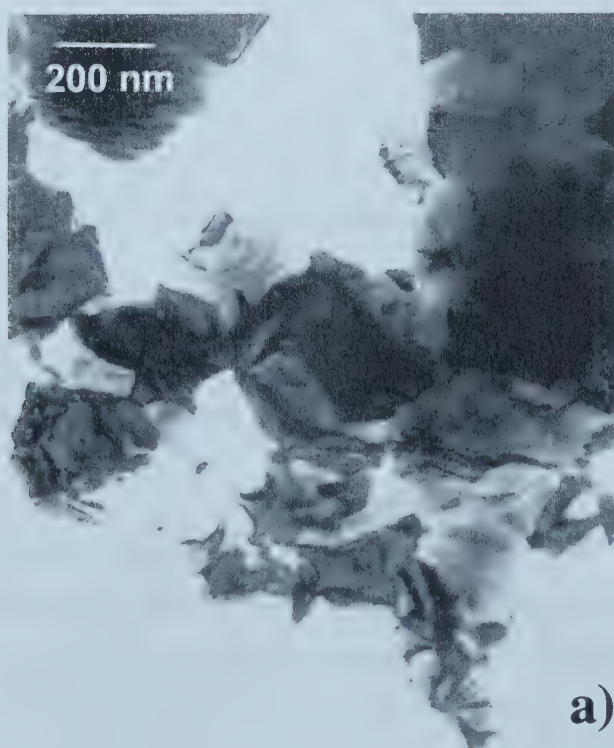
A better understanding of the deposit grain size and composition can be obtained from plan view sample. By using a several micron thick deposit to make the plan view, it ensures that the structure and composition observed is typical of an actual solder deposit. A plan view TEM image with a corresponding EDX spectrum and diffraction pattern are seen in Figure 42. From the plan view, it is possible to confirm that the average grain diameter of the sample at several microns thick remains roughly 200nm as originally indicated at 1200s. More importantly, however, is that the diffraction pattern (Figure 42b) for the Au<sub>5</sub>Sn indicates that it is the disordered phase, not the ordered phase. The ordered phase, because of the larger lattice constant, would exhibit higher order diffraction rings very close to the center spot. Since these rings are not present, it is



concluded that the disordered phase is being deposited. While it is not unusual to deposit the non-equilibrium phase, it is valuable to have confirmation that the phase being deposited is the disordered phase as originally suggested. It also helps to clarify the reason for the scatter seen in the lower plateau of Figure 24.

The EDX spectra provide extra confirmation of the composition of the deposited layer. The intensity of the Sn L-peaks, with background subtraction, is  $8580 \pm 3\%$  and the intensity of the Au L-peaks, with background subtraction, is  $59708 \pm 1\%$ . Using the previously calculated k-value, this results in an overall composition of 79%Au and 21%Sn. Although this is outside the homogeneity range of the  $\text{Au}_5\text{Sn}$  phase, given the significant errors associated with this calculation, it is suitably close to the acceptable values between 10 and 17at%Sn.

The grain size of the  $\text{Au}_5\text{Sn}$  phase is significantly larger (200nm) than the grain size of the AuSn phase (50-75nm). Again, this is a result of the current density effects of deposition. At a smaller current density, there are fewer nucleation events giving preference to the growth of existing nuclei. This ultimately results in a larger grain size than for a deposition done at a higher current density where more nucleation is possible.







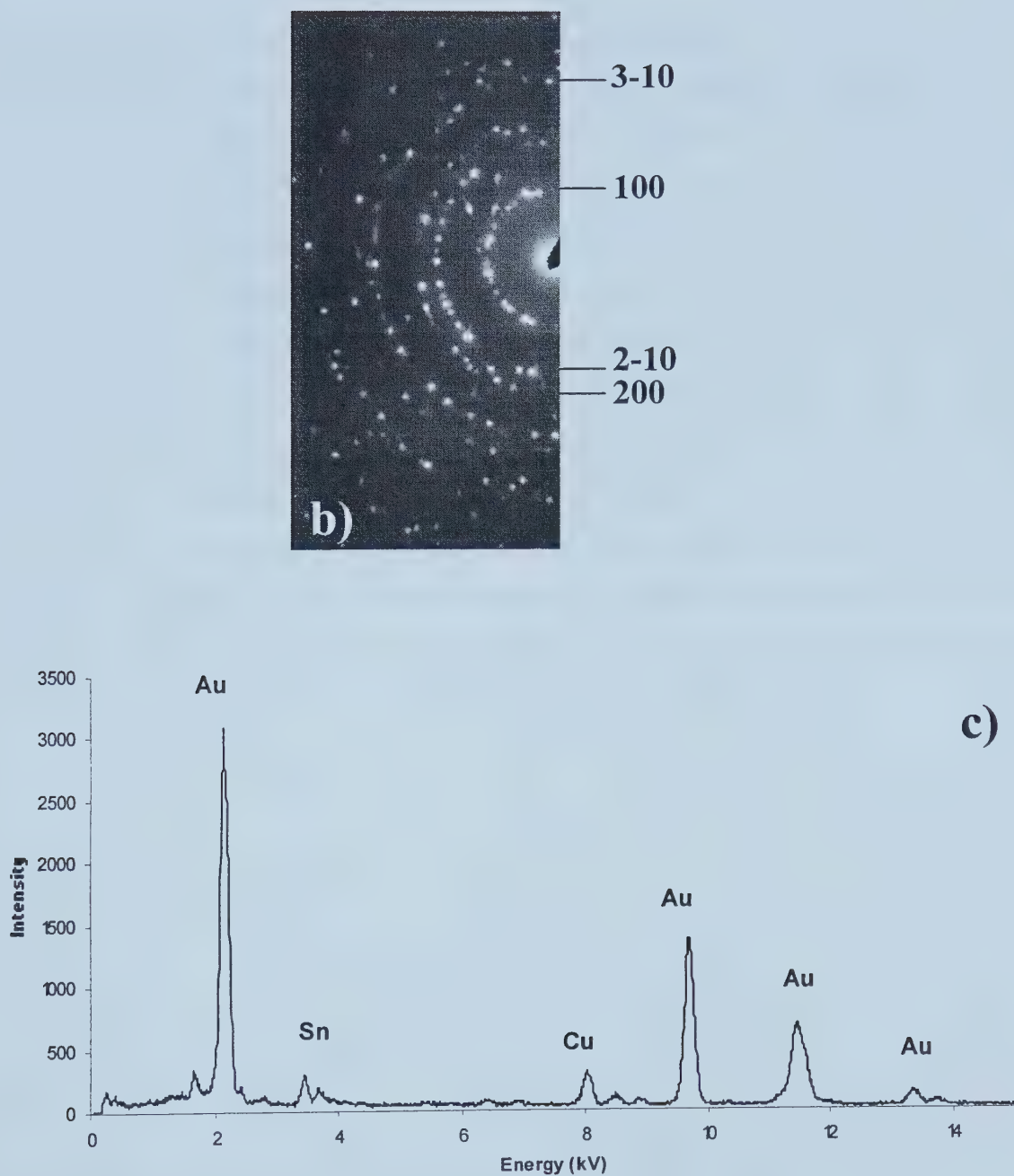


**Figure 42.** a) Plan view TEM brightfield image of  $\text{Au}_5\text{Sn}$ , b) diffraction pattern showing the  $\zeta$  phase, and c) EDS spectra confirming the composition of  $\text{Au}_5\text{Sn}$ .

The presence of copper in the EDX spectrum is an artifact from sample preparation. In order to mechanically stabilize the plan view sample, it was glued to a copper ring resulting in the presence of the copper peak in the EDX spectrum.



#### 4.5.2.2 Film Growth Mechanism-Compositional Analysis

Electron diffraction and EDX analysis were also initially employed as methods of determining which phase forms as the initial nuclei. However, because of the significant problems associated with cross-section sample preparation and subsequent tin diffusion for the AuSn phase, only XRD analysis was used for the  $\text{Au}_5\text{Sn}$  phase. Samples at 66, 180, 400, and 600 seconds were sampled. The individual spectra have been overlaid for easier comparison in Figure 43. What is important to note in this figure is that although the seed layer peaks (Pt) are quite significant at 66 seconds, some telling  $\text{Au}_5\text{Sn}$  peaks are clearly present, for instance the 006 peak. The seed layer peaks are present because there is insufficient deposit thickness on the surface to prevent the seed layer from being sampled. As time progresses, the Pt peaks become less intense as surface coverage increases. In addition, the increasing coverage allows other  $\text{Au}_5\text{Sn}$  peaks to be identified. The XRD results, clearly verify that the initial nuclei are forming as the  $\text{Au}_5\text{Sn}$  phase, and then continue to grow as that phase despite what was previously thought.

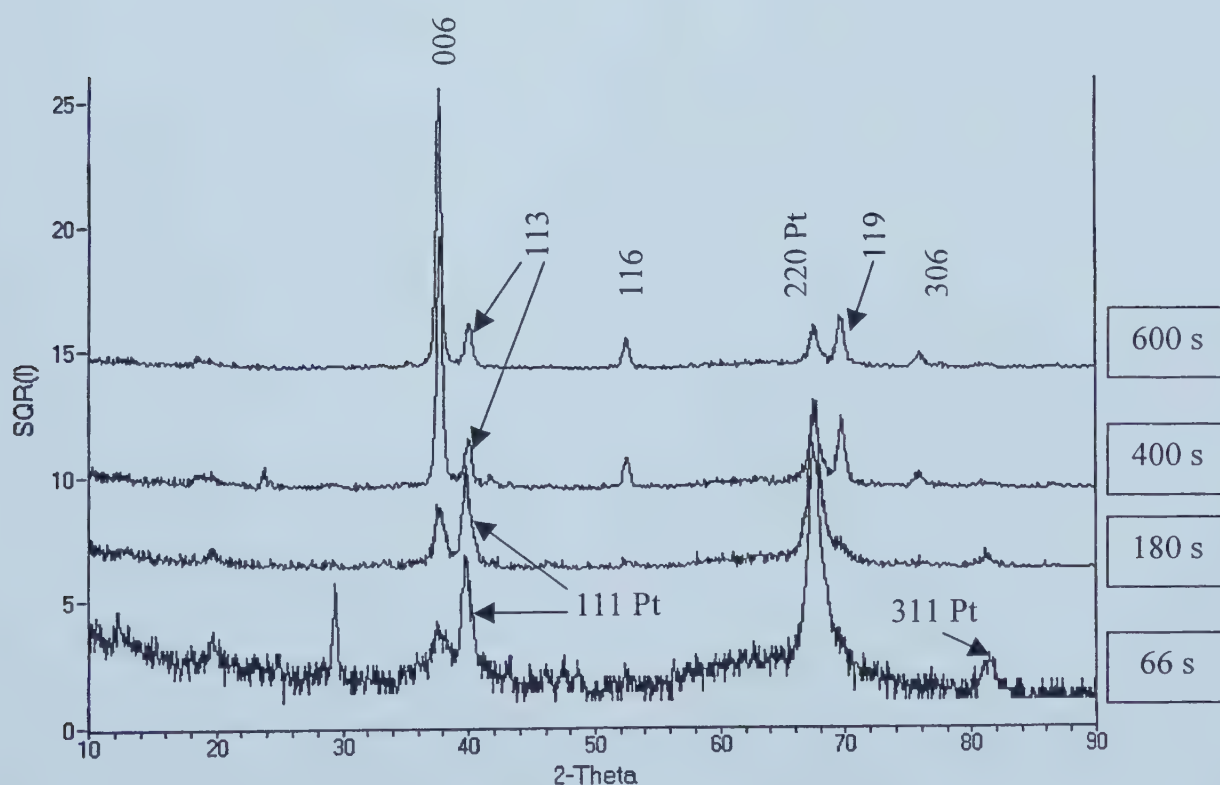


Figure 43. XRD spectra from deposits done for 66, 180, 400, and 600 seconds.



It is important that the initial phase forming is the  $\text{Au}_5\text{Sn}$  phase. When considering a structure like the composite multi-phase structure, it is important that the composition of the deposited phase remains constant throughout the layer thickness. If this were not the case, it would be very difficult to predict the final composition of the composite structure, and would introduce the concept of a minimum required thickness. In such a situation, a minimum thickness of each layer would have to account for both complete surface coverage and the appropriate composition. In the case of the  $\text{Au}_5\text{Sn}$  phase, the minimum plating time that would be most appropriate for the composite multi-layer structure should be around 600 seconds where a continuous layer has been formed. The protruding particles from the surface of the sub-layer will be easily leveled when the  $\text{AuSn}$  layer is next deposited on top. The rapid nucleation of the  $\text{AuSn}$  phase will easily compensate for any effects from having a non-level initial surface.





## 5 Conclusions

### 5.1 Solution Stability

1. The addition of EDA did not noticeably improve the stability of the solution.
2. The useful life of the solution with no EDA added was not 16 days as previously thought, when a visual change is first noticed, but was 24 hours.

### 5.2 Current Density/Composition Relationship

1. There are three distinct regions in the current density vs. composition graph that fully describe the deposition behaviour of the solution. The first region occurs from low current densities up to  $1\text{mA/cm}^2$ , where the deposition of the disordered  $\text{Au}_5\text{Sn}$  phase occurs at an average composition of 15at%Sn. The second region is a transition region where the current density and composition have no discernable relationship. The composition varies between 15 and 50 at%Sn for current densities of  $1\text{-}2\text{mA/cm}^2$ , though not with any predictable pattern. The deposits are two-phase consisting of both  $\text{Au}_5\text{Sn}$  and  $\text{AuSn}$ . The final region occurs at current densities greater than  $2\text{mA/cm}^2$ , resulting in the deposition of the  $\text{AuSn}$  phase at a composition of 50at%Sn.
2. The deposition process exhibits the typical behaviour of a regular co-deposition process as defined by Brenner.
3. The eutectic composition (30at%Sn) can be produced using a composite multi-phase layered structure. The structure consists of alternating layers of each eutectic phase ( $\text{AuSn}$  and  $\text{Au}_5\text{Sn}$ ) which combine to give an overall composition of 30at%Sn. Depositing the  $\text{AuSn}$  phase at  $2.4\text{ mA/cm}^2$  and the  $\text{Au}_5\text{Sn}$  phase at  $0.8\text{mA/cm}^2$  in a four to one time ratio ( $\text{Au}_5\text{Sn}$  to  $\text{AuSn}$ ) will result in a layer with the eutectic composition.

### 5.3 Phase Morphology

#### 5.3.1 AuSn

1.  $\text{AuSn}$  film formation is a growth-controlled process. A continuous dense layer is formed within 60 seconds. The film growth mechanism is typical of the high current density deposition mechanism described in electrocrystallization theory



with a dominant two-dimensional nucleation mechanism. The resulting layer begins with a layer of equiaxed particles that later transform into a columnar structure due to the effects of preferred growth. The final surface is quite rough.

2. At  $2.4 \text{ mA/cm}^2$ , the film nucleates as AuSn and then continues to grow as this phase.
3. The grain size of AuSn deposited at  $2.4 \text{ mA/cm}^2$  is approximately 50-75 nm. The fine grain size is a result of the relatively high deposition current density and consequent nucleation rate.
4. The high current density results in a relatively fast deposition rate.
5. Cross-section TEM sample preparation resulted in significant diffusion of tin out of the solder layer into the gold seed layer resulting in an erroneously low tin concentration. XRD is therefore a more effective method for determining the composition of the deposit.
6. Kirkendall voids that were observed in the TEM cross-sections provide additional evidence of the speed of diffusion in the Au/Sn alloy system.

### 5.3.2 **Au<sub>5</sub>Sn**

1. Au<sub>5</sub>Sn film formation is a nucleation controlled process. A continuous, dense layer forms within 600 seconds. The film growth mechanism is typical of a low current density deposit with a predominance of the lateral growth mechanism resulting in a topographically smooth deposit.
2. At  $0.8 \text{ mA/cm}^2$ , the film nucleates and grows as the Au<sub>5</sub>Sn phase.
3. The grain size of the deposit at  $0.8 \text{ mA/cm}^2$  is approximately 200nm. The grain size is significantly larger than the AuSn phase because of the lower current density used for deposition.
4. The low deposition current density also results in a relatively slow deposition rate.



## 6 Further Recommendations

At the completion of this body of work, there are still some areas of the Au/Sn electrodeposition project that need to be addressed. It is the recommendation of the author that the following issues be addressed at a later time.

1. The stability of the solution is insufficient at its current state to be very useful in a commercial setting. It would be extremely beneficial to have a solution with a lifetime of 2-3 weeks or longer; the present 24 hours is insufficient. It is clear that the addition of a stabilizing agent that improves the visual stability only of the solution is unacceptable. What must be undertaken is a study of the individual species of the solution: how they have complexed in the solution, the effects of the stabilizing agent on the metal complex, and a better understanding of the exact reactions that are occurring. This cannot be carried out through polarization tests and observation alone. It is clear that this portion of the project will require a significant understanding of chemistry and will likely involve more complicated techniques to break down the chemistry of the solution. Ultimately, this work should explain why the bath begins de-stabilizing at 24 hours. Although it is suspected that the tin is de-complexing, the exact reaction is unknown as is the actual tin complex. This work will ultimately lead to much greater commercial possibilities for the solution and the technique.
2. Equally important is to test the bonding ability of the solder layer that forms. Although it is possible to produce a eutectic composition that melts near the eutectic temperature, it is equally important for the deposited solder layer to bond with the same strength as the preforms or evaporated solder layer. This bonding can be simulated in a University setting, but that is undesirable. A better measure of the bondability of the solder is to have it bonded in a commercial setting and then evaluated. Only then can it be ascertained whether or not this is an effective method of producing the eutectic alloy for bonding applications.
3. Although there may be a use for blanket coverage of the substrate carrier with the Au/Sn eutectic solder, more often solder bumps will be used. This will require a patterned deposition process and so it is critical to try the deposition process on





patterned wafers to ensure that the eutectic alloy can be deposited using the composite multi-layer method. The process should be tested with both photoresist patterning and wafers patterned with an insulator as those are the most commonly used types in industry.

4. Another recommendation for further study would be to test the limits of the composite structure. Although the nucleation and growth work indicated appropriate minimum times for depositing each layer, it would be interesting to study the effects of greatly reducing the thickness of the individual layers of each phase in the composite structure. For instance, there may be unique results if each phase were deposited for only microseconds at a time. In order to locate the optimized layer thickness, the effects of finer and finer layers on the composite structure should be studied.



## 7 References

- Avila, A.J. Pulsed Electrodeposition of Alloys. *Theory and Practice of Pulse Plating*. Ed. Puipe and Leaman. American Electroplaters and Surface Finishers Society: Orlando, Florida, 1986.
- Bradford, Samuel. *Corrosion Control*. Van Nostrand Reinhold: New York, 1993.
- Brenner, Abner. *Electrodeposition of Alloys: Principles and Practice*. Academic Press: York, 1969.
- Castellan, G.W. *Physical Chemistry*. The Benjamin/Cummings Publishing Company, Inc: Don Mills, Ontario, 1983.
- Cheh, H.Y. Electrochemical Kinetics in Pulse Plating. *Theory and Practice of Pulse Plating*. Ed. Puipe and Leaman. American Electroplaters and Surface Finishers Society: Orlando, Florida, 1986.
- Chen, S; Yin, K; White, R. A Mathematical Model for the Electrodeposition of Alloys on a Rotating Disk Electrode. *J. Electrochem. Soc.*, 1988, **135**, 2193-2200.
- Doesburg, J.; Ivey, D.G. Microstructure and Preferred Orientation of Au-Sn Alloy Plated Deposits. *Materials Science and Engineering B*, in press, 21 manuscript pages, 2000.
- Doesburg, J.; Ivey, D.G. Co-Deposition of Gold-Tin Alloy from a Non-cyanide Solution. *Plating and Surface Finishing*, 2001, **88**, 78-83.
- Dini, J.W. *Electrodeposition*. Noyes Publications: NJ, USA, 1993.
- Duva, Robert. Pulse Plating. *Electroplating Engineering Handbook 4th Edition*. Ed Lawrence Durney. Van Nostrand Reinhold: NY, 1984.
- Duva, Robert. Pulse Plating: The Pros and Cons of Practical Application. *Finishing Highlights*, 1979, **Jan/Feb**, 40-42.
- Fluehmann, W; Reid, F; Mauesli, P; Steinemann, S. Effect of Pulsed Current Plating on Structure and Properties of Gold-Cobalt Electrodeposits. *Plating and Surface Finishing*, 1980, **67(6)**, 62-65.
- Gorbunova, K..M; Polukarov, Y.M. Electrodeposition of Alloys. *Electrodeposition of Metals and Alloys: Issue 1*. Ed .N. Khomutov. IPST Press: Jerusalem, 1969.
- Gregersen, D.; Buene, L.; Finstad, T.; Lonsjo, O.; Olsen, T. A diffusion marker in Au/Sn thin films. *Thin Solid Films*, 1981, **78**, 95-102.



- Holmbom, G; Abys, J.A.; Straschil, H.K; Svensson, M. Electrodeposition, Growth Morphology, and Melting Characteristics of Gold-Tin Eutectic Alloys. *Plating and Surface Finishing*, April, 1998, **85(4)**, 66-73.
- Ibl, N. Some Theoretical Aspects of Pulse Electrolysis. *Surface Technology*, 1980, **10**, 81-104.
- Ivey, D.G. Microstructural Characterization of Au/Sn Solder for Packaging in Optoelectronic Applications. *Micron*, 1998, **29(4)**, 281-287.
- Knodler, A. Pulsed Electrodeposition of Precious Metals. *Theory and Practice of Pulse Plating*. Ed. Puipe and Leaman. American Electroplaters and Surface Finishers Society: Orlando, Florida, 1986.
- Katz, A.; Baiocchi, F.; Lane, E.; Lee, C.H.; Hall, C.; Doting, J.; Grijsback, C.; Harris, K. Au-Sn/W and Au-Sn/Cr metallized chemical vapor deposited diamond heat Sinks for InP laser device applications. *Journal of Applied Physics*, 1994, **75(1)**, 563-567.
- Landolt, D. Electrochemical and Materials Science Aspects Of Alloy Deposition. *Electrochimica Acta*, 1994, **39**, 1075-1090.
- Landolt, D. Mass Transport in Pulse Plating. *Theory and Practice of Pulse Plating*. Ed. Puipe and Leaman. American Electroplaters and Surface Finishers Society: Orlando, Florida, 1986.
- Lee, C.H.; Wong, Y.M.; Doherty, C.; Tai, K.L; Lane, E.; Bacon, D.D.; Baiocchi, F.; Katz, A. Study of Ni as a barrier metal in AuSn soldering application for laser chip/submount assembly. *Journal of Applied Physics*, 1992, **72(8)**, 3808-3815.
- Leidheiser, H; Ghuman, A. Pulse Electroplating of Silver-Tin Alloys and the Formation of Ag<sub>3</sub>Sn. *J. Electrochem Soc*, 1973, **120(4)**, 484-487.
- Leisner, P; Neilsen, C; Tang, P; Dorge, T; Moller, P. Methods for Electrodepositing Composition-Modulated Alloys. *Journal of Materials Processing Technology*, 1996, **58**, 39-44.
- Li, Zelin; Cai, J; Zhou, S. New Insight into the Anomalous Codeposition of Alloys. *Trans. IMF.*, 1999, **77**, 149-151.
- Lyons Jr., Ernest. *Introduction to Electrochemistry*. D.C. Heath and Company: Boston, 1967.
- Massalski, T.B.; King, H. W. The Lattice Spacing Relationships in Close-Packed  $\alpha$  and  $\zeta$  Phases Based on Gold. *Acta Metallurgica*, 1960, **8**, 677-683.





- Matijasevic, G; Lee, C; Wang, C. Au-Sn Alloy Phase Diagram and Properties Related to its Use as a Bonding Medium. *Thin Solid Films*, 1993, **223**, 276-287.
- Mohler, J.B. *Electroplating and Related Processes*. Chemical Publishing Co. Inc.: New York, 1963.
- Nakahara, S.; McCoy, R. J.; Buene, L.; Vandenberg, J.M. Room temperature inter-diffusion studies of Au/Sn thin film couples. *Thin Solid Films*, 1981, **84**, 185-196.
- Nakahara, S.; McCoy, R. J. Interfacial void structure of Au/Sn/Al metallizations on Ga/Al/As light-emitting diodes. *Thin Solid Films*, 1980, **72**, 457-461.
- Nakahara, S.; McCoy, R.J. Kirkendall void formation in thin-film diffusion Couples. *Applied Physics Letters*, 1980, **37(1)**, 42-44.
- Perrin, D.D, *Organic Complexing Reagents: Structure, Behavior, and Application to Inorganic Analysis*. John Wiley and Sons: New York, 1964.
- Plumbridge, W. Review: Solders in Electronics. *Journal of Materials Science*, 1996, **31**, 2501-2514.
- Puippe, J.C. Qualitative Approach to Pulse Plating. *Theory and Practice of Pulse Plating*. Ed. Puippe and Leaman. American Electroplaters and Surface Finishers Society: Orlando, Florida, 1986.
- Puippe, J.C. Influence of Charge and Discharge of Electrical Double Layer in Pulse Plating. *Theory and Practice of Pulse Plating*. Ed. Puippe and Leaman. American Electroplaters and Surface Finishers Society: Orlando, Florida, 1986.
- Puippe, J.C. Influence of Pulse Plating on Crystallization. *Theory and Practice of Pulse Plating*. Ed. Puippe and Leaman. American Electroplaters and Surface Finishers Society: Orlando, Florida, 1986.
- Sanchez,H; Ozil, P; Chainet, E; Nguyen, B; Meas, Y. Silver-Gold Alloys Prepared by Pulse Plating: Modelling of the Chemical Composition. *J. Electrochem. Soc.*, 1997, **144(6)**, 2004-2012.
- Sun, W; Ivey, D.G. Development of an Electroplating Solution for Co-depositing Au-Sn Alloys. *Materials Science and Engineering*, 1999, **B56**, 1-12.
- Tannenberger, H. The Morphology of Gold Deposits Obtained by Pulse Plating. *Metal Finishing*, 1985, July, 35-37.
- Weil, Rolf. *Electroplating Engineering Handbook 4<sup>th</sup> Edition*. Ed. Lawrence J. Durney.



Van Nostrand Reinhold: NY, 1984.

Winand, Rene. Electrodeposition of Metals and Alloys-New results and perspectives.  
*Electrochimica Acta*, 1994, **39(8/9)**, 1091-1105.

















University of Alberta Library



0 1620 1492 0480

**B45435**